



Strålsäkerhets
myndigheten

Swedish Radiation Safety Authority

Author: Lars Olof Jernkvist
Ali Massih

Research

2015:37

Models for axial relocation of fragmented
and pulverized fuel pellets in distending fuel
rods and its effects on fuel rod heat load

SSM perspective

Background

At high burnups the components of the nuclear fuel are affected by the environment they have been exposed to. Fuel pellets can crack due to thermal effects and tensions build up inside because of fission gases. The result of this is that fuel pellets at high burnup in a situation with high temperature increase (for example at a loss of coolant accident) can break up severely and move within the fuel rod, relocate. Relocation of fuel fragments can in turn result in an increased load where fragments accumulate and an increased risk of fuel rod failure.

Within the research of fuel behavior supported by OECD/NEA at Studsvik and Halden phenomena acting in a loss of coolant situation are in focus. These tests are the basis for development of analytical tools that can predict fuel rod behavior and with analytical tools the situation in a nuclear reactor can be analyzed.

Objective

In this project Quantum Technologies AB has developed models for FRAPTRAN-1.5 for fuel fragmentation and relocation and the subsequent increase of load in the volume where fuel fragments accumulate. The models are novel in the several ways; both as models for fragmentation and relocation and for the way they are incorporated in the FRAPTRAN program.

Results

This report describes the development of the new models from the basic theory to experimental observations to the mathematical expressions that can be used in the analytical tool FRAPTRAN. Three major models have been developed; fragmentation of nuclear fuel, axial relocation of the fragments and thermal response of relocation. These models are incorporated in FRAPTRAN in way which makes it possible to calculate the feedback that fragmentation and relocation causes.

To show the capacity of the new models a calculation of one of the LOCA-tests performed in Halden is included in the report, a calculation which shows good agreement with the test.

In this process of code development interpretations of what is seen in the experimental research is vital. The fragmentation and pulverization characteristics are discussed from the point of fragment sizes and shapes and how they can be packed in a confined volume. In combination with typical nuclear fuel burnup behavior it indicates a threshold from where fragmentation and relocation becomes an issue to consider and to limit. The report also discusses how these phenomena degrade the cladding that surrounds the nuclear fuel and how the temperature and oxidation at the hot spot is affected and the time to burst is reduced.

Need for further research

Continued improvement of calculation tools are needed to accurately describe the performance of the nuclear fuel in the reactor at transient and accident conditions. In the conclusions of this report aspects that need to be further developed in analytical tools and the need for more experimental data are described. Further development is necessary for example regarding mechanisms for fragmentation and dispersal as well as the effects of dispersal. There is also a need to use this newly developed model to analyze and interpret other LOCA-tests from Halden and Studsvik.

Project information

Contact person SSM: Anna Alvestav

Reference: SSM2014-2355



Strål
säkerhets
myndigheten

Swedish Radiation Safety Authority

Author: Lars Olof Jernkvist, Ali Massih
Quantum Technologies AB, Uppsala

2015:37

Models for axial relocation of fragmented
and pulverized fuel pellets in distending fuel
rods and its effects on fuel rod heat load

Date: September 2015

Report number: 2015:37 ISSN: 2000-0456

Available at www.stralsakerhetsmyndigheten.se

This report concerns a study which has been conducted for the Swedish Radiation Safety Authority, SSM. The conclusions and viewpoints presented in the report are those of the author/authors and do not necessarily coincide with those of the SSM.

Models for axial relocation of fragmented and pulverized fuel pellets in distending fuel rods and its effects on fuel rod heat load

Report TR14-002V1, September 1, 2015

Lars Olof Jernkvist
Ali R. Massih

Quantum Technologies AB



Contents

Summary	III
Sammanfattning	IV
1. Introduction	1
2. Model description	5
2.1. Fuel fragment axial relocation	5
2.1.1. Fundamental assumptions	5
2.1.2. Computational algorithm	8
2.2. Fuel fragmentation and pulverization	11
2.2.1. Fuel fragmentation	11
2.2.2. Fuel pulverization	13
2.2.3. Packing fraction of crumbled fuel.....	15
2.2.4. Threshold for fuel fragment detachment.....	20
2.3. Modifications to thermal calculations	21
2.3.1. Radial heat conduction equation.....	22
2.3.2. Heat transfer by axial fuel relocation.....	24
2.3.3. Void volume gas temperature calculation.....	25
3. Verification of the relocation model	27
3.1. Test case 1: Single balloon	27
3.2. Test case 2: Twin balloons.....	30
4. Assessment of Halden LOCA test IFA-650.4	33
4.1. Methodology, computer programs and assumptions	33
4.1.1. Simulation of pre-irradiation	34
4.1.2. Simulation of LOCA test.....	34
4.2. Calculated results.....	37
4.2.1. Pre-irradiation.....	37
4.2.2. LOCA test.....	39
5. Concluding remarks	49
5.1. Distinguishing features of the proposed model.....	49
5.2. Main conclusions.....	50
5.3. Suggestions for further work	52
6. References	55
Appendix A: Fuel fragmentation and pulverization	A.1
Appendix B: Effective thermal conductivity of crumbled fuel	B.1
Appendix C: The Halden LOCA test IFA-650.4	C.1

Summary

Loss-of-coolant accidents (LOCAs) in light water reactors may lead to overheating of the fuel rods, significant distension of the cladding tubes and axial relocation of fuel pellet fragments inside the “ballooned” part of the fuel rods. The fuel relocation may localize the heat load to a particular part of the rod, thereby increasing the risk for cladding failure and aggravating local oxidation of the cladding. It may also increase the amount of fuel dispersed into the coolant, should the cladding fail. Recent LOCA tests have revived interest in the relocation and dispersion phenomena among nuclear regulators, since the test results suggest that high burnup (> 65 MWd/kgU) UO_2 fuel pellets may pulverize into very fine (< 0.2 mm) fragments, with a higher potential for axial relocation and subsequent dispersal than observed earlier for low to medium burnup fuel.

To analyse these issues, a computational model for axial relocation of fuel fragments during LOCA and its effects on the fuel rod heat load and failure processes is developed and introduced in SSM’s version of FRAPTRAN-1.5, a computer program intended for fuel rod thermo-mechanical analyses of transients and accidents. The fuel relocation is calculated on the basis of estimated fuel fragment size distributions and the calculated cladding distension along the fuel rod, and its effects on the axial redistribution of stored heat and power are accounted for in thermo-mechanical analyses of the fuel rod. Hence, our model fully considers thermal feedback effects from the fuel relocation, in contrast to existing relocation models. It also provides estimates of the amount of fuel that may potentially be ejected into the coolant upon cladding failure anywhere along the fuel rod.

The model is validated by comparisons with measured data and discussed in light of tests and experiments. In particular, we study the IFA-650.4 integral LOCA test in the Halden reactor, Norway. This test was done on a very high burnup (92.3 MWd/kgU) UO_2 fuel rodlet and it resulted in extensive fuel pulverization, axial relocation and fuel dispersal into the coolant. Our simulations of this test suggest that thermal feedback effects from axial fuel relocation are strong enough to significantly affect the dynamics of cladding ballooning and rupture, even though the calculated duration of these processes is no more than 7–8 seconds. Moreover, for the considered LOCA test, the axial relocation has a strong effect on the calculated peak cladding temperature and oxidation after rupture.

Finally, our work suggests that the aforementioned pulverization mechanism of high burnup fuel is important to axial fuel relocation during LOCA as it may increase the packing fraction of crumbled fuel. The pulverization thereby eases axial movements of the fuel pellet column and raises the local heat load in regions where fuel fragments accumulate. Our calculations indicate that fuel with a pellet average burnup around 70–75 MWd/kgU would be particularly prone to axial relocation, due to its expected fragment size distribution.

Sammanfattning

Haverifall med kylmedelsförlust (LOCA) i lättvattenreaktorer kan leda till överhettning av bränslestavar, utvidgning av stavarnas kapslingsrör, samt axiell omflyttning av bränslekutsfragment i de delar av stavarna som expanderat. Bränsleomflyttningen kan koncentrera värmebelastningen till en begränsad del av stavarna och därigenom öka risken för kapslingsskador och förvärra kapslingsrörens oxidation lokalt. Den kan också medföra att mängden bränsle som sprids ut i kylvattnet ökar i händelse av kapslingsskada. Nyligen genomförda LOCA-experiment har återuppväckt tillsynsmyndigheternas intresse för dessa fenomen, då provresultaten antyder att högutbränt ($> 65 \text{ MWd/kgU}$) UO_2 -bränsle kan pulveriseras till mycket små ($< 0.2 \text{ mm}$) fragment, vilket leder till en större risk för omflyttning och efterföljande utspridning i kylvattnet än vad som tidigare observerats för bränsle med låg eller medelhög utbränning.

För att analysera dessa frågor utvecklas här en beräkningsmodell för axiell omflyttning av bränslefragment under LOCA och dess effekter på bränslestavens värmebelastning och skadeprocesser. Modellen införs i SSM:s version av FRAPTRAN-1.5, ett beräkningsprogram avsett för termomekanisk analys av bränslestavar under transienter och olyckor. Bränsleomflyttningen beräknas på grundval av uppskattad storleksfördelning för bränslefragmenten samt kapslingsrörets beräknade deformationsprofil längs bränslestaven, och bränsleomflyttningens inverkan på axiell omfördelning av effekt och lagrad värme beaktas i termomekaniska analyser av bränslestaven. Vår modell tar således full hänsyn till termiska återkopplingseffekter av bränsleomflyttningen, i motsats till existerande beräkningsmodeller. Den tillhandahåller även uppskattningar av den bränslemängd som potentiellt kan spridas ut i kylvattnet vid kapslingsbrott i någon del av staven.

Modellen valideras genom jämförelser mot mätdata och diskuteras mot bakgrund av experimentella resultat. I synnerhet studerar vi LOCA-experiment IFA-650.4, som genomförts i Haldenreaktorn, Norge. Provet gjordes på en högutbränd (92.3 MWd/kgU) UO_2 -provstav, och resulterade i omfattande bränslepulverisering, axiell omflyttning och bränsleutspridning i kylvattnet. Våra simuleringar av detta prov antyder att termiska återkopplingseffekter från den axiella bränsleomflyttningen är tillräckligt starka för att märkbart påverka dynamiken för kapslingens deformation och brott, trots att den beräknade varaktigheten hos dessa processer är högst 7–8 sekunder. Dessutom har den axiella bränsleomflyttningen stor inverkan på kapslingens beräknade maximala temperatur och oxidation efter kapslingsbrottet för det beaktade LOCA-experimentet.

Avslutningsvis skall nämnas att vårt arbete pekar mot att ovan nämnda pulveriseringsmekanism för högutbränt bränsle är betydelsefull för axiell bränsleomflyttning, då den kan öka bränslefragmentens packningstäthet. Pulveriseringen underlättar därmed axiella rörelser hos bränslekutspelaren och ökar den lokala värmebelastningen i områden där kutsfragment ansamlas. Våra beräkningar antyder att bränsle med en genomsnittlig kutsutbränning runt $70\text{--}75 \text{ MWd/kgU}$ torde vara särskilt benäget för axiell omflyttning, på grund av dess förväntade fragmentstorleksfördelning.

1. Introduction

Axial relocation of oxide fuel fragments inside distending cladding tubes of light water reactor (LWR) fuel rods was first reported about 35 years ago when in-reactor experiments on fuel rod behaviour during loss-of-coolant accidents (LOCAs) were conducted in Germany and the USA [1-4]. Post-test examinations revealed that significant amounts of fuel fragments could relocate and accumulate in ballooned regions of the test rods, provided that the cladding distension was sufficiently large. From these early tests, it was also clear that the fuel relocation could occur both before and concurrently with cladding rupture [1]. The findings raised concern that the relocation would increase the local heat load in ballooned parts of fuel rods, which would then result in higher temperature and faster cladding oxidation than normally considered in safety analyses. Some of the earliest computational studies of these potential consequences were in fact carried out in Sweden, and the results were quite alarming [5, 6]. However, in a seminal modelling work on axial fuel relocation, Siefken [7] stated that ballooning in most cases would *lower* the cladding temperature. The reason is that disorderly stacked, mm-sized, fuel fragments in the ballooned part of the fuel rod have a fairly low packing fraction, which means that the cladding tube diameter has to increase significantly to accommodate additional fuel. As a result, the increase in coolable area caused by the large cladding distension more than compensates for the increased amount of hot fuel within the cladding.

Although axial fuel relocation was still considered an issue by regulators [8, 9], the analysis presented by Siefken in 1983 was reassuring, and little attention was paid to the phenomenon until 2006, when a LOCA test (IFA-650.4) on a very high burnup fuel rod in the Halden reactor, Norway, resulted in cladding rupture with concomitant dispersal of a large amount of fuel fragments into the coolant. Subsequent post-test examinations revealed that a large part of the fuel pellet column had relocated axially and been ejected into the coolant through the fairly small rupture opening. This kind of behaviour had not been observed in earlier tests, which were limited to fuel rods with burnups lower than $35 \text{ MWd}(\text{kgU})^{-1}$. The IFA-650.4 test was soon followed by similar tests on other high burnup fuel rods, both integral in-reactor LOCA tests in Halden [10] and out-of-reactor LOCA simulation tests in Studsvik, Sweden [11]. These tests have shown that, when overheated, high burnup UO_2 fuel may pulverize into very fine ($< 0.2 \text{ mm}$) fragments. These fragments seem to have a higher potential for axial relocation and subsequent dispersal into the coolant than the fairly large fuel fragments typically observed in early LOCA tests on low to medium burnup fuel. As will be shown in this report, the fine fragments formed by pulverization of high burnup fuel may also increase the packing fraction of crumbled and relocated fuel in ballooned regions of the fuel rod, which may lead to higher local heat loads than for the coarse fragments typically seen in low burnup fuel. Hence, Siefken's conclusions do not necessarily hold for high burnup fuel.

The observed difference in behaviour between low and high burnup fuel during LOCA has revived interest in the fuel fragmentation, relocation and dispersion phenomena among nuclear regulators [12, 13]. In comparison with the 1980s, the regulatory focus has somewhat shifted from the effects of axial fuel relocation on the local heat load to its effects on fuel dispersal upon cladding rupture. The fuel dispersal is an issue with regard to energetic fuel-coolant interaction, radiological consequences, criticality and long-term coolability of the material ejected into the coolant.

Along with the recent LOCA tests on high-burnup fuel, some computational models have been proposed for the observed fuel relocation. For example, already in 2006, Aounallah and co-workers made some simple estimates of fuel fragment relocation when evaluating the Halden IFA-650.4 test with the FALCON fuel analysis program [14]. A year later, Khvostov et al. [15] presented a more thorough analysis of the same test, using FALCON and a simple stand-alone model for assessing the thermal effects caused by the relocation. The IFA-650.4 test was also recently evaluated by Govers and Verwerft, who developed a computational model for axial fuel relocation that they used together with the FRAPTRAN computer program [16]. All these relocation models estimated the extent of fuel fragment relocation based on the cladding distension along the fuel rod, as calculated with the fuel rod analysis program (FALCON or FRAPTRAN). However, the models were not fully integrated with these programs, and the effects of relocation on the axial redistribution of fuel mass, stored heat and power were only partially accounted for in the thermo-mechanical analyses of the fuel rods.

The computational model for axial fuel relocation presented in this report is implemented as an integral part of FRAPTRAN-1.5, a computer program used for fuel rod thermo-mechanical analyses of transients and accidents [17]. Our relocation model is distinguished by its close integration with the solution methods for radial heat transfer in this program. Hence, in contrast to hitherto presented relocation models, the model considers thermal feedback effects from the fuel relocation in a complete and consistent way. It also uses submodels to calculate the packing fraction and effective thermal conductivity of particle beds formed by crumbled fuel in ballooned regions of the fuel rod, based on the estimated state of fragmentation for the fuel pellets. In particular, these submodels estimate the mass fraction of fine fuel fragments formed by pulverization of overheated high burnup fuel. As already mentioned, the pulverization phenomenon increases the packing fraction of disorderly stacked fuel fragments. This eases axial movement of the fuel, and it also strengthens thermal feedback from the relocation; both effects are considered in our model.

The relocation model and its supporting submodels for the fuel fragment packing fraction, effective thermal conductivity, fuel fragmentation and pulverization, are presented in section 2 of the report. The experimental studies and data, on which the latter models are based, are presented in Appendix A. A separate part of sec-

tion 2 is devoted to the modifications made to the equations for radial heat transfer in FRAPTRAN-1.5 in order to account for thermal feedback effects from the fuel relocation and to address the change in fuel geometry from a cylindrical, dense, fuel column to a porous particle bed. In section 3, we apply the model to two simple test cases to verify its correctness and to illustrate its functionality. The model is then validated against the Halden IFA-650.4 LOCA test in section 4, where calculated results are discussed in light of measured data. Finally, in section 5, we draw some general conclusions from the presented study and make suggestions for further work.

2. Model description

Three submodels are dealt with in this section. The first and most important treats axial relocation of fuel fragments. This submodel, which is presented in section 2.1, requires input in terms of cladding tube deformations and estimates of the fragment size distribution for the fuel pellet column. The latter are given by submodels for fuel fragmentation and pulverization, described in section 2.2. The relocation model provides output in terms of the change in fuel mass distribution along the fuel rod. This is used as input to thermal calculations by the host code, in our case FRAPTRAN-1.5 [17], so that the radial heat transfer equation is modified in those parts of the fuel rod where fuel relocation occurs. These modifications are described in section 2.3.

2.1. Fuel fragment axial relocation

2.1.1. Fundamental assumptions

The model is based on two postulated prerequisites for axial relocation of fuel fragments within a distending fuel rod. Firstly, the cladding distension along at least one axial segment of the discretized fuel rod must be sufficient to accommodate relocated fuel fragments in a disordered (crumbled) configuration, which is assumed to contain a lot more void volume than the original, pellet-like configuration. In a specific axial segment of the fuel rod, henceforth referred to by subscript k , the disordered configuration is defined by the packing fraction of fuel fragments

$$\phi_k = V_k^f / V_k . \quad (1)$$

Here, V_k^f is the volume occupied by fuel fragments and V_k is the total volume enclosed by the cladding tube in the k :th segment. In an axial segment of length L_k , the total volume is $V_k = \pi L_k R_{cik}^2$, where R_{cik} is the cladding inner radius in the k :th axial segment. An alternative way of characterizing the crumbled fuel is by the void fraction in the segment, which is simply $1 - \phi_k$.

As already mentioned, ϕ_k is very close to unity under normal fuel operation, since the fuel fragments are then densely packed and retained in the original, cylindrical configuration of the pellets. The void volume is then made up essentially of pellet dishes, cracks and possibly a narrow pellet-cladding gap. When the cladding tube distends under LOCA, the gap gradually widens and may reach a size that make the fuel pellet column collapse. The fuel fragments then move radially outward and turn into a disordered pattern with ϕ_k significantly lower than unity. Here, we make the assumption that local collapse of the fuel pellet column in an axial seg-

ment occurs when more fuel can be accommodated in a crumbled configuration than in the original, pellet-like, configuration. This condition on fuel pellet column collapse can be written as

$$m_k^M > m_k^i, \quad (2)$$

where m_k^i is the initial (as-fabricated) fuel mass in the k :th segment and m_k^M is the fuel mass in the segment in case it is completely filled with crumbled fuel:

$$m_k^M = \phi_k \rho_f V_k = \phi_k \rho_f \pi L_k R_{cik}^2. \quad (3)$$

Here, ρ_f is the density of the fuel material and ϕ_k is the packing fraction of the crumbled fuel. We treat this packing fraction as a model parameter that is independent of the cladding distension. Hence, when fuel relocates from higher elevations, the packing fraction of disordered fragments in ballooned segments that receive fuel is assumed to remain equal to the packing fraction just after fuel column radial collapse. This assumption is justified by the early work of Siefken [7], who measured the packing fraction of crumbled fuel in eight ballooned fuel rods with low ($< 17 \text{ MWd}(\text{kgU})^{-1}$) burnup after LOCA tests in the Power Burst Facility (PBF) reactor, USA. He found that the packing fraction in regions where the fuel pellet column had collapsed into a crumbled state did not change much as the cladding tube continued to distend [7]. In our model, it is assumed that this characteristic packing fraction of disordered fuel fragments, which is a key model parameter, depends on the fragment size distribution of the fuel. This, in turn, depends on burnup and operating life of the fuel. From theory and experiments, the packing fraction is expected to be fairly low (0.6–0.7) for low burnup fuel that contains mostly mm-sized fragments. It is expected to be higher for higher burnup fuel, which contains some amount of much finer fragments that will fill up the gaps between the larger fragments and between the fragments and the cladding inner surface. The method for calculating ϕ_k from the state of fuel fragmentation is defined in section 2.2.3.

The condition on fuel pellet column collapse defined by eqs. (2) and (3) will preclude axial relocation until the cladding radius in some axial segment reaches a threshold deformation, roughly given by $\phi_k R_{cik}^2(t) \approx R_{cik}^2(0)$, where the right-hand-side quantity is the as-fabricated cladding inner radius. In terms of cladding hoop logarithmic strain, $\varepsilon_{\theta\theta}(t) \approx \ln(R_{cik}(t)/R_{cik}(0))$, the condition for relocation can thus be written

$$\varepsilon_{\theta\theta}(t) > \varepsilon_{\theta\theta}^{th}(t) \approx -\ln(\phi_k)/2, \quad (4)$$

where $\varepsilon_{\theta\theta}^{th}$ can be interpreted as a cladding threshold strain (logarithmic) for fuel pellet column collapse and onset of fuel fragment axial relocation. Equation (4) is plotted in Fig. 1. It is clear that the threshold strain is sensitive to the value assumed for the packing fraction of crumbled fuel.

Equation (4) defines a necessary condition on the cladding hoop strain for fuel fragments that fall down from higher elevations of the fuel pellet column to be accommodated in a disordered configuration within a ballooned segment of the

fuel rod. The second prerequisite for axial relocation is given by the fact that no fragments will detach and fall down, unless the cladding tube is sufficiently distended to allow fragments to break away from their close-packed arrangement by gravity, thermal expansion/shrinkage, or flow induced vibrations of the fuel rod. More precisely, we prescribe a threshold for the pellet-cladding gap size, henceforth denoted g^{th} , which is used to define whether there is enough space for fuel fragments to detach from their original close-packed configuration and relocate downwards. One may hypothesize that this threshold gap size would depend on the typical size of fuel fragments at the pellet rim; large fragments are likely to detach only in fairly wide pellet-cladding gaps, whereas small fragments may detach also in narrow gaps. However, there are currently no data to support this hypothesis; see section 2.2.4, where g^{th} is further discussed.

It should be remarked that the model accounts for the possibility that part of the fuel pellet column moves downwards while maintaining the pellet fragments in their original, pellet-like, configuration. Hence, in segments with $g > g^{th}$ and $m_k^M < m_k^i$, the fuel pellet column may move downward without breaking the close-packed structure of the fuel pellet fragments. This part of the fuel column thus relocates while maintaining a fragment packing fraction close to unity. It is clear from in-reactor LOCA tests that this kind of relocation occurs in a fairly large region above extensively ballooned segments of the fuel rod [1, 10].

In our model, it is assumed that axial relocation of fuel fragments changes the distribution of fuel mass along the fuel rod, and consequently, also the axial distributions of stored heat and heat generation. The assumptions made regarding effects of fuel relocation on temperature calculations are presented in section 2.3.

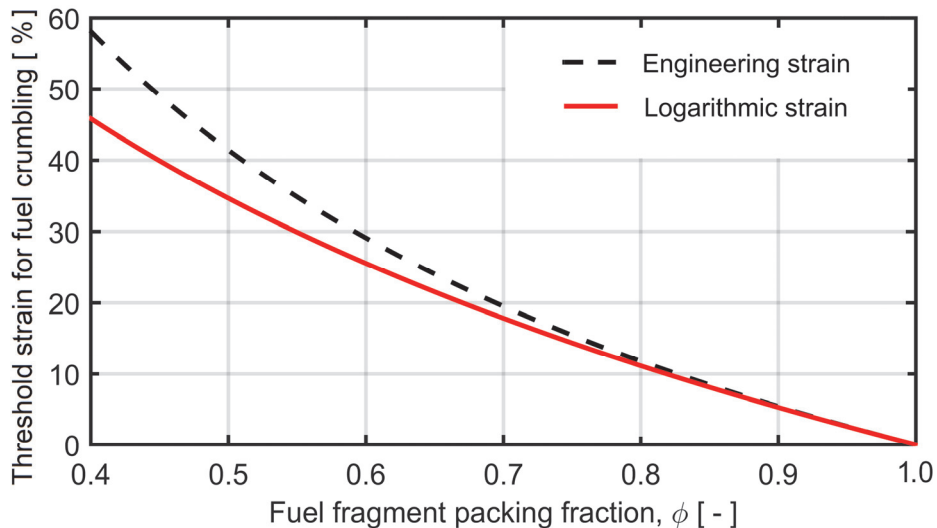


Fig. 1: Cladding hoop logarithmic threshold strain for fuel pellet column collapse and onset of axial fuel relocation, as defined by eq. (4). For comparison, the relocation threshold is also plotted in terms of engineering strain (relative elongation).

2.1.2. Computational algorithm

The axial relocation of fuel fragments is calculated through an algorithm that is similar to the one proposed by Govers and Verwerft [16]. The algorithm is called at the end of each time step taken by the host computer program, FRAPTRAN-1.5 [17]. The algorithm calculates the redistribution of fuel mass during the time step, using the current state of fuel pellet fragmentation and cladding tube distension as input. The updated axial distribution of fuel mass along the fuel rod is applied in thermal-mechanical analyses for the next time step taken by FRAPTRAN, but the current time step is *not* recalculated with the updated mass distribution. Hence, the relocation model is placed *outside* the iterative loop for coupled thermo-mechanical analyses.

The algorithm makes two loops over the N axial segments that are used for discretizing the active length of the fuel rod. There are no restrictions on the number of segments or their lengths; they may have equal or different lengths. Henceforth, the segment numbering is assumed to run bottom-up, and subscript k refers to the k :th segment from the bottom. We consider a time step that starts at time t_o , and assume that the fuel mass in each axial segment is known for this point in time. This mass is henceforth denoted m_k^o , whereas m_k denotes the unknown fuel mass at end of the time step. This quantity is to be calculated by the algorithm.

In the first loop, the aforementioned requirement on a minimum pellet-cladding gap size for fuel mobility is used for calculating the amount of fuel, m_k^r , that each axial segment may receive from higher elevation segments. Since m_k^r may contain contributions from many axial segments, the loop starts from the top segment (N) and runs downwards, as illustrated in Fig. 2. If the current local gap exceeds the threshold gap size for fuel mobility, g_k^{th} , it is assumed that almost all fuel in the segment may fall down. More precisely, it is postulated that at least a fraction x^r of the initial (as-fabricated) fuel mass, m_k^i , will always remain in the segment. This fraction represents small fuel fragments that are bonded to the cladding inner surface. The remaining fuel mass fraction x^r is treated as a model parameter, henceforth set to 0.01.

The second loop is run to update the fuel mass in each axial segment in case relocation actually occurs; see the flowchart in Fig. 3. From section 2.1.1, we recall that collapse of the fuel pellet column that triggers subsequent axial fuel relocation takes place only if $m_k^M > m_k^i$, i.e. if the initial fuel mass in the segment is less than the mass that can be accommodated by the distending cladding, considering that the disorderly stacked fuel fragments have a packing fraction $\phi_k < 1$. As indicated in Fig. 3, there are also two additional constraints on the fuel relocation; it may occur only in the downward direction, and only if detached fuel fragments are available in axial segments at higher elevations. These conditions can mathematically be expressed by

$$\sum_{j=1}^k m_j^o \leq m_k + \sum_{j=1}^{k-1} m_j \leq m_k^r + \sum_{j=1}^k m_j^o. \quad (5)$$

The centre part of eq. (5) defines the total fuel mass up to the k:th axial segment at end of the current time step. The left-hand condition ensures downward relocation, since it states that the total fuel mass in all axial segments up to the k:th segment should not decrease during the considered time step. The right-hand condition in eq. (5) states that the mass increase for the k:th segment during the time step is limited by the availability of detached fuel fragments in segments at higher elevations; m_k^r is the available fuel mass, evaluated during the first loop of the algorithm.

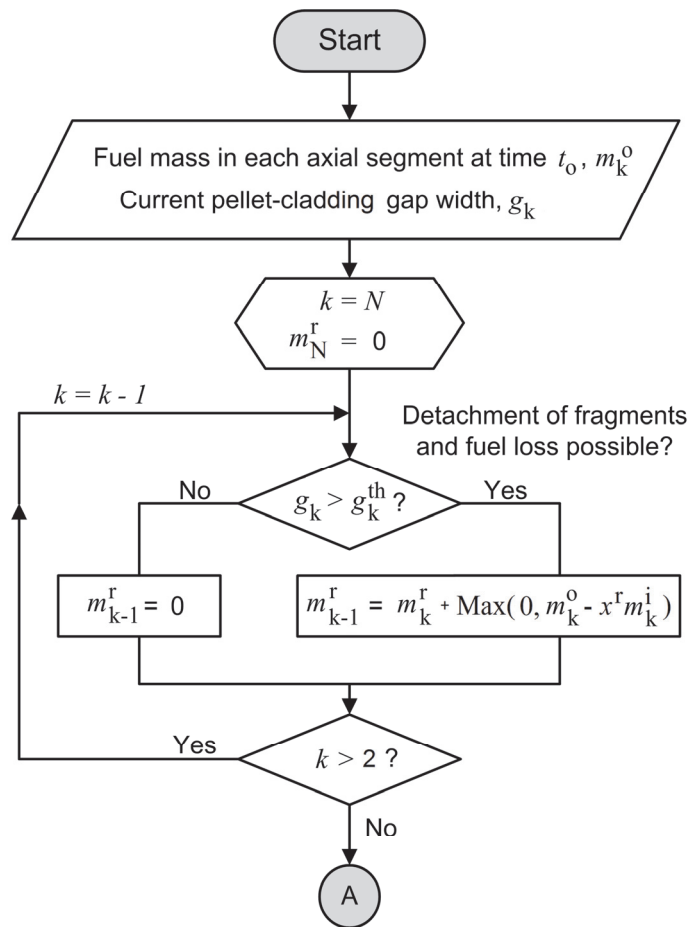


Fig. 2: First loop over axial segments is run to determine the fuel mass that *may* relocate (fall down) into each segment, m_k^r .

Equation (5) can be cast into

$$m_k = \text{Max}(m_k^M, m_k^L) \text{ or } m_k = \text{Max}(m_k^i, m_k^L), \quad (6)$$

$$m_k = \text{Min}(m_k^M, m_k^U) \text{ or } m_k = \text{Min}(m_k^i, m_k^U), \quad (7)$$

where m_k^M is the trial value for m_k , defined by eq. (3), and the lower and upper constraint values are given by

$$m_k^L = \sum_{j=1}^k m_j^o - \sum_{j=1}^{k-1} m_j, \quad (8)$$

$$m_k^U = m_k^r + \sum_{j=1}^k m_j^o - \sum_{j=1}^{k-1} m_j. \quad (9)$$

It should be remarked that the left-hand-side branch of the condition inside the loop in Fig. 3 handles the case with relocation of fuel that maintains its original pellet-like geometry, without disordering the fuel fragments. This kind of relocation typically occurs in axial segments with moderate cladding distension above the ballooned region of the fuel rod. It occurs without changing the fuel mass for most axial segments, but an empty axial space is created between the part of the fuel column that is free to relocate downward ($g > g^{th}$) and the part that is stuck by contact with the cladding tube ($g < g^{th}$). The behaviour is illustrated in section 3 of the report.

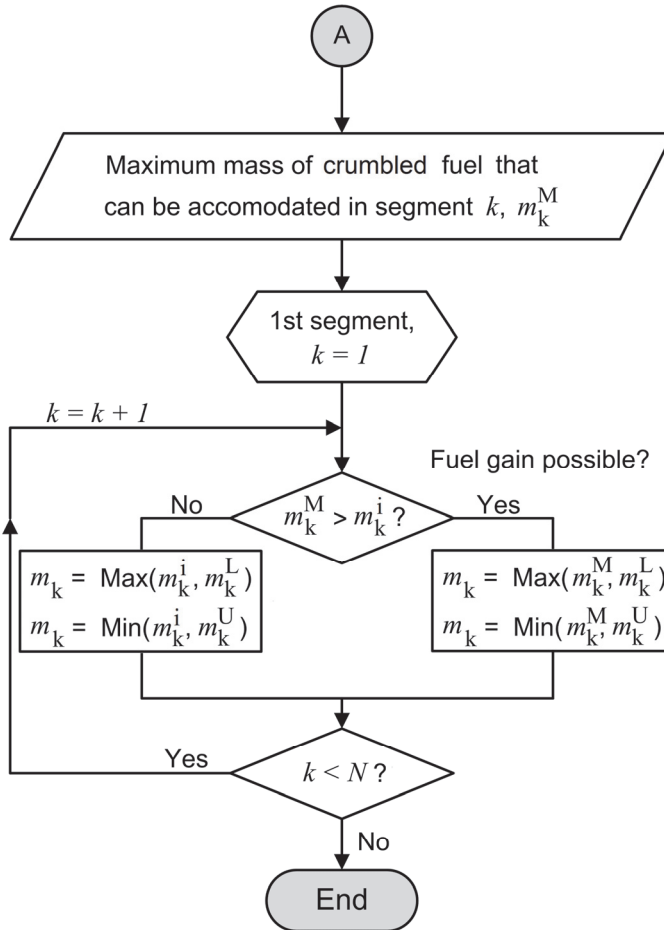


Fig. 3: Second loop over axial segments. The constraints on the updated fuel mass, m_k , enforced by the min/max conditions, are explained in the text.

It should be remarked that the relocation model provides an upper bound for the fuel mass that may be ejected into the coolant, should the cladding fail in the k:th axial segment. Assuming that the ejected fuel will include all fuel above the cladding breach that is free to move downward (m_k^r) and all fuel within the k:th segment, except for the aforementioned residual part $x^r m_k^i$, the upper bound for the ejected fuel mass is $m_k^r + \text{Max}(0, m_k^o - x^r m_k^i)$. Possible improvements of this upper bound estimate are discussed in section 5.3.

2.2. Fuel fragmentation and pulverization

As mentioned in section 2.1, the key parameters ϕ and g^{th} in our relocation model are assumed to depend on the state of fragmentation for the fuel pellet column. The applied methodology and the correlations used for quantifying these dependencies are described below. Henceforth, we discriminate between fuel fragmentation and fuel pulverization: Fuel fragmentation inevitably occurs under normal reactor operation by thermally induced stresses in the fuel pellets, and the fragments formed are usually fairly large (> 1 mm). Fuel pulverization, on the other hand, occurs when high burnup fuel is transiently overheated. As the name indicates, the phenomenon produces a “pulver”, consisting of very fine (< 0.2 mm) fuel fragments. The two mechanisms are treated in subsections 2.2.1 and 2.2.2, where empirically based submodels for estimating the state of fuel fragmentation and pulverization from information on the operating life of the fuel are presented. The experimental studies and data, on which these empirical models are based, are presented in Appendix A. Subsections 2.2.3 and 2.2.4 deal with the calculation of the key model parameters ϕ and g^{th} from the estimated state of fuel fragmentation and pulverization. A review of the fuel fragmentation and pulverization phenomena with emphasis on their importance for fuel rod behaviour under loss-of-coolant accidents can be found in [12].

2.2.1. Fuel fragmentation

Fuel fragmentation is a fairly well known phenomenon, since it occurs during normal operation of oxide nuclear fuel. As explained in Appendix A, the fragmentation is caused mainly by internal stresses induced by the strong radial temperature gradient in the fuel pellets. Ceramographic investigations [18] of irradiated fuel show that the fragments are inversely correlated in size to the peak linear heat generation rate (LHGR) experienced by the fuel during its reactor life time. The fuel fragment size is also known to decrease slightly with increasing burnup. Empirical correlations have been proposed in the literature, by which the crack density and/or fuel fragment size can be estimated from fuel pellet average burnup and peak LHGR; these correlations are reviewed in Appendix A.

Fuel fragments formed by thermally induced stresses during normal reactor operation are fairly large; as shown in Appendix A, reported fragment sizes typically range from about 2 to 4 mm. As revealed by ceramographic investigations of irradiated fuel directly before and after LOCA testing, there is very little additional cracking of the fuel during a typical LOCA for fuel pellets with an average burnup below about $60 \text{ MWd}(\text{kgU})^{-1}$. In fuel pellets with higher burnup, fuel pulverization may occur; see section 2.2.2.

Based on the aforementioned observations, it is assumed in our model that the mm-sized fragments formed during normal reactor operation do not crack further during LOCA, unless the fuel burnup and temperature are high enough for fuel pulverization to occur. Moreover, for ease of modelling, the mm-sized fragments are considered to have the shape of right triangular prisms, where the height and all base side lengths are equal. This approximation is based on the results from ceramographic investigations, see Appendix A. From these results, it also follows that the characteristic side length of the prismatic fragments can be estimated from

$$l_f = D_{FP} \text{Min}(1, \pi/n_f), \quad (10)$$

where D_{FP} is the fuel pellet diameter and n_f is the number of radial cracks intersecting the pellet outer surface at a particular axial cross section. Here, n_f is calculated from the pellet average burnup and the peak LHGR experienced by the fuel during its lifetime through the empirical correlation by Walton and Matheson [19], presented in Appendix A. The characteristic fragment size defined by eq. (10) is plotted for a typical 17×17 pressurized water reactor (PWR) fuel rod with $D_{FP} = 8.26 \text{ mm}$ in Fig. 4.

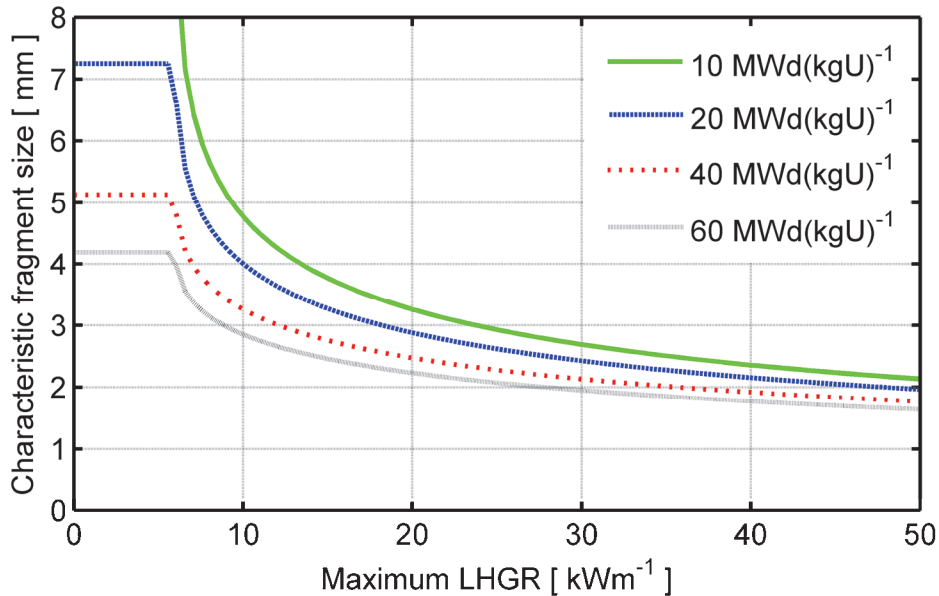


Fig. 4: Characteristic fuel fragment size, l_f , versus fuel burnup (legend) and maximum LHGR experienced by the fuel during its lifetime. Here, l_f is calculated from eq. (10), assuming a fuel pellet diameter of 8.26 mm.

As shown by Fig. 4, the calculated characteristic fragment size is 2–3 mm for typical values of maximum LHGR ($25\text{--}40 \text{ kWm}^{-1}$) experienced by the fuel in commercial power reactors. This fragment size is well in line with those reported from ceramographic investigations; see Appendix A.

2.2.2. Fuel pulverization

The mechanisms responsible for pulverization of high burnup fuel are poorly understood. The prevailing hypothesis is that the pulverization occurs by cracking initiated at overpressurized bubbles and pores that contain gaseous fission products [20-22]. Hence, a critical overpressure in the pores must be reached for pulverization to occur. This means that the material must be sufficiently overheated with regard to its steady-state irradiation temperature. Moreover, the overheating needs to be fairly fast to preclude stress relaxation by creep or re-resolution of gas into the material surrounding the pores. According to a recent review [20-22], experiments show that the average size of the fuel fragments formed by pulverization decreases with increasing heating rate and maximum temperature reached. The hypothesis also implies that cracking can be suppressed by a confining hydrostatic pressure, imposed by pellet-cladding mechanical interaction. This suppression has been experimentally confirmed [20-22].

Appendix A summarizes available studies and data on the pulverization phenomenon. Based on the results of these studies, we make the following empirically based assumptions in our model:

- Fuel pulverization may occur only in those parts of the fuel pellets that have a local burnup above $70 \text{ MWd}(\text{kgU})^{-1}$. This threshold burnup is similar to the local burnup at which a porous high burnup structure (HBS) forms at the pellet periphery, the so called rim zone microstructure [23, 24]. However, in our model, the pulverization is not confined to the re-structured material in the pellet rim.
- Pulverization occurs in the high burnup material only if the local temperature exceeds a critical threshold and the pellet-cladding contact pressure is lower than 50 MPa. The applied temperature threshold is the one recently proposed in [20-22], based on available data. It is shown Fig. 5.
- The fuel fragments formed by pulverization are octahedral in shape and have equal size. This size, l_p , is a model parameter. From the analysis presented in section 2.2.3, l_p is set to 100 μm .

When applying the temperature threshold defined in Fig. 5, the local fuel temperature and burnup is calculated by the host computer program, in our case an extended version of FRAPTRAN-1.5.¹ The amount of pulverized fuel is thus calcu-

¹ The local burnup is in fact calculated in a pre-processing step by the FRAPCON-3.5 program [25], using the TUBRNP micro burnup model [26]. FRAPCON is used for generating burnup dependent initial conditions for transient analyses with FRAPTRAN.

lated by comparing the local state of the fuel with the burnup dependent temperature threshold in Fig. 5. For illustration, we have calculated the volume fraction of material that may pulverize versus the pellet radial average burnup for a typical fuel design and operating history. The calculations, which are thoroughly described in [27], were done for a 15×15 type PWR fuel rod. The results are shown in Fig. 6. The step-like nature of the calculated curves reflects the radial discretization of the fuel pellet used in FRAPCON; the pellet is here divided into 25 annuli.

In conclusion, the calculated results in Fig. 6 show that the volume fraction of fuel that may pulverize start to increase rapidly as the fuel pellet radial average burnup exceeds about 65 MWd(kgU)⁻¹. Above 82 MWd(kgU)⁻¹, the entire pellet may pulverize if transiently overheated, since the local burnup then exceeds 70 MWd(kgU)⁻¹ everywhere. The calculated volume fraction of pulverized fuel presented in Fig. 6 is in fair agreement with unpublished data from out-of-reactor heating tests on high burnup UO₂ fuel that have recently been carried out in Studsvik, Sweden.

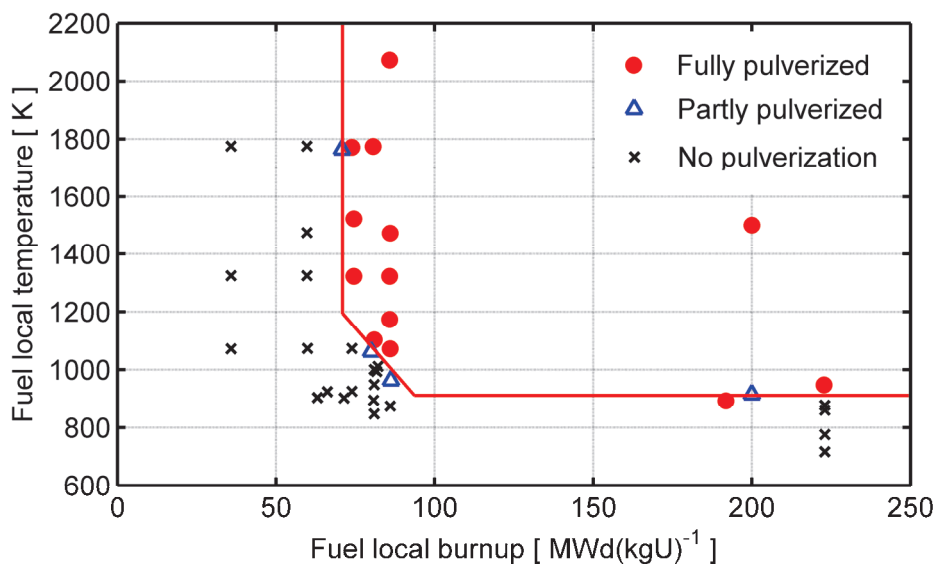


Fig. 5: Temperature threshold for pulverization in comparison with experimental data. The threshold is empirically based [20-22]; see Appendix A. The two breakpoints in terms of fuel local burnup and temperature are (70 MWd(kgU)⁻¹, 1200 K) and (94 MWd(kgU)⁻¹, 910 K).

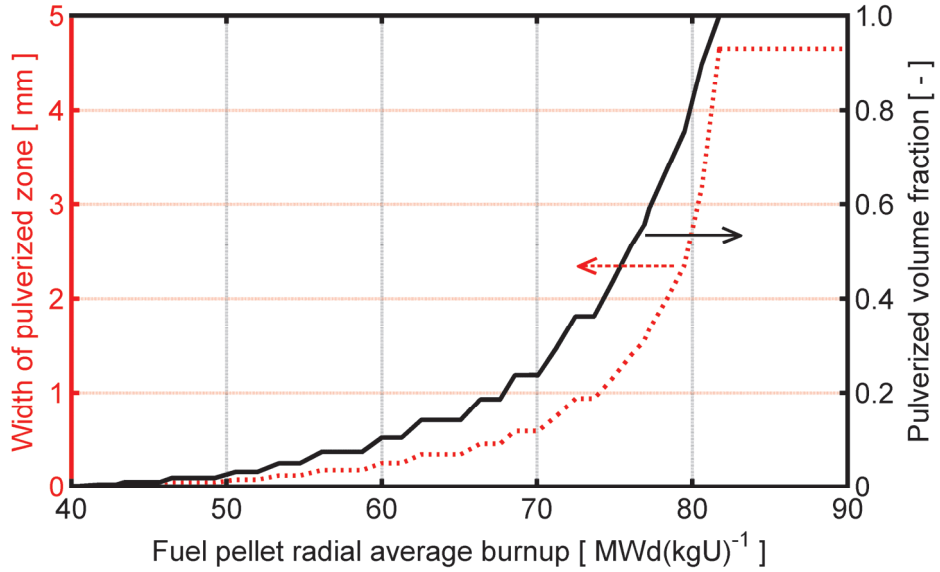


Fig. 6: Calculated width of pulverized zone (i.e. a zone with local burnup > 70 MWd/kgU) and the corresponding volume fraction of pulverized material versus fuel pellet radial average burnup. The calculations pertain to a 15×15 type PWR fuel rod with a pellet diameter of 9.30 mm; see [27] for further details.

2.2.3. Packing fraction of crumbled fuel

The packing fraction, ϕ , of crumbled fuel in ballooned segments of the fuel rod depends on the shape and size distributions of the disorderly stacked fragments; introductions to the subject of particle packing are provided in [28, 29]. For uniformly shaped and sized particles, it is well-established that the packing fraction generally increases with increasing sphericity of the fragments. Sphericity, ψ , is mathematically defined as the ratio of the surface areas between a sphere and a particle of the same volume as the sphere. Hence,

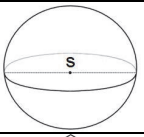
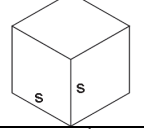
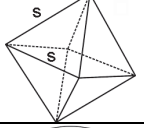
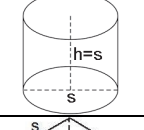
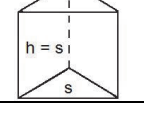
$$\psi = \frac{\pi^{1/3} (6V_p)^{2/3}}{A_p}, \quad (11)$$

where A_p and V_p are the particle surface and volume. By definition, spheres have $\psi = 1$. The sphericity of other basic particle shapes is presented in Table 1.

For monosized particle beds, i.e. for cases where all particles have the same size and shape, the packing fractions for randomly packed beds range from 0.60 to 0.75 for the particles listed in Table 1. Higher packing fractions can be reached if particles with different sizes are mixed, since small particles may fill the voids between large particles. There are no simple theories or models that successfully describe the relationship between a general particle size distribution and packing fraction [30]. However, such models do exist for *binary* mixtures of particles, i.e. mixtures consisting of two types of monosized particles with well defined shapes.

These models are sufficient for our needs, since we consider two types of fuel fragments: prismatic fragments with a typical size of a few millimetres, and octahedral fragments that are a 1–2 orders of magnitude smaller. In the following, we will refer to properties of these two types of fragments by use of subscripts L and S (Large and Small).

Table 1: Sphericity, ψ , and equivalent packing diameter, D_p , for selected idealized particle shapes with volume V_p and area A_p .

Shape and dimension		ψ	D_p	V_p	A_p
Sphere with diameter s		1.000	s	$0.5236s^3$	πs^2
Cube with side s		0.806	$1.147s$	s^3	$6s^2$
Octahedron with side s		0.846	$0.895s$	$0.4714s^3$	$3.4641s^2$
Ideal cylinder, h=s		0.874	$1.069s$	$0.7854s^3$	$4.7124s^2$
Triangular prism, h=s		0.716	$0.910s$	$0.4330s^3$	$3.8660s^2$

A widely used relation for characterizing the packing fraction of binary particle mixtures is due to Westman [31], who considered a mixture of large (L) and small (S) particles with known mass fractions x^L and $x^S = 1 - x^L$, respectively. The packing fractions of mono-component beds of the large and small particles are also assumed to be known and denoted ϕ^L and ϕ^S . The overall packing fraction of the binary mixture, ϕ , can then be estimated from a simple relation

$$a^2 + 2Gab + b^2 = 1, \quad (12)$$

where

$$a = \frac{\phi^S (\phi^L - x^L \phi)}{\phi \phi^L}, \quad (13)$$

$$b = \frac{\phi^S \phi^L - \phi \phi^L (x^S + x^L \phi^S)}{\phi \phi^S (1 - \phi^L)}, \quad (14)$$

and G is a parameter that depends on the differences in particle shape and size between the two components of the mixture. This parameter can be fitted empirically to a specific binary mixture, but some general expressions for estimating G based on the particle characteristics also exist in the literature [32, 33]. Here, we will calculate G from

$$G = \begin{cases} 0.738(D_p^S / D_p^L)^{-1.566}, & D_p^S / D_p^L \leq 0.824 \\ 1, & D_p^S / D_p^L > 0.824 \end{cases}, \quad (15)$$

where D_p^S and D_p^L are the equivalent packing diameters of the small and large particles. The equivalent packing diameter is calculated from the particle volume V_p and sphericity ψ through

$$D_p = \left(3.9431 - \frac{4.5684}{\psi} + \frac{1.8660}{\psi^2} \right) V_p^{1/3}. \quad (16)$$

Equations (15) and (16) have been proposed by Yu et al, based on measurements of packing fractions for a large variety of binary mixtures [32]. Calculated values for the equivalent packing diameter of the various particles are given in Table 1. For our applications, G ranges from about 40 to 150, depending mainly on the relative difference in fragment size between the large and small fragment class.

In order to apply eqs. (11)-(16) to the putative binary mixture of fuel fragments in ballooned parts of the fuel rod, we need to define the packing fractions of mono-component beds of large and small fuel fragments, i.e. the parameters ϕ^L and ϕ^S . For the packing fraction of large fragments, we rely on the measured data presented by Siefken for eight fuel rods tested in the PBF [7]. The investigated rods had burnups up to $16.6 \text{ MWd}(\text{kgU})^{-1}$. Gamma scanning and photomicrography of selected cross sections were used to determine the packing fraction of the collapsed fuel pellet column in ballooned parts of the test rods after LOCA testing. The measured packing fractions ranged from 0.62 to 0.79, with an average value of 0.69. This value is in line with those reported for particles of similar shape in monosized particle beds [29].

The packing fraction of small fragments formed by pulverization of high burnup fuel must be estimated, since measured data are unavailable. From Appendix A, we recall that the fuel pulverization mechanism is reported to produce fragments over a fairly wide size range; observed fragment sizes typically range from 20 to 200 μm . For this reason, it is likely that the fragment packing fraction is higher than obtained for monosized particle beds. Pending reliable data, we assume a packing fraction of 0.72 for the small fragments resulting from pulverization.

Hence, the packing fractions entering eqs. (13) and (14) are $\phi^L = 0.69$ and $\phi^S = 0.72$. The mass fraction of small fuel fragments, x^S , is calculated by applying the fuel pulverization threshold in section 2.2.2, and parameter G is calculated from the size difference between large and small fragments. The typical size of

large fragments is calculated through eq. (10), whereas the size of small fragments from the pulverized part of the fuel pellets is treated as a free parameter.

Fig. 7 shows the calculated fuel fragment packing fraction as a function of the small fragment mass fraction, x^S , in the mixture. All calculations were made for a fixed size of 2.0 mm for the large fragments, whereas five different sizes were assumed for the small fragments. According to the calculations presented in Fig. 7, the binary mixture reaches a maximum packing fraction when the mass fraction of small fragments is between 0.25 and 0.35. The peak value, as well as the location of the peak, depends on the difference in fragment size between the large and small fragment class. For the small fragment class that results from fuel pulverization, we note that very small fragments are able to fill the gaps between the mm-sized fuel pieces more efficiently than larger fragments. A theoretical maximum for ϕ can be calculated by letting the small fragment size tend to zero [29]. This asymptotic maximum is $\phi = \phi^L + \phi^S - \phi^L \phi^S$, or 0.9132 with our choice of ϕ^L and ϕ^S (0.69 and 0.72). From Fig. 7, it is clear that the calculated peak for the case with 25 μm -size fragments is close to this theoretical maximum.

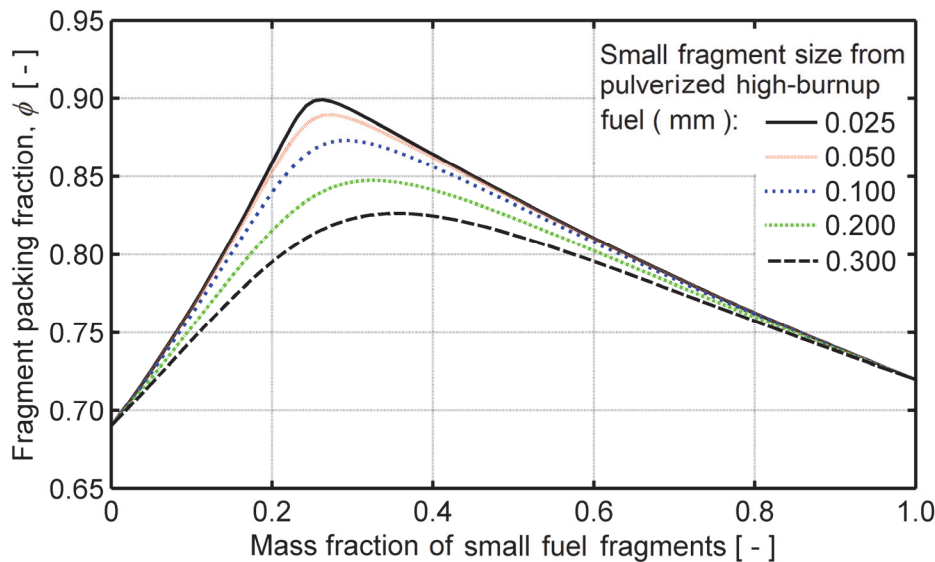


Fig. 7: Fuel fragment packing fraction versus relative amount of small fragments from pulverized high burnup fuel, calculated through eqs. (11)-(16). The large fragment size was assumed to be 2.0 mm throughout the calculations.

It is also clear from Fig. 7 that the calculated packing fraction of the fragment mixture is not so sensitive to the assumed size of the small fragments produced by the pulverization mechanism: The peak packing fraction changes merely from 0.90 to 0.85 as the fragment size is increased from 25 to 200 μm . This fairly moderate change suggests that our relocation model will not be particularly sensitive to the assumed fragment size. Henceforth, we assume that the small fragments produced by pulverization of high burnup fuel are 100 μm in size.

By combining the calculated curve for the 100 μm fragment size in Fig. 7 with eq. (4), we may calculate the cladding threshold strain for collapse of the fuel pellet column into a crumbled state versus the relative amount of small fuel fragments. The results, which are presented in Fig. 8, show that the threshold strain decreases rapidly as the mass fraction of small fragments increases from zero to about 30 %, and then increases again. By combining the results put forth in Fig. 8 with those in Fig. 6, we may conclude that fuel with a pellet radial average burnup of about 72 $\text{MWd}(\text{kgU})^{-1}$, which is estimated to contain about 30 weight percent small fragments, would be particularly sensitive to axial relocation. We note that this happens to be close to the burnup of rodlets 12 and 13 in the Halden IFA-650 series of in-reactor LOCA tests. Post-irradiation examinations give clear evidence of axial fuel relocation in both these BWR fuel rodlets [34].

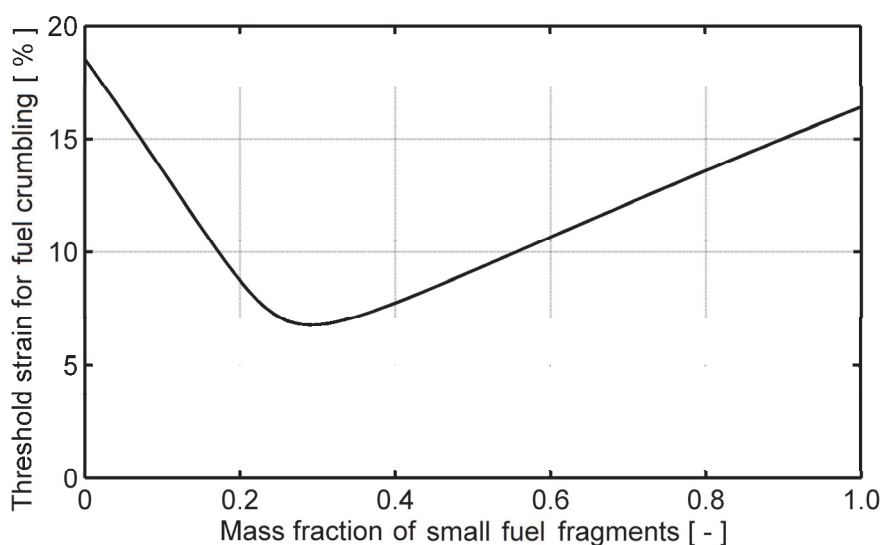


Fig. 8: Cladding hoop logarithmic threshold strain for fuel pellet column collapse and onset of axial fuel relocation versus relative amount of small fuel fragments. Here, the assumed size of large and small fragments in the binary mixture is 2.0 and 0.1 mm, respectively.

It may be interesting to compare the calculated threshold in Fig. 8 with threshold strains for axial relocation reported from experiments: Siefken [7] evaluated eighteen in-reactor LOCA tests done in the PBF reactor, USA, and Forschungsreaktor 2 (FR2), Germany. The evaluated test rods had burnups in the range of 0 to 35 $\text{MWd}(\text{kgU})^{-1}$, which means that small fuel fragments formed by pulverization did not exist [12]. Siefken concluded that no axial relocation of fuel occurred in these rods for cladding hoop strains less than 17 %. This value is in very good agreement with our calculated threshold for a case without small-size fuel fragments. Later, Raynaud [12] reported a threshold cladding strain of 13–17 % for two Halden IFA-650 test rodlets with burnups of 56 and 61 $\text{MWd}(\text{kgU})^{-1}$. From Fig. 6, we expect the mass fraction of small fragments from pulverized fuel to be 0.05–0.10 for this burnup range, and from Fig. 8, we expect the corresponding

threshold strain to be 13–17 %. Hence, the calculated results are in perfect agreement with the observed strain thresholds. Moreover, the calculated trend of a decreasing threshold strain with burnup over this range also agrees with the observations [12].

Finally, it should be remarked that much higher threshold strains for fuel column collapse and axial relocation have been reported from out-of-reactor tests, carried out in the 1980s by the United Kingdom Atomic Energy Authority (UKAEA) on rodlets sampled from irradiated commercial PWR fuel rods [35, 36]. Internally pressurized samples with lengths from 450 to 800 mm were electrically heated to temperatures around 800 °C until the cladding ballooned. In some of the tests, X-ray radiography was used to monitor the deformation of the fuel pellet column in real time during the ballooning. Vibrations or end-loading of the fuel pellet column were applied during some tests to simulate the in-reactor conditions expected during the reflood phase of the LOCA. Unfortunately, detailed information on these tests seems to be unavailable in public libraries and archives, but it is reported that, in general, the fuel pellet column did not collapse axially into the balloon until a cladding hoop strain of about 50 % was reached [36]. For lower strains, the fuel pellet column retained points in contact with the cladding by adopting a spiral configuration. Moreover, neither end-loading nor vibrations significantly affected the behaviour of the fuel pellet column [36].

2.2.4. Threshold for fuel fragment detachment

As described in section 2.1.1, our relocation model makes use of a threshold for the pellet-cladding gap size, g^{th} , which defines the minimum space needed for fuel fragments to detach from their original close-packed configuration and relocate downwards. This threshold gap size must be settled based on results of post-test examinations. To this end, we consider six fuel rods that were subjected to LOCA simulation experiments in Studsvik, Sweden [11]. Following the simulated LOCA transient, bend tests were conducted on the rods to measure the mechanical strength of the ballooned and ruptured region. The two halves of each broken rod were then inverted and gently shaken, in order to dislodge any loose fuel fragments within the cladding tube. The “mobile” part of the fuel column fell out, whereas fuel fragments restricted from moving remained within the fuel cladding. By correlating the position of the emptied part of the fuel column with cladding diameter measurements, Raynaud [12] determined a threshold hoop strain for fuel mobility for each of the six test rods. With a few exceptions, the measured threshold strains were in the range from 3 to 6 %; the average value was 4.5 % [12]. No significant influence of fuel pellet burnup on the threshold strain could be determined; two test rods had a burnup of about 60 MWd(kgU)⁻¹ and an average threshold strain of 5.4 %, the remaining four rods had burnups of about 78 MWd(kgU)⁻¹ and an average threshold strain of 4.1 %.

From the results of these measurements, we set the threshold pellet-cladding gap size for pellet fragment detachment, g^{th} , to 0.2 mm in our model. This gap size corresponds to a cladding hoop strain of about 4.4–4.8 %, depending on the cladding tube dimensions. More experimental data, similar to those discussed above, are needed to determine whether g^{th} depends on fuel burnup or any other parameter. It should be remarked that the results presented above are consistent with observations from post-test investigations of fuel rods in the Halden IFA-650 LOCA test series. From these investigations, it is reported that the local cladding hoop strain must exceed about 5 % to produce visible fuel cracking and to allow fragment separation and movement [34].

2.3. Modifications to thermal calculations

The axial relocation of fuel fragments changes the axial distributions of stored heat and power along the fuel rod. This must be accounted for in calculations of the fuel rod temperature distribution. Moreover, when the fuel pellet column collapses and fuel fragments move radially outward in ballooned segments of the fuel rod, it is no longer justified to calculate the fuel radial temperature distribution based on the usual geometrical assumptions of a solid cylindrical fuel pellet surrounded by an annular gas-filled pellet-cladding gap [17]. When the balloon is filled with crumbled fuel from the collapsed fuel pellet column, the pellet-cladding gap is significantly reduced. At the same time, gas-filled voids open up between the disorderly stacked fuel fragments. As the volume fraction of gas is typically 20–30 %, the macroscopic thermal conductivity of the crumbled fuel in the balloon is much lower than that of solid fuel material. Consequently, the main results of fuel crumbling on the fuel radial temperature distribution are a lower fuel temperature close to the cladding surface (due to a reduced pellet-cladding gap) and a steeper radial temperature gradient (due to a low macroscopic thermal conductivity of the solid-gas mixture). Fuel fragment axial and radial relocation also changes the distribution and temperature of free volume gas within the fuel rod. In particular, some axial segments of the fuel rod may be partly or completely emptied of fuel, which necessitates a modified strategy for calculating the gas temperature in these segments.

The following subsections deal with the modifications made to the thermal calculations in our version of FRAPTRAN-1.5. When introducing these modifications, several bugs and inconsistencies were found in the source code and algorithms used for fuel rod temperature calculations in the original version of FRAPTRAN-1.5 [37]. These errors are corrected in our extended version of FRAPTRAN-1.5, and the general thermo-mechanical solution strategy is modified, such that the fuel rod deformations are fully accounted for in thermal analyses.

2.3.1. Radial heat conduction equation

The fuel temperature calculations are carried out in FRAPTRAN-1.5 by solving the radial heat conduction equation,

$$\rho_f c_{pf} \frac{\partial T}{\partial t} - \frac{1}{r} \frac{\partial}{\partial r} \left(\lambda_f r \frac{\partial T}{\partial r} \right) = q'''(t, r), \quad (17)$$

in each axial segment of the fuel rod individually. Hence, axial symmetry is assumed, and any axial heat conduction in the fuel pellet column is neglected. In eq. (17), T is temperature, r is the radial coordinate, q''' denotes the volumetric heat source, and ρ_f , λ_f and c_{pf} are the density, thermal conductivity and specific heat capacity of the fuel material. The thermal conductivity and specific heat capacity are calculated through correlations, considering the material composition, local fuel temperature and burnup. It is assumed that the fuel material is identical in all axial segments, but an axially varying gadolinia concentration may be modelled, and the existence of a central hole in part of the fuel pellet column can be considered [17]. The volumetric heat source in the right-hand-side of eq. (17) is prescribed as input, and is allowed to differ from one axial segment to another. In FRAPTRAN-1.5, eq. (17) is solved by an implicit time stepping scheme, and a finite difference method is used for the spatial discretization [17, 38].

As explained in section 2.1.1, our model assumes that the fuel pellet stack collapses and the fuel fragments fall radially outward into the balloon when the cladding distension in the considered axial segment is large enough to accommodate the fragments in a disordered configuration, characterized by the packing fraction ϕ . Hence, there is a sudden transition to a new geometrical configuration. When this transition occurs in an axial segment, eq. (17) is modified such that it henceforth represents an *effective* continuum material that consists of fuel fragments surrounded by stagnant gas. The term *effective* is used to communicate the concept that the material is assumed to be homogeneous on a macroscopic scale. This means that eq. (17) can still be applied, but the material properties must be modified. The following changes are made to eq. (17) when the fuel pellet column collapses:

- The radial positions of the nodes used for solving eq. (17) by the finite difference technique are scaled, such that the collapsed pellet surface comes into partial contact with the cladding inner surface. In other words, the pellet-cladding gap is nearly closed; only a small residual gap, g' , remains, as illustrated in Fig. 9. The residual gap, which is a model parameter, accounts for the fact that the crumbled fuel is only in point wise contact with the cladding surface. Once the fuel pellet column has collapsed, the radial positions of the pellet nodes are continuously updated, such that the pellet-cladding radial gap is maintained at g' as the cladding distends further. It should be remarked that Fig. 9 illustrates the instant of transition from a pellet-like configuration to a

porous bed; the radial temperature distribution will subsequently change as a result of the modified fuel geometry and thermal conductivity.

- The fuel effective density is changed from ρ_f to $\phi\rho_f$, to reflect the transition from densely packed and ordered fuel fragments to a porous bed of fragments. Likewise, the volumetric heat source is changed from q''' to $\phi q'''$, since it is proportional to the fuel density.
- The fuel thermal conductivity is changed from λ_f to λ_{eff} , which is an effective thermal conductivity for the crumbled fuel. The effective thermal conductivity applied in our model depends on the thermal conductivities of the fuel fragments and the surrounding gas, and on the packing fraction of the fuel fragments. The model used for λ_{eff} is described and validated against experimental data in Appendix B.

The modified heat conduction equation thus reads

$$\phi\rho_f c_{pf} \frac{\partial T}{\partial t} - \frac{1}{\tilde{r}} \frac{\partial}{\partial \tilde{r}} \left(\lambda_{eff} \tilde{r} \frac{\partial T}{\partial \tilde{r}} \right) = \phi q'''(t, \tilde{r}) . \quad (18)$$

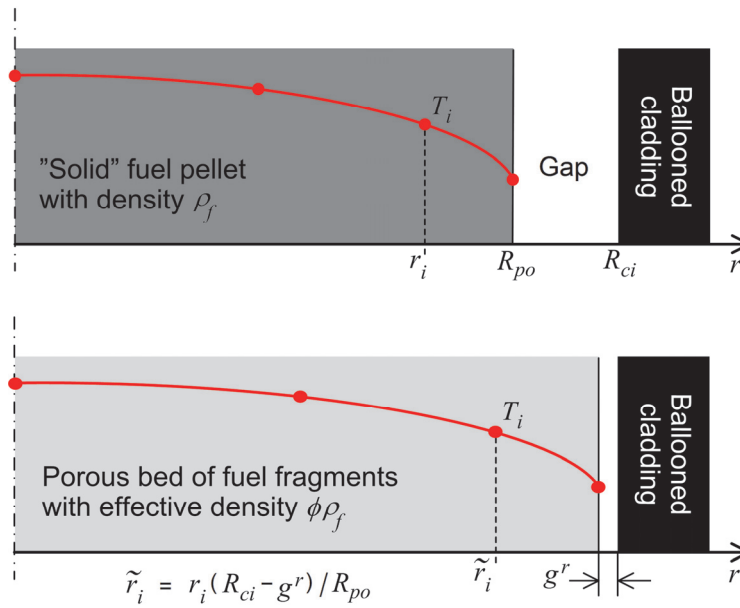


Fig. 9: Assumed change of fuel geometry and effective fuel density following collapse of the fuel pellet column into a ballooned part of the cladding tube. Node positions in the fuel are scaled, such that only a residual pellet-cladding gap, g^r , remains after fuel crumbling.

It can be easily shown that the fuel mass and radial average enthalpy within the considered axial segment are unaffected by the modifications listed above at the very moment of transition. After the transition, however, the fuel mass within the segment may change by axial relocation, and the radial average enthalpy may change as a result of the modified radial temperature distribution. It should be remarked that eq. (18) is used also in axial segments that are fully or partly emptied of fuel ($x^r < \phi < 1$). However, λ_f and the original radial positions of the pellet

nodes are maintained in axial segments where the fuel pellet column has not collapsed.

2.3.2. Heat transfer by axial fuel relocation

Our model for axial fuel relocation in section 2.1.2 solves the conservation equations for fuel mass, but it does not solve the conservation equation for energy with regard to the axial direction. This simplification could have some impact on the calculated fuel temperatures, in case large axial gradients in fuel temperature exist along the part of the rod where fuel relocation occurs. To illustrate this issue, we consider the enthalpy per unit length of the fuel column, henceforth denoted H' . The conservation equation for this property can be written as

$$\frac{\partial H'}{\partial t} + \frac{\partial}{\partial z} (H' u_z) = q' - 2\pi R_{ci} h_{gap} \Delta T_{gap}, \quad (19)$$

where u_z is the axial velocity of the relocating fuel fragments, q' is the fuel linear heat generation rate, h_{gap} is the pellet-cladding gap heat transfer coefficient and ΔT_{gap} is the temperature drop across the gap. Consider now the k :th axial segment of the fuel rod, which extends from $z = z_1$ to $z = z_2$. The rate of change for the average fuel enthalpy, H_k , within this segment is obtained by integration of eq. (19) over z

$$\frac{dH_k}{dt} + H'(z_2)u_z(z_2) - H'(z_1)u_z(z_1) = L_k (q' - 2\pi R_{cik} h_{gap} \Delta T_{gap}), \quad (20)$$

where $L_k = z_2 - z_1$ is the length of the axial segment. The axial velocity of the fuel at the upper and lower boundaries of the segment, $u_z(z_2)$ and $u_z(z_1)$, can be obtained from the axial relocation algorithm in section 2.1.2, but the fuel enthalpy per unit length at these positions is not calculated. For this reason, we introduce the approximation $H'(z_1) \approx H'(z_2) \approx H'_k$ in eq. (20), which results in

$$\frac{dH_k}{dt} + H'_k (u_z(z_2) - u_z(z_1)) \approx L_k (q' - 2\pi R_{cik} h_{gap} \Delta T_{gap}). \quad (21)$$

This equation is solved by our modified heat transfer model in FRAPTRAN. It accounts for changes in total fuel enthalpy in the k :th axial segment by accumulation, $u_z(z_2) < u_z(z_1)$, or loss, $u_z(z_2) > u_z(z_1)$, of fuel fragments. However, it neglects that fuel fragments falling down into the considered segment may have different temperature and specific enthalpy than fragments already in the segment and/or fragments exiting the segment at the bottom.² Consequently, the approximation is justified as long as the axial fuel relocation occurs between segments with about the same fuel temperature and specific enthalpy. Cases with steep axial temperature gradients along those parts of the fuel rod that are affected by fuel relocation will be poorly reproduced by the model.

² Compare with the complete conservation equation for enthalpy in eq. (20), from which it is clear that H_k will change also when $u_z(z_2) = u_z(z_1)$, if $H'(z_2) \neq H'(z_1)$.

Also axial gradients for other properties than fuel temperature are neglected when axial fuel relocation is calculated by the model. For example, in our model, the radial distributions of burnup, power and fission products in an axial segment are not changed, even though the segment may receive fuel from higher elevations with different burnup and different radial distributions of power and fission products. Likewise, the fuel fragment size distribution in the segment is not changed as a result of incoming fragments from higher elevations. To take these effects into account by solving the axial conservation equations for a number of properties in combination with the radial heat conduction equation is clearly beyond the scope of FRAPTRAN. Models of this kind would also be very difficult to verify experimentally, since it is currently unclear whether the fuel pellet rim, with its particularly high burnup, fission product content and decay power, is more prone to relocate axially than the inner part of the fuel pellet. It has been speculated that this is the case in high burnup fuel, when the rim is pulverized. Gamma scanning of fuel fragments accumulated in ballooned regions of high burnup fuel rods has been used in order to confirm this hypothesis [39], but these investigations showed no evidence that the relocated fuel originated predominantly from the pellet rim. However, it should be remarked that the resolution in the gamma scan data was low, and the investigators stated that higher resolution data are needed to draw firm conclusions as to the original radial position of the relocated fuel [39].

2.3.3. Void volume gas temperature calculation

The collapse of the fuel pellet column into the balloon involves a practically instantaneous outward movement of fuel fragments, concurrent with an inward movement of the gas within the pellet-cladding gap; see Fig. 9. This redistribution of gap gas and its consequences for the gas temperature and fuel rod internal gas pressure are accounted for in our model. In FRAPTRAN, it is assumed that the gap gas temperature in a particular axial segment is the average of the pellet outer surface and cladding inner surface temperature. Here, we assume that gas moving into voids between fuel fragments after collapse of the fuel pellet column attains the radial average fuel temperature; this is consistent with the way FRAPTRAN treats the gas accumulated in pellet cracks [17]. In axial segments where the fuel pellet column has not collapsed, we assume that the entire gas volume is at the gap gas temperature, i.e. at the average temperature of the gap boundaries within the segment. The gas volume within the k :th axial segment, V_k^g , is calculated from

$$V_k^g = (1 - \phi_k)V_k = (1 - \phi_k)\pi L_k R_{cik}^2, \quad (22)$$

in consistency with eq. (1).

3. Verification of the relocation model

In the following, the numerical implementation of the computational algorithm for axial fuel relocation in section 2.1.2 is verified by applying the relocation model to two test cases with simple boundary conditions. More precisely, two hypothetical axial profiles for the cladding deformation are prescribed along a full-length fuel rod, and the resulting fuel relocation is calculated as a function of time as the cladding distension is postulated to gradually increase. The relocation model is tested outside the FRAPTRAN program, which means that thermal feedback effects from the relocation are not considered.

In both test cases considered below, the active length of the fuel rod is assumed to be 3.60 m, and the fuel pellet diameter is 9.0 mm. Moreover, the pellet-cladding gap is assumed to be closed at beginning of the tests, and the fuel is in a state such that a fragment packing fraction of 0.75 is reached after fuel crumbling in ballooned regions. For simplicity, this packing fraction is presumed to be independent of space and time. In all calculations, the fuel rod is discretized into 36 equal-length axial segments along the active length of the fuel rod.

3.1. Test case 1: Single balloon

In the first test case, we consider a fairly uniform cladding deformation, defined by a sine-shaped balloon with its peak at the fuel rod mid-plane ($z=1.8$ m). The prescribed cladding deformation is defined by

$$R_{ci}(t, z) = 4.5 \times 10^{-3} + 2.0 \times 10^{-5} t \sin(\pi z / L_a), \quad (23)$$

where R_{ci} is the inner radius of the cladding and z/L_a is the relative position along the active length (L_a) of the fuel rod. The time t is in units of seconds.

The cladding deformation (evolution of R_{ci}) is shown by the solid black line in Fig. 10. The dotted red line in the same figure refers to the calculated fuel pellet radius. From the dotted red line, it is easily seen where the cladding deformation is large enough for collapse of the fuel pellet column to occur. With reference to eq. (2) in section 2.1.1, the dotted red line thus defines in which axial segments, k , the condition for fuel crumbling is satisfied.

Fig. 11 presents the calculated axial relocation of fuel fragments. The plot shows the calculated fuel mass fraction in each of the 36 axial segments along the fuel rod; the mass fraction is defined as m_k / m_k^i , i.e. the current fuel mass in the segment divided by the initial, as-fabricated mass. At $t = 36$ s, fuel starts to accumulate in the most distended part of the rod, while fuel is lost from a region about 0.4 m below the top of the pellet column. Above this region, the pellet-cladding gap is

< 0.2 mm, and thus not large enough for fuel fragments to detach from their original position; see section 2.2.4. As the cladding distension increases, the emptied region of the cladding grows, and so does the region where relocated fuel fragments accumulate in a disordered pattern. Up to about $t = 70$ s, there exists an intermediate region, where fuel moves downward without causing any net change of the local fuel mass; the fuel just slides down through this region in its original pellet-like configuration. At $t = 100$ s, the entire upper part of the fuel rod has been emptied of fuel, except for the uppermost axial segment.

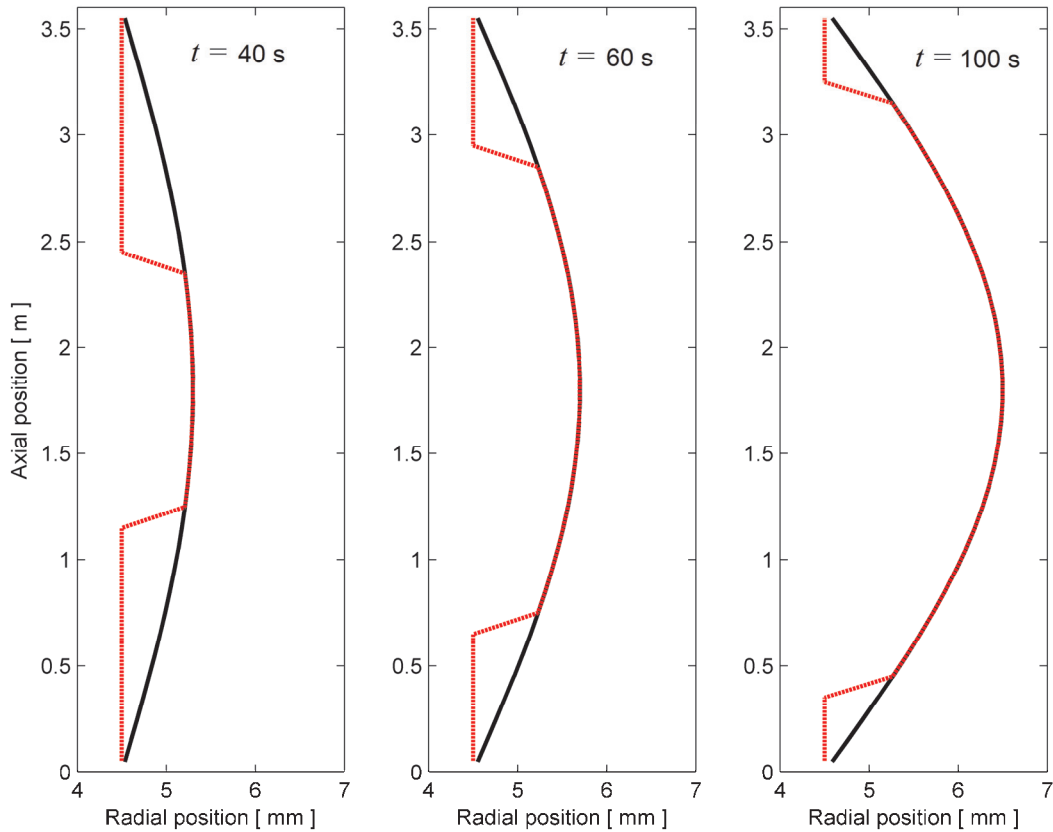


Fig. 10: Deformation pattern for test case 1. Solid black line: Cladding inner radius, as defined by eq. (23). Dotted red line: Calculated fuel pellet radius, indicating the region where crumbling of the fuel pellet column may occur.

It is clear from Fig. 10 and Fig. 11 that a fairly large cladding distension is needed to obtain an appreciable change in local fuel mass. This is illustrated in Fig. 12, which shows the calculated relationship between fuel relative mass change and cladding hoop logarithmic strain at the fuel rod mid-plane position. For the considered case of an initially closed pellet-cladding gap and an assumed fuel fragment packing fraction of 0.75 after crumbling of the fuel pellet column, the local fuel mass starts to increase when the cladding hoop strain reaches about 14 %. This result is consistent with the calculated threshold strain for relocation, presented in Fig. 1, section 2.1.1. We note that a hoop strain of about 35 % will increase the local fuel mass by about 50 % in the considered case.

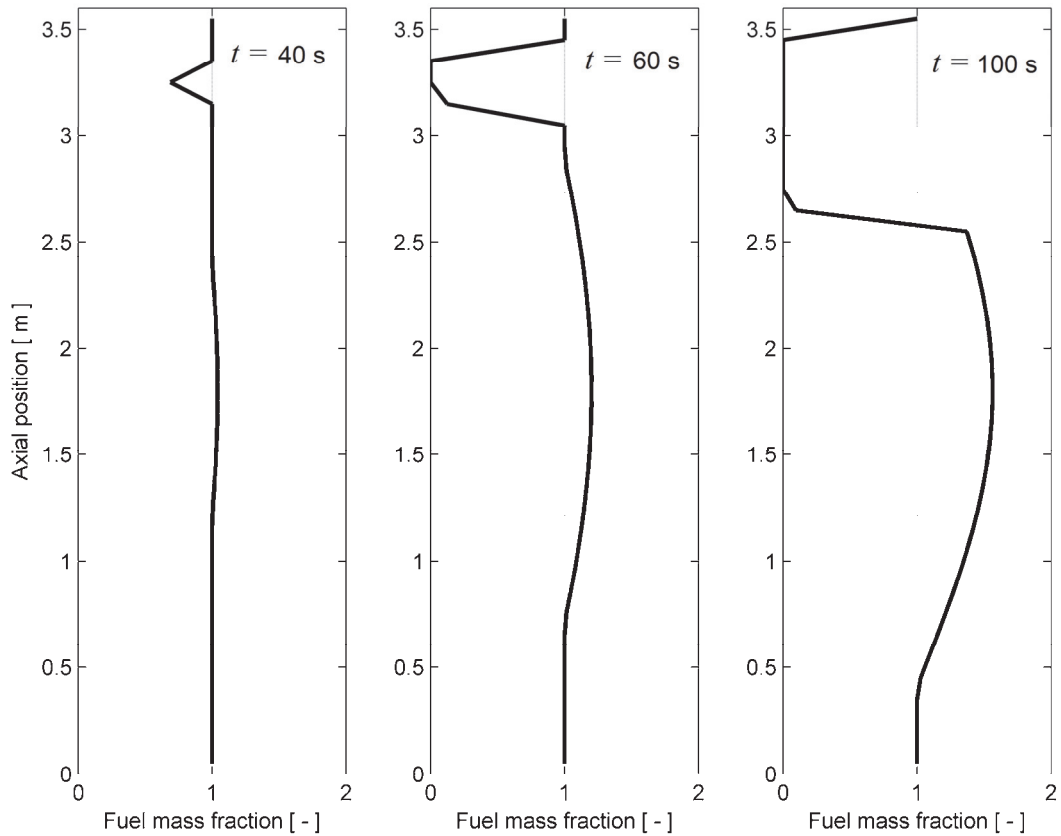


Fig. 11: Calculated space-time variation in fuel mass fraction (local ratio of current fuel mass to initial mass) for test case 1.

A simple relationship between the relative change in local fuel mass, $\Delta m/m^i$, and the cladding hoop logarithmic strain can be derived for any assumed packing fraction of the fuel fragments. In a general case with solid, cylindrical fuel pellets, the relative change in local fuel mass after the fuel pellet column has collapsed and become crumbled is

$$\Delta m/m^i = \phi \left(R_{ci}(t)/R_p \right)^2 - 1, \quad (24)$$

where R_p is the pellet radius (before fuel crumbling). This relation follows from eq. (3). Assuming that the pellet-cladding gap is closed at start of the LOCA, here defined by time $t = 0$, we may use the identity $R_p = R_{ci}(t=0)$ in eq. (24). Hence,

$$\Delta m/m^i = \phi \left(R_{ci}(t)/R_{ci}(0) \right)^2 - 1 = \phi \exp(2\varepsilon_{\theta\theta}(t)) - 1, \quad (25)$$

where the right hand side follows directly from the definition of cladding hoop logarithmic strain. Equation (25) is a useful relationship, from which the relative change in local fuel mass and linear heat generation rate can be calculated from the extent of cladding ballooning for any assumed packing fraction.

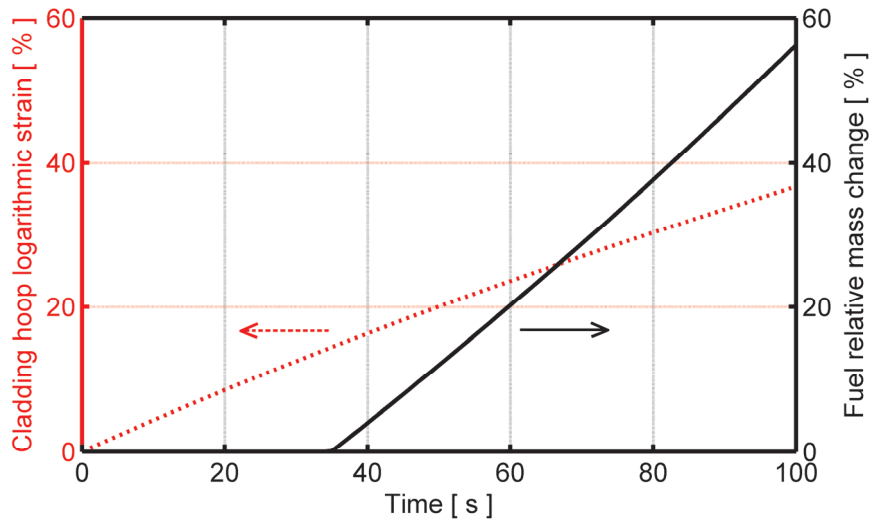


Fig. 12: Calculated relative change in local fuel mass versus local hoop cladding strain of the cladding. Fuel rod mid-plane position, test case 1.

3.2. Test case 2: Twin balloons

The cladding deformation considered for test case 1 in section 3.1 is hypothetical, and deemed unrealistic for fuel rods experiencing loss-of-coolant accidents in light water reactors. Results from a LOCA simulation program in the early 1980s, where assemblies of full-length PWR fuel rods were tested in the Canadian NRU reactor [40], show that cladding ballooning is significantly restrained at spacer grid positions. It is therefore believed that spacer grids will act as choke points for axial fuel relocation during a LOCA, and experiments are planned in the Halden test reactor to elucidate this issue [34].

To verify that our model is capable of handling more realistic deformation patterns, we now consider a case where the cladding deformation is restrained at the fuel rod mid-plane ($z = 1.8$ m). The deformation pattern, which is shown in Fig. 13, is obtained by prescribing the cladding inner radius through

$$R_{ci}(t, z) = 4.5 \times 10^{-3} + 2.0 \times 10^{-5} t \left| \sin(2\pi z / L_d) \right|. \quad (26)$$

Fig. 14 shows the calculated axial relocation of fuel fragments that results from the postulated cladding deformation. The relocation behaviour is similar to that in test case 1, but it occurs independently and concurrently in the upper and lower halves of the fuel rod. The two parts are separated by a plug of immobile fuel fragments at the fuel rod mid-plane, where the cladding deformation is insufficient for the fuel fragments to detach from their original position. This plug thus blocks any relocation of fuel fragments from the upper to the lower balloon. This kind of constraint is expected at spacer grids.

It should be remarked that FRAPTRAN, in general, does not account for thermo-mechanical effects of spacer grids. However, with some modifications to the program, thermal and mechanical effects of spacer grids on the fuel rod could be accounted for by prescribing certain properties and/or boundary conditions for those axial segments of the rod that coincide with the spacer grid positions.

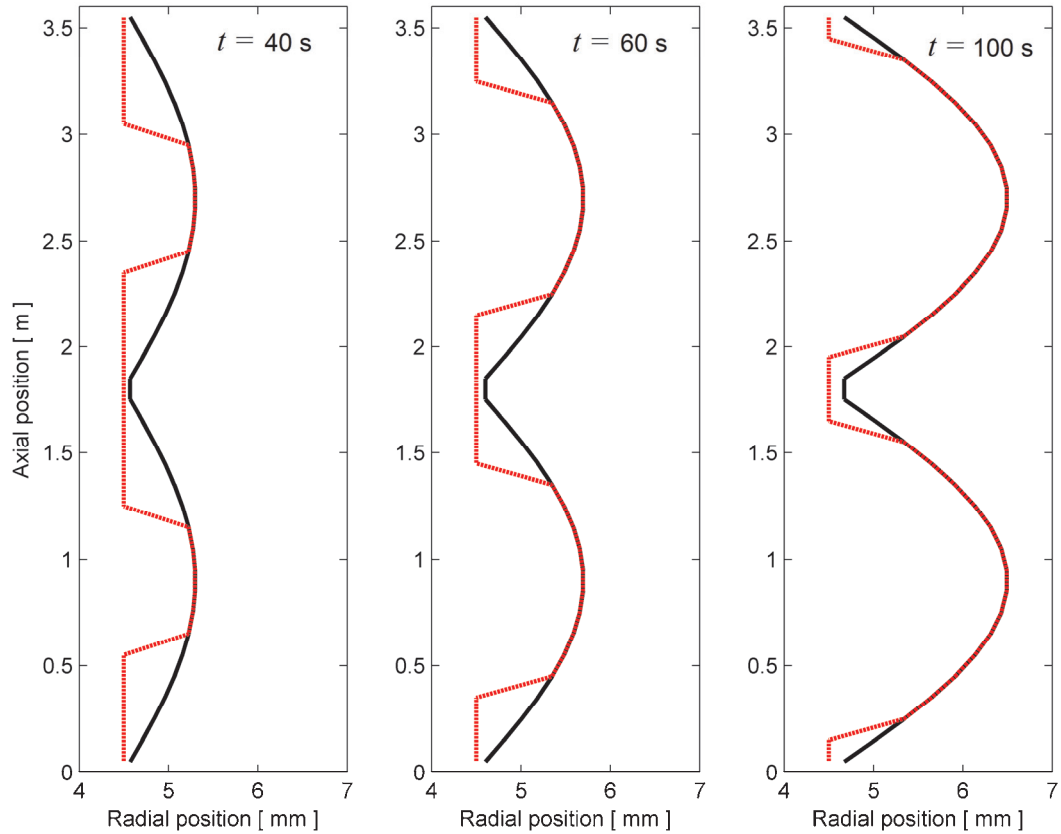


Fig. 13: Deformation pattern for test case 2. Solid black line: Cladding inner radius, as defined by eq. (26). Dotted red line: Calculated fuel pellet radius, indicating the regions where crumbling of the fuel pellet column may occur.

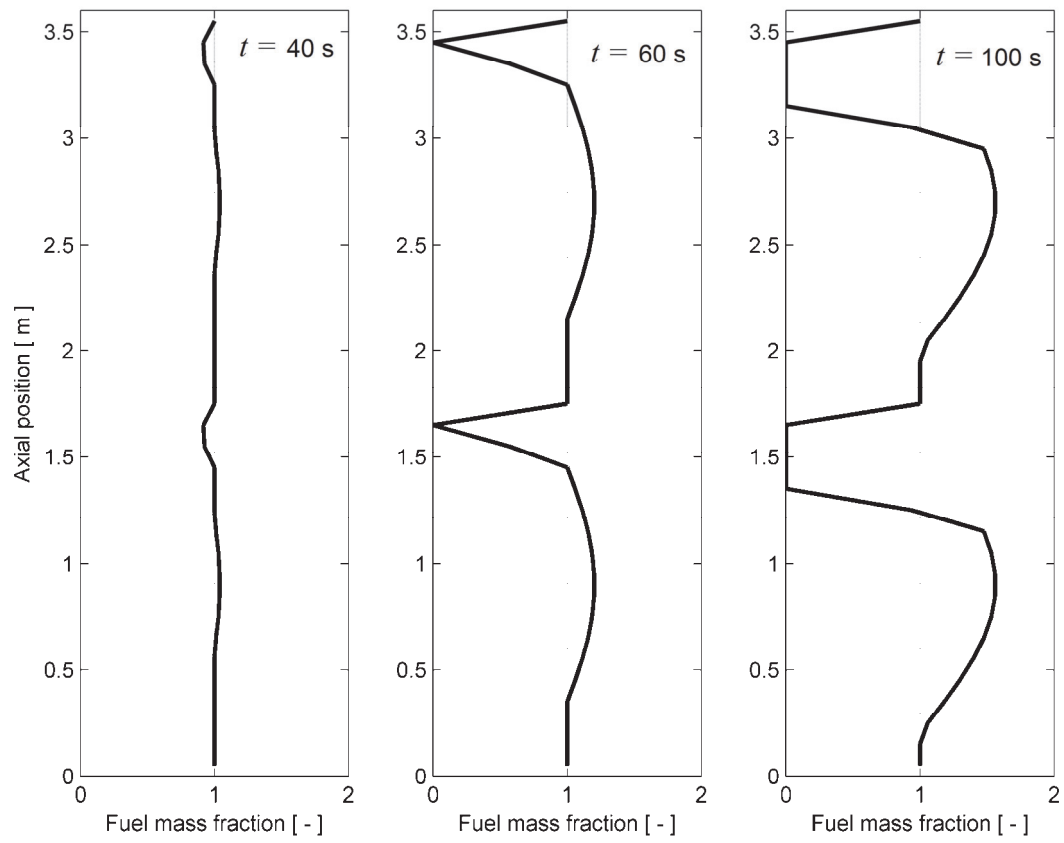


Fig. 14: Calculated space-time variation in fuel mass fraction (local ratio of current fuel mass to initial mass) for test case 2.

4. Assessment of Halden LOCA test IFA-650.4

In this section, we simulate the Halden IFA-650.4 LOCA test with our extended version of FRAPTRAN-1.5. The aim is to validate the new models introduced in the program. The test is simulated twice, with and without consideration of axial fuel relocation, in order to assess the importance of the relocation to the thermo-mechanical behaviour and high temperature degradation of the tested fuel rod.

The fourth test in the Halden IFA-650 LOCA test series was conducted in April 2006, using a test rodlet with an average fuel burnup of $92.3 \text{ MWd}(\text{kgU})^{-1}$ that had been sampled from a PWR fuel rod after seven operating cycles in a commercial power reactor. The test, which is described in Appendix C, resulted in cladding ballooning and burst, as well as significant axial fuel relocation and dispersal of pulverized fuel into the coolant. The fact that this happened at a cladding temperature more than 400 K below the allowable peak temperature postulated in existing acceptance criteria for LOCA caused concern about the applicability of these criteria to high burnup fuel [13].

Over the years, the IFA-650.4 test has been analysed with a number of computer programs and models to better understand the mechanisms behind the unexpectedly large fuel dispersal observed in the test [14-16, 41-44]. Fuel pulverization and axial relocation of the fine fragments have been identified as important mechanisms that ease the fuel dispersal. It should be remarked that the IFA-650.4 LOCA test has been evaluated by Quantum Technologies in the past [43, 44]. These evaluations did not address fuel pulverization or axial relocation. They also differed from the assessment presented here with regard to applied methodology and computer programs, as clarified in section 4.1 below.

4.1. Methodology, computer programs and assumptions

The computer analyses of the IFA-650.4 LOCA test were carried out in two steps. In the first step, the pre-irradiation of the fuel rod segment that was later re-fabricated into the IFA-650.4 test rodlet was modelled by use of FRAPCON-3.5. More precisely, the pre-irradiation in the Gösigen nuclear power plant was modelled with the standard version of the program [25], as delivered by Pacific Northwest National Laboratory (PNNL), without introducing any modifications or extensions to the program. The procedure is described in section 4.1.1 below.

Calculated results from FRAPCON-3.5, defining the pre-test conditions for the test fuel rodlet, were used as input to the second analysis step. This step involved simulations of the IFA-650.4 LOCA test with our extended version of FRAPTRAN-1.5. In addition to the models for fuel fragmentation, pulverization and

axial relocation described in this report, this version of FRAPTRAN-1.5 also includes a set of models that treat cladding high temperature metal-water reactions, solid-solid phase transformation, creep and failure in a unified fashion [45, 46]. As already mentioned, a number of errors were discovered in the course of work and corrected [37]. The applied version is thus very different from the standard version of FRAPTRAN-1.5 delivered by PNNL [17]. Both FRAPCON and FRAPTRAN are best-estimate computational tools, and the presented analyses should be considered as best-estimate; no uncertainty or sensitivity analyses were carried out. However, the analysis of the LOCA test was done twice: with and without the fuel relocation model. Except for this difference, the two calculations were done with identical models and input data.

It should be remarked that no computer program was used for calculating the transient thermo-hydraulic boundary conditions that are needed for fuel rod analyses with FRAPTRAN. These boundary conditions were derived from measured temperatures and pressures in the IFA-650.4 test rig; the applied methodology and assumptions are described in section 4.1.2.

4.1.1. Simulation of pre-irradiation

The pre-irradiation of the 480 mm long fuel rod segment that was later re-fabricated into the IFA-650.4 test rodlet was simulated by use of the standard version of FRAPCON-3.5 [25]. Input for the simulations, in terms of rod design data and operation history in the Gösgen PWR, are given in section C.2, Appendix C. For simplicity, the power history was modelled as consisting of seven equally long reactor cycles, where the fuel rod LHGR was held constant over each cycle. Nominal core average thermo-hydraulic conditions for the Gösgen PWR was used in the simulations, but the coolant inlet temperature was increased to 574.8 K to represent the local conditions at the fifth span of the full length mother fuel rod.

Twenty four equal-length axial segments (nodes) were used to discretize the 480 mm long sample for the fuel rodlet. Recommended default models and options for FRAPCON-3.5 were used in the calculations. In particular, the thin-shell mechanical model was used for the cladding tube, rather than the finite element based model. The Duplex-type cladding material of the rodlet was represented by models for M5® cladding, which are available in FRAPCON-3.5 [25]. These models were selected, since the M5® alloy has similar performance with regard to water-side corrosion as the Zr-2.6wt%Nb surface liner in the Duplex cladding.

4.1.2. Simulation of LOCA test

The IFA-650.4 LOCA test was simulated with our extended version of FRAPTRAN-1.5, using previously developed high temperature models for the cladding tube [45] in combination with a slightly modified version of the finite element

based mechanical solution module [47]. All calculations were done with an axial discretization consisting of 24 equal-length segments for the active part of the test rodlet. The radial discretization comprised 44 annuli in the fuel pellet and one element across the cladding thickness. A constant time step length of 10 ms was used, and the simulation covered the first 500 seconds of the LOCA test. An average LHGR of 0.95 kWm^{-1} was prescribed for the rodlet and held constant during the simulated part of the LOCA test. The axial power profile used throughout the simulation is shown in Fig. 37, Appendix C.

The test rodlet was filled with a low-conductivity gas mixture, consisting of 95 vol% argon and 5 vol% helium; see section C.2, Appendix C. This gas mixture was postulated for the calculations with FRAPTRAN. The fill gas pressure at room temperature was reported to be 4.0 MPa. We used a slightly lower cold pressure of 3.86 MPa in our calculations, in order to match the calculated “hot” pre-test pressure to the measured value of 6.95 MPa. Transient fission gas release from the high burnup fuel was not considered in the calculations, and possible restrictions of rod internal gas flow during the test were neglected. Hence, the internal gas was assumed to have uniform pressure and composition along the rod and in the plenum volume. Since transient fission gas release was not modelled, the gas composition remained unchanged until cladding rupture was calculated to occur. By default in FRAPTRAN-1.5, steam is assumed to replace the initial fill gas from the time of cladding rupture [17].

Other pre-test conditions of the IFA-650.4 rodlet were defined by the end-of-life fuel rod conditions after operation in Gösgen, as calculated with FRAPCON-3.5. Calculated results for the permanent deformations of fuel and cladding, cladding oxide layer thickness and hydrogen content, as well as the radial distributions of fuel burnup and power, were imported to FRAPTRAN input from FRAPCON output. Most of these data are presented and discussed in section 4.2.1.

The first 500 seconds of the IFA-650.4 LOCA test were simulated with our extended version of FRAPTRAN-1.5. The fuel and heater power was held constant during this period, and no water was sprayed into the test rig. Consequently, it is fairly easy to define the thermo-hydraulic boundary conditions for the fuel rod during this period. The later part of the test was not simulated, since the test rig conditions were then made more complex by water spraying, reduced heater power and reactor scram; see section C.3, Appendix C.

The time dependent thermo-hydraulic boundary conditions required by FRAPTRAN for calculating the fuel rod behaviour during the considered part of the LOCA test were derived from temperatures and pressures measured in different parts of the test rig. The source of data for each required input parameter is defined in Table 2, and time histories for some of the parameters are plotted in Fig. 15. The coolant conditions were assumed to be uniform in the calculations, i.e. any spatial variations in the coolant properties listed in Table 2 were neglected.

Table 2: Time dependent input parameters defining the thermo-hydraulic boundary conditions for FRAPTRAN. Time histories for all parameters were derived from measured data, as indicated below. See also section C.3, Appendix C.

Input parameter	Utilized source of measured data
Coolant pressure	Measured loop pressures at rig inlet and outlet (average value)
Coolant temperature	Measured heater temperature at upper part of the test rig (TCH2)
Clad-to-coolant heat transfer coefficient	Estimated from measured temperature difference between cladding and heater (TCC1 – TCH2) and fuel rod linear heat generation rate
Plenum gas temperature	Measured cladding surface temperature at gas plenum position (TCC3)

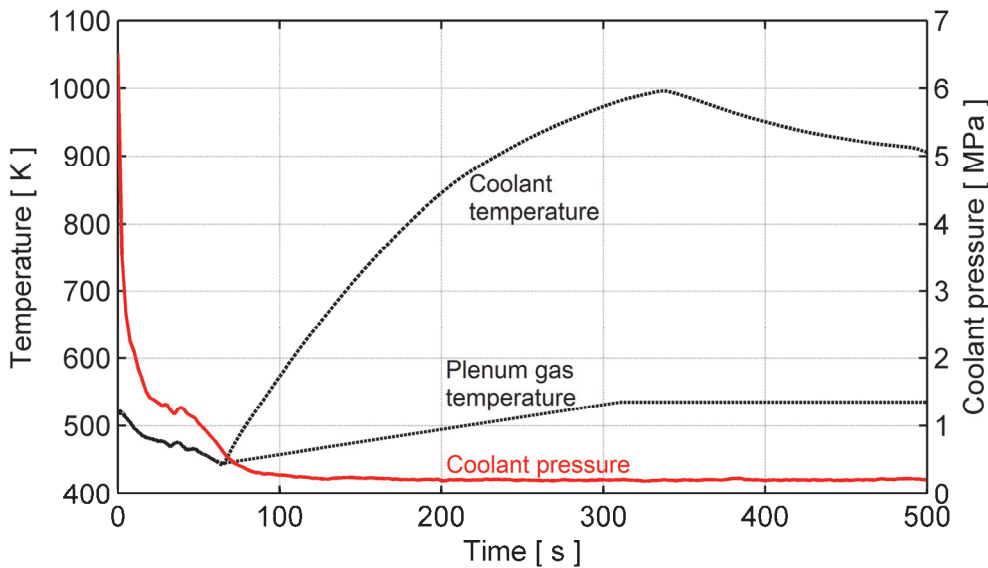


Fig. 15: Time dependent boundary conditions applied in simulations of the first 500 seconds of the IFA-650.4 LOCA test with FRAPTRAN.

The electrical heater could not be explicitly modelled in FRAPTRAN. Instead, the measured heater temperature was used for defining the coolant bulk temperature, and an equivalent clad-to-coolant heat transfer coefficient was derived from the known linear heat generation rate for the test rodlet and the measured temperature difference between the cladding and heater surfaces (thermocouples TCC1 and TCH2). This temperature difference was typically 50–70 K and surprisingly steady during the heat-up and high temperature phases of the test. In light of the constant rod power during the test, this consistency suggests that the heat transfer coefficient did not change much over time. By use of an iterative procedure, it was found that the following expression for the clad-to-coolant heat transfer coef-

ficient, h_{cc} , resulted in a good match between calculated and measured cladding temperatures

$$h_{cc}(t) = \text{Max} \left(200, 4\sigma T_{sh}^3(t) \right). \quad (27)$$

Here, h_{cc} is in units of $\text{W}(\text{m}^2\text{K})^{-1}$, σ is the Stefan-Boltzmann constant, and T_{sh} is the measured surface temperature of the electrical heater. Equation (27) implies that radiation dominates the heat transfer when $T_{sh} > 960$ K; the formula is an approximate form of Stefan-Boltzmann's law for a perfect blackbody, whose temperature is close to that of the surroundings [48]. At lower temperature, the heat transfer coefficient is nearly constant and relates to conduction and convection in overheated steam.

None of the temperature dependent criteria for cladding high temperature rupture that are available in our version of FRAPTRAN-1.5 [45] worked well for the IFA-650.4 test, since the calculations resulted in contact between the distending cladding tube and the surrounding heater before rupture occurred. Once in contact, the heater acted as a die, forcing the cladding balloon to grow in the axial direction until it finally ruptured. For this reason, we postulated a threshold for the effective creep strain, at which the cladding was assumed to fail. The threshold effective strain (logarithmic) was set to 0.75, since this value resulted in cladding failure just before the cladding came into contact with the surrounding heater; see Fig. 19. In addition, we scaled the cladding creep rate in FRAPTRAN, with the aim to match the calculated and measured time to cladding rupture. A scale factor of 0.4 was found to give a good match when fuel relocation was considered in the calculations. To allow meaningful comparisons of the calculated cases with and without fuel relocation, this scale factor was used in all calculations. Except for the scaled creep rate and the ad-hoc rupture criterion, models in our extended version of FRAPTRAN-1.5 were not modified or tuned. The model parameters used in our relocation model were those defined in section 2; $l_p = 0.10$ mm, $g^{th} = 0.20$ mm, $g^r = 5.0$ μm , $x^r = 0.01$, $\phi^L = 0.69$, and $\phi^S = 0.72$.

4.2. Calculated results

4.2.1. Pre-irradiation

Key results of the simulated pre-irradiation of the IFA-650.4 test rodlet in the Gösgen nuclear power plant with the FRAPCON-3.5 computer program are summarized in Table 1. Measured data are included for comparison, when available. The calculated cladding corrosion (hydrogen pickup and oxide layer thickness) is in fair agreement with measurements. We recall from section 4.1.1 that the non-standard Duplex-type cladding material of the rodlet was represented by models for M5@ in our calculations with FRAPCON-3.5 [25], in order to reproduce the corrosion performance. The calculated pre-test cladding corrosion corresponds to

consumption of 1.5–1.7 % of the cladding wall thickness. Hence, the calculated pre-test ECR (equivalent cladding reacted³) was about 1.6 %.

Table 3: Pre-test conditions of the IFA-650.4 test rodlet, calculated with the FRAPCON-3.5 computer program.

Parameter		Calculated	Measured
Rodlet average burnup	[MWd(kgU) ⁻¹]	92.2	92.3
Pellet radial average burnup	[MWd(kgU) ⁻¹]	92.2	-
Pellet centre burnup	[MWd(kgU) ⁻¹]	78.1	-
Pellet surface burnup	[MWd(kgU) ⁻¹]	258	-
Cladding hydrogen concentration	[wppm]	67 - 76	50
Cladding oxide layer thickness	[μm]	14 - 16	10

Fig. 16 shows the calculated distributions of burnup and power across the fuel pellet at end of life in the Gösgen reactor. These distributions are assumed to be valid for the entire length of the IFA-650.4 test rodlet, since the irradiation conditions were fairly uniform along the sampled rod segment.

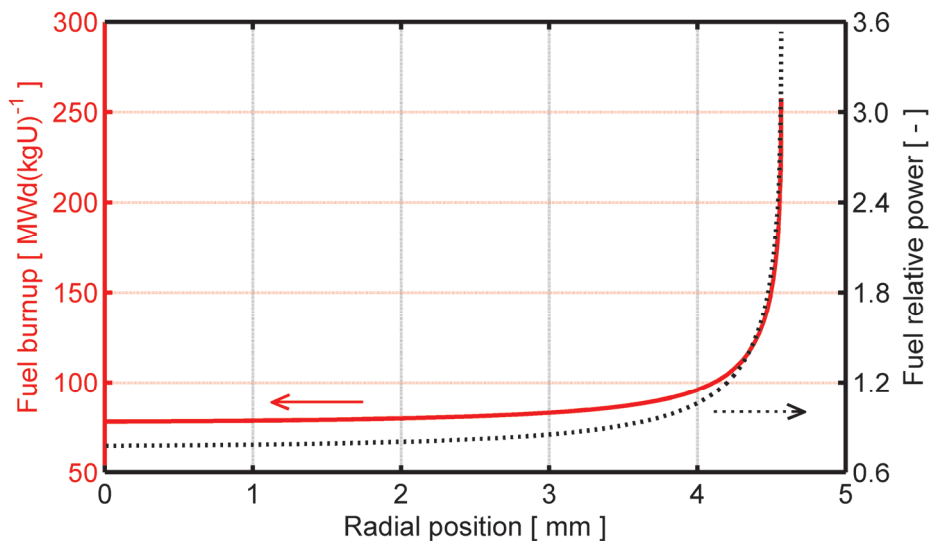


Fig. 16: Distributions of burnup and power across the fuel pellets in the IFA-650.4 test rodlet, as calculated by the FRAPCON-3.5 computer program.

The distributions in Fig. 16 are used for defining the radial profiles of burnup and power in subsequent analyses of the IFA-650.4 test with our extended version of FRAPTRAN-1.5. It is assumed that the distributions do not change with time during the test – not even when fuel crumbling occurs. As explained in section 2.3.1,

³ ECR is a widely used acceptance criterion for licensing emergency core cooling systems. It is defined as the percentage of the cladding thickness that would be oxidized, if all the oxygen from the cladding-water reactions stayed in the oxide layer as ZrO₂.

fuel crumbling is modelled by changing the pellet material properties and positions of pellet nodes when solving the radial heat conduction equation. The radial distributions of power, burnup or any other property that may affect the heat conduction are considered to be unaffected by fuel crumbling.

It should be remarked that the local fuel burnup exceeds $78.1 \text{ MWd}(\text{kgU})^{-1}$ across the entire cross section of the fuel pellet. According to the fuel pulverization threshold applied in our model (see section 2.2.2), this burnup leads to complete pulverization of the fuel for temperatures above 1100 K. We also note that the calculated average size of fuel fragments in the IFA-650.4 rodlet is 1.87 mm before the LOCA test. This follows from eq. (10) and the empirical fuel fragmentation model detailed in Appendix A, considering that the peak power experienced by the fuel during irradiation in Gösgen was 33.5 kWm^{-1} .

4.2.2. LOCA test

Next, we consider the results of our simulations of the IFA-650.4 LOCA test. Calculated results are presented graphically for the cases with and without fuel relocation considered in the analyses with our modified version of FRAPTRAN-1.5. Measured data are included in the graphs for comparison, whenever data are available. Throughout the presentation, time zero refers to the start of the LOCA test, defined by the opening of valves between the in-core pressure flask and the blowdown tank; see Appendix C.

Fig. 17 shows the calculated and measured evolution of rod internal gas pressure during the test. From section 4.1.2, we recall that the gas pressure is calculated on the basis of calculated temperatures and deformations along the active length of the rodlet, together with a postulated temperature history for the gas within the rod plenum. We also recall that the initial cold pressure was reduced from its reported value of 4.0 MPa to 3.86 MPa in our calculations, in order to match the calculated “hot” pre-test gas pressure to the measured value (6.95 MPa). The calculated gas pressure is in close agreement with measurements for $t < 290 \text{ s}$, but overestimated for the remaining 46 seconds preceding cladding rupture. The most likely explanation to this deviation is that ballooning of the cladding starts earlier and progresses more gradually than calculated with our version of FRAPTRAN-1.5.

The calculated curves for the cases with assumed relocation (“relo”) and without relocation (“norelo”) coincide up to $t = 328 \text{ s}$. This is the time at which fuel fragments start to relocate axially, according to our calculations. The calculated time of cladding failure is 335.2 s for the case with fuel relocation and 352.1 s without. These results suggest that cladding ballooning, collapse of the fuel pellet column, and axial relocation of fuel take place in a fairly short (7–8 s) period before cladding rupture, but that the thermal feedback effects are still strong enough to affect the rupture process. For the considered test, the calculated time to rupture was shortened by no less than 17 seconds, as a result of thermal feedback effects from

fuel crumbling and relocation. As already mentioned, the deviation between the calculated and measured gas pressure time histories in Fig. 17 indicates that the ballooning and relocation in test IFA-650.4 may actually have occurred over a longer period than suggested by our calculations. If so, the impact of thermal feedback effects on the rupture process would have been even more important.

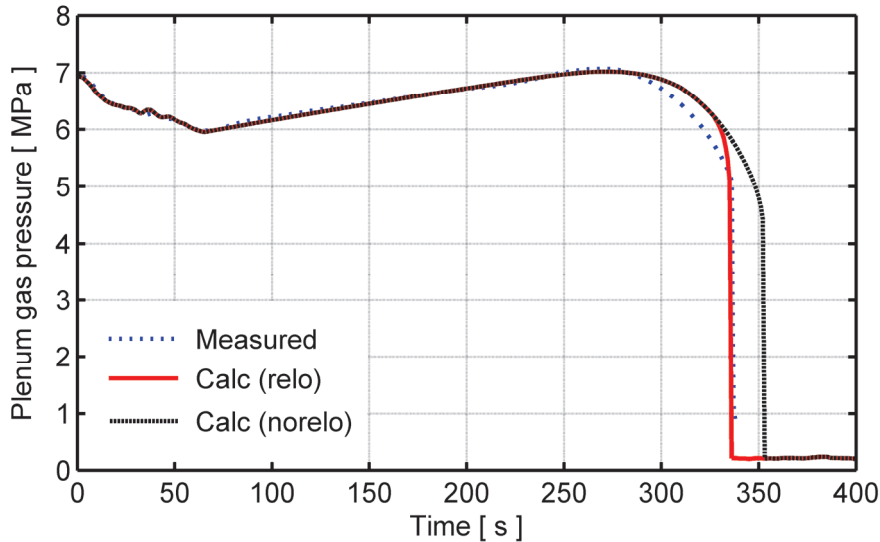


Fig. 17: Calculated evolution of rod gas pressure in comparison with measurements. Calculations were done with (relo) and without (norelo) assumed axial fuel relocation.

Fig. 18 shows the calculated evolution of cladding deformation and axial fuel relocation during the last seven seconds before cladding rupture. The thick red line shows the calculated state at the time of cladding rupture. This is also the state expected after the test is completed, since no further deformation or relocation is supposed to take place after rupture and depressurization of the rodlet. The family of thinner black lines to the left represent the calculated conditions 1, 2, 3,...,7 seconds before cladding rupture. The leftmost curve thus shows the conditions about the time when the balloon starts to grow and fuel starts to relocate.

The calculations suggest that the local fuel mass is increased by about a factor of three in the most distended cross section of the test rod. The relocated fuel originates from the uppermost, 120 mm long, part of the fuel pellet column, which has disappeared completely. This is well in line with the results reported from the test: Gamma scan (see insert in Fig. 18) as well as ceramography showed that the uppermost part of the fuel pellet column was completely missing after the test; no remaining fuel fragments were detected. The length of the missing fuel part was 190 mm, which is 70 mm longer than calculated with our model. The difference is understandable, since a significant amount⁴ of fuel had been expelled through the cladding breach and was found just above the balloon and at the bottom of the

⁴ The weight of dispersed fuel in the IFA-650 series of tests was not determined. Only qualitative assessments of the dispersal in each test, based on gamma scan results, are available [10, 34].

pressure flask after the test [49]. This dispersal of fuel fragments, which is not accounted for by our model, most certainly increased the amount of fuel lost from the upper part of the fuel rod.

Finally, we note that the calculated fuel temperature is in the range of 1100 to 1159 K, when relocation starts at $t = 328$ s. This means that, according to our model, the entire fuel column has been pulverized into fine (< 0.2 mm) fragments, and that the crumbled fuel has an assumed packing fraction of 0.72 everywhere in the ballooned region; see sections 2.2.2 and 2.2.3.

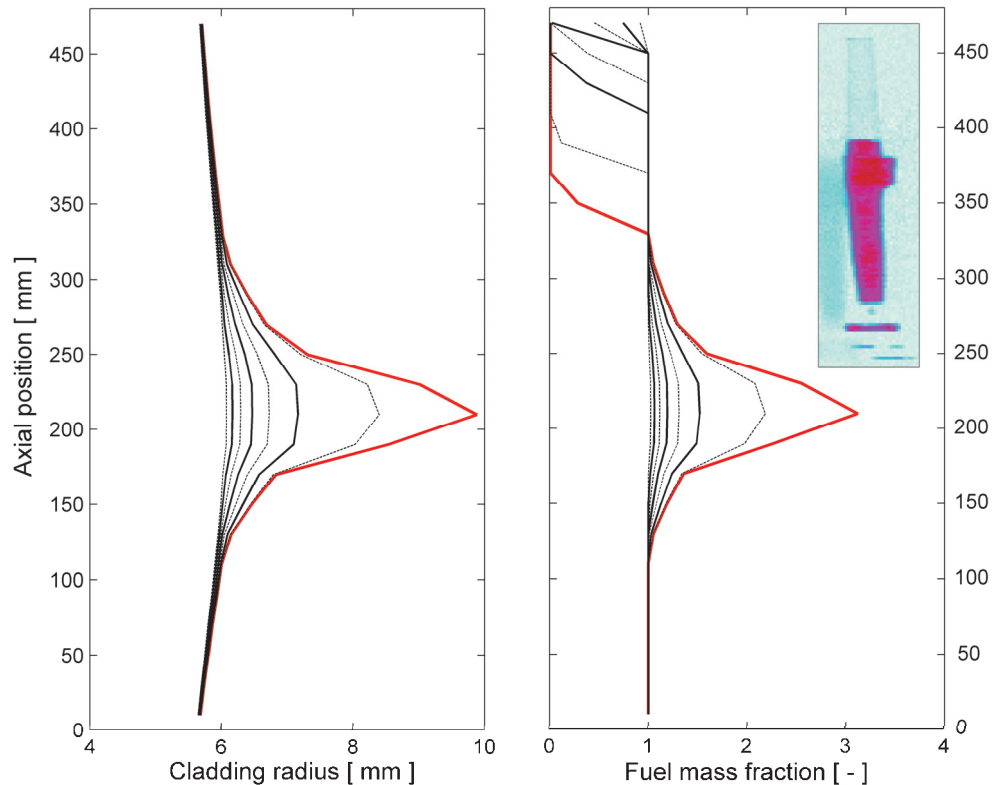


Fig. 18: Calculated evolution of cladding deformation (left) and fuel relocation (right) during the last seven seconds before cladding rupture. The rightmost curve (red) represents the conditions at time of rupture, while the seven curves to the left of it show the calculated state 1, 2,...,7 seconds before rupture. Post-test gamma scan image of the IFA-650.4 rig is included for comparison [49].

Fig. 19 shows the calculated post-test diameter profile of the IFA-650.4 rodlet in comparison with measurements. The latter were obtained by metallography of thirteen cross sections, for which the clad tube diameter was measured in two perpendicular directions. Hence, the data also provide some information on the degree of cylindrical symmetry for the deformation. The calculated peak deformation is the same for the two considered cases, since the same failure criterion in terms of a threshold for the local effective strain was used for both of them. However, the calculated deformation profiles differ. As expected, the fuel relocation tends to concentrate, or localize, the cladding deformation. The reason is the con-

concentrated heat load, resulting from fuel crumbling and accumulation of fuel fragments in the ballooned region of the rod.

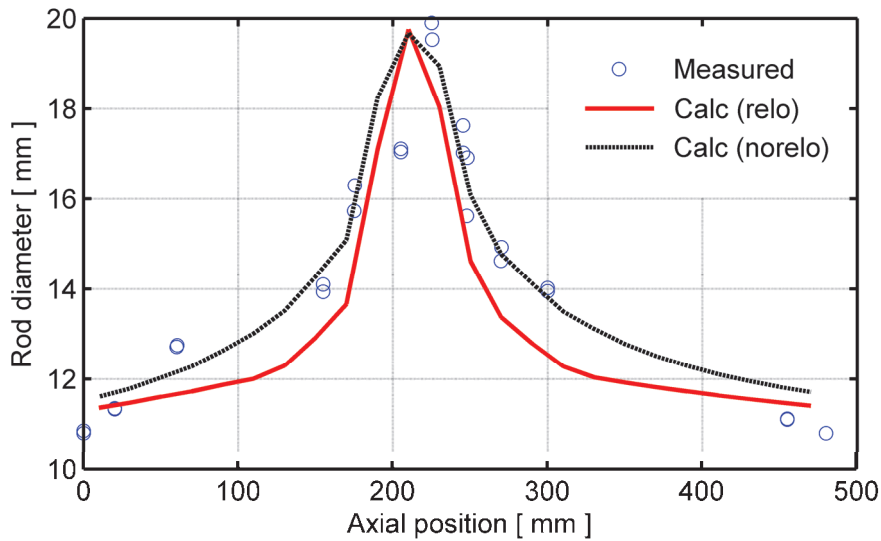


Fig. 19: Calculated and measured post-test diameter profiles for the IFA-650.4 rodlet [49].

Consequently, we next consider the thermal effects of fuel relocation and their impact on the cladding failure behaviour. Fig. 20 shows the cladding outer surface temperature versus axial position at time of cladding rupture, calculated with and without consideration of axial fuel relocation. Evidently, the calculated cladding surface temperature in the ballooned region is 30–40 K higher at time of rupture when axial fuel relocation is considered. This temperature difference explains the localization of deformation to the balloon, and also why rupture is calculated to occur 17 seconds earlier when fuel relocation is considered.

Fig. 20 shows that the calculated temperature increase caused by fuel relocation is almost uniform within the ballooned region. This may seem somewhat surprising, considering that the calculated axial distribution of fuel mass and heat load within this region is far from uniform; compare the right panel of Fig. 18. However, the cladding temperature increase just after fuel crumbling is caused not so much by the local increase of fuel mass, but by closure of the pellet-cladding gap as the fuel pellet column collapses and hot fuel fragments come into contact with the cladding inner surface. This makes the calculated pellet-to-cladding heat transfer coefficient suddenly increase by a factor of about 25 in the region with crumbled fuel, as shown in Fig. 21. The abrupt change is a consequence of going from a 0.7–0.8 mm wide annular gap, filled with gas of very low thermal conductivity, to a gap with an effective width (g^*) of only 5 μm . As explained in section 2.3.1, this is how the transition from a cylindrical fuel pellet column to a crumbled state is treated in our extended version of FRAPTRAN-1.5 for solving the radial heat conduction equation. It may be questioned if this modelling assumption of an abrupt transition is realistic; see section 5.3.

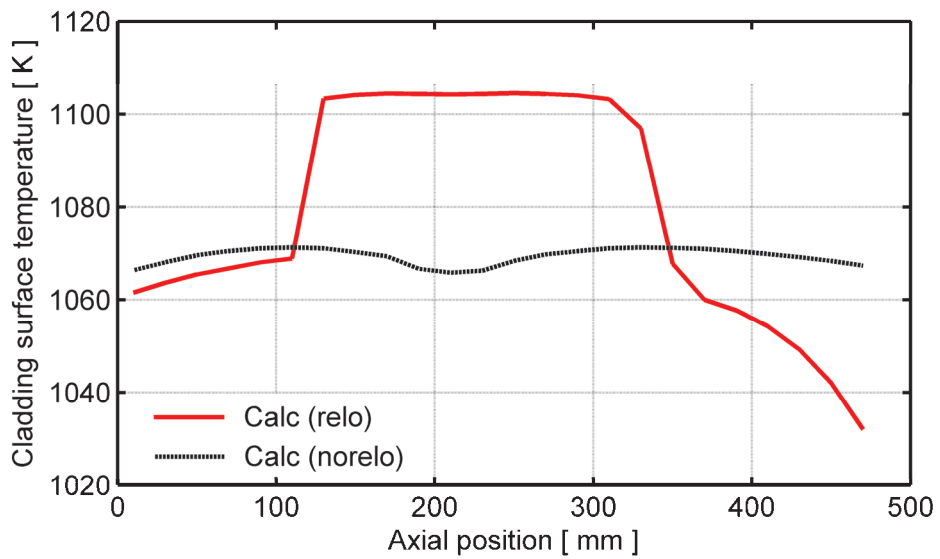


Fig. 20: Calculated cladding outer surface temperature versus axial position at time of cladding rupture, with and without consideration of axial fuel relocation.

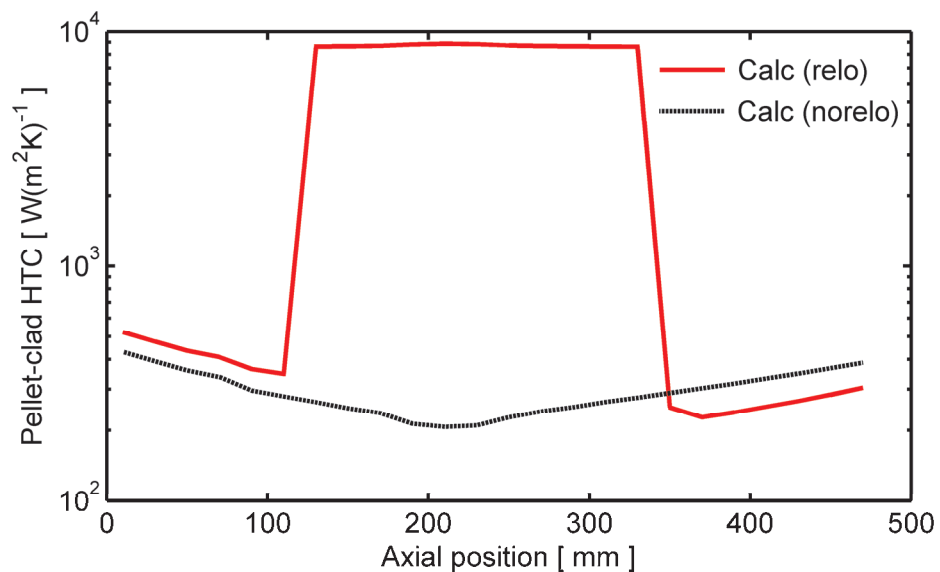


Fig. 21: Calculated pellet-cladding heat transfer coefficient versus axial position at time of cladding rupture, with and without consideration of axial fuel relocation.

The post-failure longer term effect of fuel crumbling and axial relocation on the cladding temperature distribution is illustrated by Fig. 22, which shows the calculated cladding outer surface temperature versus axial position at time $t = 500$ s. At this point in time, 165 seconds after cladding rupture, transient effects from the collapse of the fuel pellet column into the balloon have decayed and the temperature distribution reflects a quasi-steady condition. It is obvious that the calculated

temperature field for the case with axial fuel relocation is governed by the axial distribution of fuel mass and power; compare the right panel of Fig. 18. We note that the case without axial fuel relocation in Fig. 22 shows the opposite trend; the calculated cladding temperature has a minimum in the ballooned region, due to the local increase in coolable surface area.

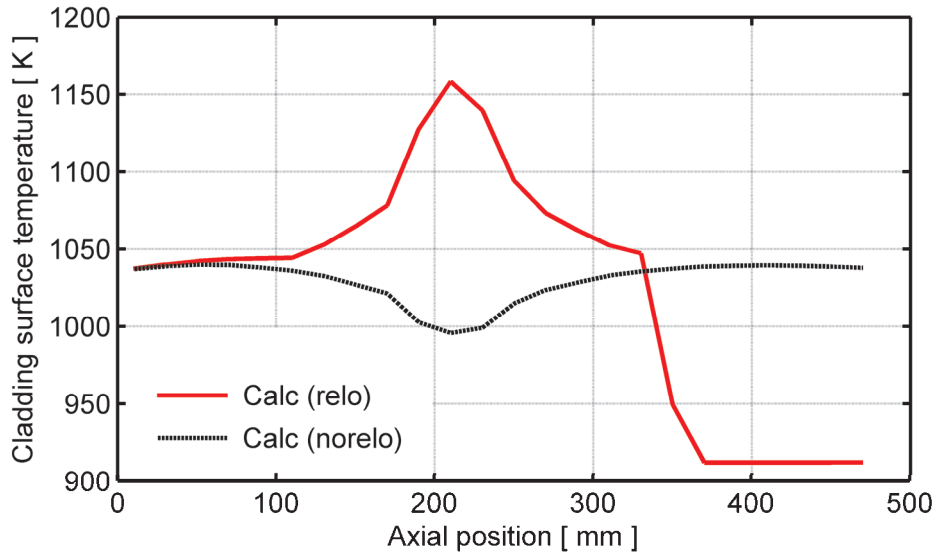


Fig. 22: Calculated cladding outer surface temperature versus axial position at time $t = 500$ s, with and without consideration of axial fuel relocation.

The long-term change in temperature distribution caused by the axial fuel relocation has a noticeable effect on the post-failure oxidation of the cladding. Fig. 23 shows the calculated equivalent cladding reacted versus axial position at time $t = 500$ s. We recall from section 4.2.1 that the calculated pre-test ECR from low temperature oxidation in Gösigen was about 1.6 %; this pre-test oxidation is included in the curves presented in Fig. 23. From the figure, it is clear that the calculated contribution to the peak ECR from the LOCA test is about twice as large when axial fuel relocation is considered. These results underline the importance of axial fuel relocation in computational predictions of ECR as part of licensing analyses [12].

The calculated results presented in Fig. 23 cannot be directly verified against experimental data, since no post-test measurements were made of the axial variation in cladding oxide thickness or metal oxygen concentration. However, the outer surface oxide layer thickness was measured at some positions in the ballooned region after the test. It ranged from about 10 to 13 μm , and the thickest oxide was found at the lower end of the balloon [49]. These results indicate that the peak ECR would be around 3.3 %, i.e. somewhere between our calculated results for the cases with and without fuel relocation. This is not surprising, considering that fuel fragments were ejected from the failed balloon into the coolant during the test. The fuel ejection, which is not accounted for in our simulations of the test,

lowered the fuel fragment packing fraction in the balloon. More precisely, the post-test area fraction covered by fuel fragments was estimated to be no more than 0.4–0.5 in the balloon, based on image analyses [49]. The low fragment packing fraction that resulted from the fuel ejection most certainly limited the the thermal feedback effects of axial fuel relocation in the experiment.

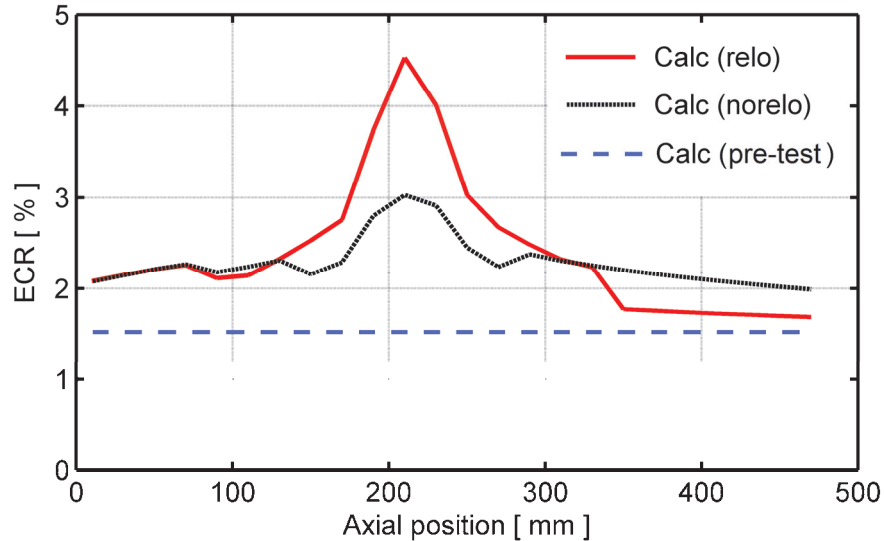


Fig. 23: Calculated equivalent cladding reacted versus axial position at time $t = 500$ s, with and without consideration of axial fuel relocation. The calculated pre-test ECR is included for comparison.

The calculated curve for the case without axial fuel relocation in Fig. 23 has an undulating shape, with several local minima. The shape arises as a consequence of the axial profiles for fuel power and cladding deformation, where the deformation has several, partly counteracting, effects on the ECR. It increases the local surface area, which on one hand promotes the metal-water reactions, but on the other hand lowers the cladding temperature and thereby the reaction rates. The deformation also leads to a thinning of the tube wall, which affects the ECR. In total, all these effects lead to the rather complex waviness of the curves in Fig. 23.

Fig. 24 shows a comparison of the calculated cladding surface temperature with measured data from thermocouple TCC1. This was one of two thermocouples located 80 mm below the top of the fuel pellet column, i.e. in the part that was completely emptied of fuel upon cladding rupture; see section C.3, Appendix C. The cladding temperature at this position is slightly underestimated for $65 < t < 250$ s in our calculations. The most likely explanation to the deviation is our simplified modelling of the clad-to-coolant heat transfer coefficient, which is assumed to be constant, $200 \text{ W(m}^2\text{K)}^{-1}$, for low temperatures; see section 4.1.2.

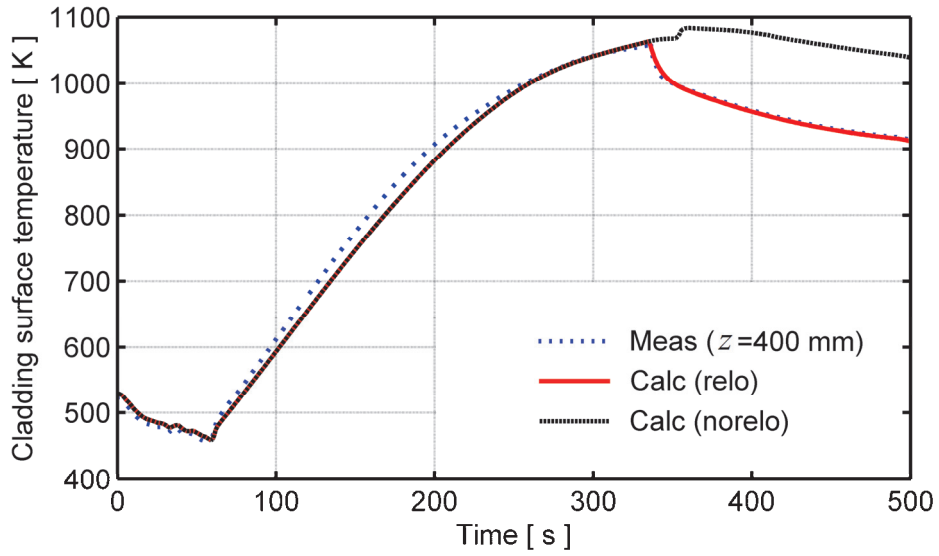


Fig. 24: Calculated and measured cladding surface temperature versus time. The temperature refers to the position of thermocouples TCC1 and TCC2, 400 mm above the bottom of the fuel pellet column. Measured data are from TCC1.

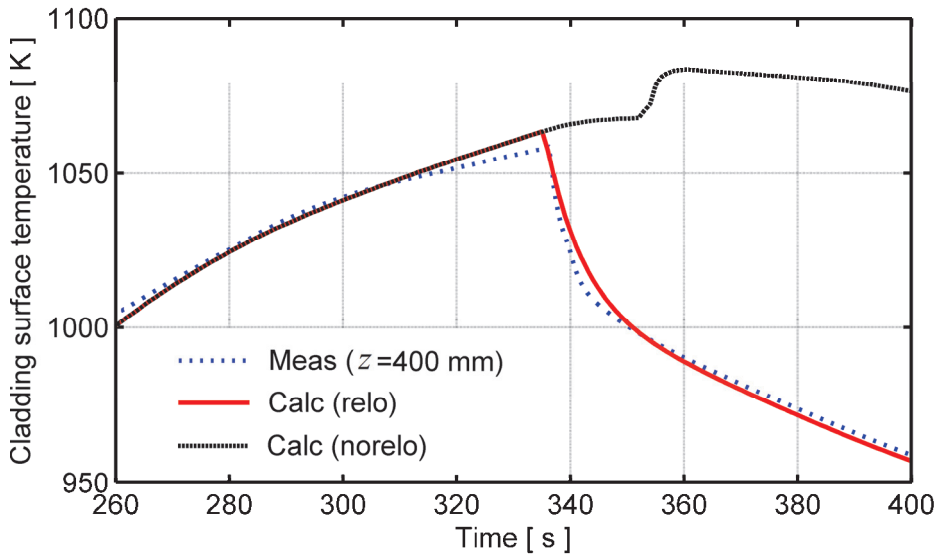


Fig. 25: Calculated and measured cladding surface temperature about the time of cladding rupture (336 s); close-up of Fig. 24.

Fig. 25 is a close-up of Fig. 24, showing the calculated and measured temperature variation about the time of cladding rupture (336 s in experiment, 335 and 352 s in calculations with and without fuel relocation, respectively). The calculated curve for the case with axial fuel relocation is very close to the measured data. This confirms that thermal feedback effects due to the complete fuel loss from the upper part of the rodlet are accurately captured by our model. When the fuel is lost, the cladding temperature approaches that of the surrounding coolant and heater; this is why the calculated and measured curves virtually coincide for $t > 350$ s.

For the calculated case without axial fuel relocation, the temperature increases after cladding rupture at $t = 352$ s. The temperature rise is a result of improved pellet-cladding heat transfer, since FRAPTRAN by default models instantaneous ingress of steam from the coolant channel to the pellet-cladding gap upon cladding rupture. The steam has higher thermal conductivity than the 95%Ar + 5%He fill gas.

5. Concluding remarks

5.1. Distinguishing features of the proposed model

Our model for axial relocation of fuel fragments during LOCA is based on the same assumptions as in all models hitherto proposed for the phenomenon, namely, that the relocation is essentially controlled by the cladding distension along the fuel rod and the fragment packing fraction attained by crumbled fuel in ballooned regions of the rod. The cladding distension is normally calculated by a suitable computer program for thermo-mechanical fuel rod analyses, in our case FRAPTRAN-1.5 [17], while the packing fraction is treated as a model parameter. Nonetheless, our model has a number of features that make it stand out from earlier relocation models.

First and foremost, our relocation model is integrated with the equations used for calculating the space-time variation of fuel and cladding temperature in FRAPTRAN-1.5. This means that thermal feedback effects from the axial redistribution of power and stored heat that axial fuel relocation brings about are fully accounted for in the transient fuel rod analysis. Earlier relocation models [14-16] have been designed and used as post-processors to various computer programs for fuel rod analysis, meaning that the programs have calculated the fuel rod thermo-mechanical behaviour with no or only partial consideration of fuel relocation.

Secondly, we consider in our model the state of fuel fragmentation and pulverization when estimating the packing fraction of crumbled fuel in ballooned regions of the fuel rod. As already mentioned, the packing fraction is a key parameter that controls the degree of fuel relocation, given the deformed configuration of the cladding tube. We have taken the novel approach of estimating the fuel fragment packing fraction from a simple semi-empirical model, which is based on the assumption that the crumbled fuel consists of two different size classes of fragments: The first class includes mm-size fragments, created by thermal stresses in the fuel during normal operation, and the second class comprises fine (< 0.2 mm) fragments, created during LOCA by overheating high burnup fuel. The second fragment class thus exists only under certain conditions, and a recently proposed empirical “pulverization threshold” [20-22] is used in our model for calculating the mass fraction of small fuel fragments, based on the distributions of burnup and temperature in the fuel.

Thirdly, when solving the radial heat conduction equation in our extended version of FRAPTRAN-1.5, we account not only for the changes in local fuel mass and heat load caused by axial fuel relocation, but also for the changes in fuel column geometry and material properties caused by fuel crumbling in ballooned regions of the rod. For example, the thermal conductivity of the particle bed of crumbled

fuel in the balloon is calculated through an effective medium model for solid particles surrounded by stagnant gas. According to this model, which has been verified against thermal conductivity data for UO_2 particle beds in various gases, the effective thermal conductivity of the particle bed depends on the thermal conductivities of the fuel fragments and the surrounding gas, and on the packing fraction of the fuel fragments.

5.2. Main conclusions

In section 4, we used the relocation model and its supporting submodels, implemented in our extended version of FRAPTRAN-1.5, for simulating the Halden IFA-650.4 LOCA test. This particular test is well suited for model validation, since it was carried out on an extensively instrumented fuel rodlet with very high burnup and resulted in significant fuel relocation. On the other hand, it should be borne in mind that the test was deliberately designed to amplify axial fuel relocation, and it may therefore not be representative of actual conditions under LOCA in commercial power reactors [13]. For example, the cladding tube was allowed to distend to a much larger diameter than what would be possible to reach in a typical LWR fuel assembly design. Here, we recapitulate the main conclusions from the simulations and discuss them in light of results from other investigations.

Firstly, our simulations of the IFA-650.4 test suggest that ballooning of the cladding, and the fuel relocation that resulted from it, occurred over a short (7–8 s) period, just before cladding rupture. The close agreement between the calculated and measured temperature drop that suddenly occurred in the upper part of the test rod just before cladding rupture (see Fig. 25) corroborates that the time of fuel relocation is accurately retrodicted by our model. The results are interesting, and it should be remarked that there has been some dispute in the past as to whether axial fuel relocation during LOCA occurs before or after cladding rupture. Today, there is clear experimental evidence from two in-reactor LOCA tests that fuel relocation may precede cladding rupture. These are test E5, conducted in the German FR2 reactor [1], and test IFA-650.14, recently carried out in the Halden reactor [50, 51]. The cladding did not rupture in either of these tests, but post-test neutron radiography revealed that extensive axial relocation had nevertheless taken place inside the ballooned cladding during both tests.

Secondly, our simulations suggest that thermal feedback effects from fuel relocation are strong enough to influence the dynamics of cladding ballooning and rupture, notwithstanding the short duration of these processes. For the simulated IFA-650.4 test, the calculated time to cladding rupture was shortened by no less than 17 seconds, as a result of thermal feedback effects. According to our calculations, the most important thermal feedback effect during the short period from onset of axial fuel relocation to cladding rupture is caused by the collapse of the fuel pellet column, which makes hot fuel fragments come into direct contact with the expanding cladding. The local increase of fuel mass in ballooned regions results in

minor thermal feedback effects *before* cladding rupture, but it has significant effects on the local cladding temperature and oxidation rate *after* rupture. Our simulations suggest a doubling of peak ECR (equivalent cladding reacted) during the IFA-650.4 test, due to a threefold increase of local fuel mass and linear heat generation rate at the most distended cross section of the test rodlet. These results are in line with those reported from analyses of postulated LWR LOCAs. For example, computational analyses of a postulated large break LOCA in a 900 MWe PWR by the French Institut de Radioprotection et de Sûreté Nucléaire (IRSN) show a similar effect of fuel relocation on peak ECR for the considered accident scenario, as well as a significant increase in calculated peak cladding temperature [8, 9]. These results are interesting with regard to LOCA licensing analyses, since they indicate that conservative assumptions have to be made in the analyses, unless fuel relocation and its consequences to cladding local temperature and oxidation are accounted for in the computational evaluation models.

Thirdly, we recapitulate that our submodel for estimating the fuel fragment packing fraction from the calculated state of fuel fragmentation and pulverization suggests that fuel with a pellet average burnup around $70\text{--}75 \text{ MWd}(\text{kgU})^{-1}$ would be particularly prone to axial relocation. This follows from the fact that the highest packing fractions, and thus the most favourable conditions for fuel relocation, are obtained when the weight fraction of small ($< 0.2 \text{ mm}$) fuel fragments, resulting from pulverization of high burnup fuel, is about 0.3. From typical burnup distributions in LWR fuel and the aforementioned pulverization threshold [20-22], this weight fraction of small fragments is expected in overheated fuel with a pellet average burnup around $72 \text{ MWd}(\text{kgU})^{-1}$.

Finally, we note that ballooning of the cladding tube is a local phenomenon that results from plastic instability. The balloons observed after in-reactor LOCA simulation experiments generally have an axial extension less than 100 mm [1, 10, 40]. In order to resolve this localized deformation with sufficient accuracy in computer simulations, the calculations have to be done with a fine axial discretization of the fuel rod, at least in the region where ballooning takes place. In our simulations of the Halden IFA-650.4 test, we used an axial discretization consisting of 24 segments, each 20 mm long. To carry out analyses of a full length (3.6 m) LWR fuel rod with such a discretization is impracticable. Computer programs used for analyses of ballooning must therefore allow local refinement of the discretization at axial positions of particular interest. FRAPTRAN has this capacity [17]. However, it should be remarked that the cladding ballooning model (BALON2) that is available in FRAPTRAN-1.5 cannot be used together with our model for fuel relocation. The reason is that the BALON2 model considers only the local behaviour of the cladding; collapse of the fuel pellet column into the balloon and its thermal feedback effects are not accounted for.

5.3. Suggestions for further work

Our validation of the relocation model against the Halden IFA-650.4 LOCA test shows excellent results. Yet, it is strongly recommended to continue the evaluation against additional experiments. Among the most suitable LOCA tests for model validation are:

Halden IFA-650.9: In-reactor test on a PWR fuel rodlet with a burnup of 89.9 MWd(kgU)⁻¹. Both the test rodlet and the test conditions were very similar to those of IFA-650.4, except that the rod power was significantly higher. The IFA-650.9 rodlet failed in its lower end, and considerable fuel pulverization and axial relocation was observed [10].

Halden IFA-650.14: In-reactor test on a boiling water reactor (BWR) fuel rodlet with a burnup of 70.8 MWd(kgU)⁻¹. As mentioned in section 5.2, the test was interrupted when the cladding started to balloon, i.e. before rupture [50]. Post-test examinations of the rodlet revealed extensive fuel relocation within the non-failed cladding, but very little pulverization [51].

Studsvik LOCA test 192: Out-of-reactor test on a PWR fuel rodlet with a burnup of 78 MWd(kgU)⁻¹. The test resulted in extensive fuel pulverization, axial relocation and fuel ejection into the coolant [11].

The two tests in the IFA-650 series can be modelled and evaluated in much the same way as the IFA-650.4 test in this report; see section 4.1. The Studsvik LOCA test requires a somewhat different treatment of the thermo-hydraulic boundary conditions, since the rodlet was furnace heated. It should be mentioned that the Halden IFA-650.9 and Studsvik LOCA test 192 have been identified as priority experiments for model validation in the recently initiated IAEA coordinated research project on fuel modelling in accident conditions (known as CRP FUMAC) [52], in which SSM and Quantum Technologies participate. Detailed information and data on these tests are made available to the participants in the project, in order to provide the best possible basis for modelling.

The tests listed above could widen the supporting database for key parameters used in the relocation model. Among these parameters are the fuel fragment packing fractions for fuel with no/complete pulverization, i.e. ϕ^L and ϕ^S , as defined in section 2.2.3. Another parameter is g^{th} , which defines the minimum pellet-cladding gap size needed for fuel fragments to detach from their original, close-packed configuration and relocate downwards; see section 2.2.4. Pending a better model, this threshold is set to 0.2 mm, and for simplicity, it is currently assumed to be independent of fuel fragment size and also of axial gas pressure gradients that may exist in the pellet-cladding gap.

Fuel crumbling, i.e. collapse of the fuel pellet column with its close-packed fuel fragments into a porous particle bed, is in our model treated as an abrupt change

in geometrical configuration when the pellet-cladding radial gap reaches a width of about 0.7–0.8 mm. As seen in section 4.2.2, this modelling approach has consequences to the short-term thermal response of the cladding tube upon fuel crumbling. These consequences should be investigated, and if deemed necessary, fuel crumbling and radial relocation of fuel fragments into the wide pellet-cladding gap under LOCA conditions should be modelled as a more gradual process. Post-test neutron radiography of ballooned fuel rodlets [1, 10, 51] suggests that the assumption of a cylindrical fuel pellet column surrounded by a wide annular pellet-cladding gap is unrealistic; gap filling by *radial* relocation of fuel fragments seems to occur gradually as the cladding distends and need not immediately result in *axial* fuel relocation.

The weight fraction of fine fuel fragments is in our model calculated by use of an empirical threshold for pulverization of high burnup fuel during temperature excursions [20-22]. This simple threshold for local temperature versus local burnup, which is based largely on proprietary data, represents the current state of knowledge regarding the pulverization phenomenon. Mechanistic models for the phenomenon, linking pulverization to the local fuel porosity and distribution of gaseous fission products in the fuel, are currently unavailable but underway [53]. In addition, separate effect tests, planned for example in the third phase of the Studsvik Cladding Integrity Project (SCIP-III), will shortly shed light on the phenomenon. Progress in our understanding of the pulverization phenomenon is thus expected in the near future, and the empirical threshold currently used in our model should be modified or replaced as better models and/or more experimental data become available. Of particular interest for modelling is the impact of mechanical constraint from the cladding and effects of pre-LOCA operating history for the fuel.

We also note that the work presented in this report suggests that the fuel fragment packing fraction is particularly high for fuel containing about 30 wt% fine fragments. This particular fragment size distribution would be obtained by overheating LWR fuel with a pellet average burnup around $72 \text{ MWd}(\text{kgU})^{-1}$. Unfortunately, there are currently no measured data on the fuel fragment packing fraction versus fuel burnup that can confirm or refute this modelling result. Such measurements are warranted, not least since computer analyses suggest that the effects of axial fuel relocation on peak cladding temperature and ECR under a loss-of-coolant accident would depend strongly on the fragment packing fraction [6, 9, 54]. We recapitulate from section 2.2.3 that data on the packing fraction exist for fuel with low ($< 16 \text{ MWd}(\text{kgU})^{-1}$) burnup, but to our knowledge, there are currently no open literature data at all for higher burnup fuel.

Our relocation model provides, for each axial segment of the fuel rod, an upper bound of the fuel mass that may be ejected into the coolant, should the cladding fail within the considered axial segment. As explained in section 2.1.2, the calculated amount of dispersed fuel is based on the assumption that all fuel above the cladding breach that is free to move downward will be ejected through the breach.

This is a crude upper bound estimate, since the fuel dispersal will most likely be limited by the rupture opening and by choke points for the axial relocation at spacer grid positions. Considering the observed effects of spacers [40], it is probably realistic to assume that no relocation will take place past spacer grids. Hence, fuel located above the spacer grid that is nearest above the cladding breach may be precluded from the amount of fuel that could be ejected through the breach. Moreover, it would be possible to correlate the estimated amount of ejected fuel to the fuel fragment size distribution and to the expected area of the rupture opening. It is known that this area depends on the phase composition of the cladding metal at the time of rupture [55]. The area of the rupture opening is also known to increase with the internal overpressure in the fuel rod [56] and to decrease with the cladding hydrogen concentration [10]. In conclusion, it would be possible to extend our relocation model such that it provides more realistic estimates of fuel dispersal. To this end, a submodel for axial gas flow, induced by pressure gradients along the pellet-cladding gap, should be introduced in FRAPTRAN-1.5. This is because the dynamics of pressure equilibration will affect both the cladding rupture size (through the magnitude of the local overpressure at time of ballooning and burst) and the propensity for fuel ejection (through the magnitude and duration of axial pressure gradients after burst that may entrain fuel fragments in the flowing gas).

6. References

1. Karb, E.H., et al., *LWR fuel rod behavior in the FR2 in-pile tests, simulating the heatup phase of a LOCA*, 1983, Report KfK-3346, Kernforschungszentrum Karlsruhe, Karlsruhe, Germany.
2. Cook, T.F., *An evaluation of fuel rod behavior during test LOC-11*, 1979, Report NUREG/CR-0590, U.S. Nuclear Regulatory Commission, Washington, DC, USA.
3. Broughton, J.M., et al., *PBF LOCA test series: Test LOC-3 and LOC-5 fuel behavior report*, 1981, Report NUREG/CR-2073, U.S. Nuclear Regulatory Commission, Washington, DC, USA.
4. Broughton, J.M., et al., *PBF LOCA test LOC-6 fuel behavior report*, 1983, Report NUREG/CR-3184, U.S. Nuclear Regulatory Commission, Washington, DC, USA.
5. Bergquist, P., et al., *Impact on the calculated peak clad temperature of a redistribution of fuel after cladding swelling and rupture at PWR LOCA conditions*, 1978, Report FV-78-0010/01, AB Fjärrvärme, Trosa, Sweden.
6. Bergquist, P., *A parameter study concerning the impact on the calculated peak clad temperature of a redistribution of the fuel after cladding swelling and rupture*, 1979, Report FV-79-0017/2, AB Fjärrvärme, Trosa, Sweden.
7. Siefken, L.J. *Axial fuel relocation in ballooning fuel rods*, 1983. In: 7th International Conference on Structural Mechanics in Reactor Technology (SMiRT-7), August 22-26, 1983, Chicago, IL, USA.
8. Guillard, V., et al. *Use of CATHARE2 reactor calculations to anticipate research needs*, 2004. In: SEGFSM Topical Meeting on LOCA Issues, May 25-27, 2004, Argonne National Laboratory, Lemont, IL, USA.
9. Grandjean, C., et al. *High burnup UO₂ fuel LOCA calculations to evaluate the possible impact of fuel relocation after burst*, 2001. In: OECD Topical Meeting on LOCA Fuel Safety Criteria, March 22-23, 2001, Aix-en-Provence: OECD Nuclear Energy Agency, Committee on the Safety of Nuclear Installations, Report NEA/CSNI/R(2001)18, Paris, France, pp. 239-266.
10. Wiesenack, W., *Summary of the Halden Reactor Project LOCA test series IFA-650*, 2013, Report HPR-380, OECD Halden Reactor Project, Halden, Norway.
11. Flanagan, M., et al., *Post-test examination results from integral, high-burnup, fueled LOCA tests at Studsvik Nuclear Laboratory*, 2013, Report NUREG-2160, U.S. Nuclear Regulatory Commission, Washington, DC, USA.
12. Raynaud, P.A.C., *Fuel fragmentation, relocation and dispersal during the loss-of-coolant accident*, 2012, Report NUREG-2121, U.S. Nuclear Regulatory Commission, Washington, DC, USA.
13. Wiesenack, W., *Safety significance of the Halden IFA-650 LOCA test results*, 2010, Report NEA/CSNI/R(2010)5, OECD Nuclear Energy Agency, Paris, France.

14. Aounallah, Y., et al. *Simulations of the Halden IFA-650.3/4 high burnup LOCA tests with TRACE and FALCON; A preliminary study on axial relocation*, 2006. In: 2006 International Meeting on LWR Fuel Performance (TopFuel 2006), October 22-26, 2006, Salamanca, Spain: European Nuclear Society, pp. 305-311.
15. Khvostov, G., et al. *Modeling the effects of axial fuel relocation in the IFA-650.4 LOCA test*, 2007. In: Enlarged Halden Programme Group Meeting, March 12-15, 2007, Storefjell, Norway: OECD Halden Reactor Project, Halden, Norway.
16. Govers, K. and M. Verwerft. *Simulation of ballooning and relocation in the Halden LOCA tests with FRAPTRAN*, 2014. In: Enlarged Halden Programme Group Meeting, September 7-12, 2014, Røros, Norway: OECD Halden Reactor Project, Halden, Norway
17. Geelhood, K.J., et al., *FRAPTRAN-1.5: A computer code for the transient analysis of oxide fuel rods*, 2014, Report NUREG/CR-7023, Vol. 1, Rev. 1, Pacific Northwest National Laboratory, Richland, WA, USA.
18. Walton, L.A. and D.L. Husser, *Fuel pellet fracture and relocation*, 1983. In: Water Reactor Fuel Element Performance Computer Modelling, J.H. Gittus, Editor. Applied Science Publishers: London, UK.
19. Walton, L.A. and J.E. Matheson, *FUMAC - A new model for light water reactor fuel relocation and pellet-cladding interaction*. Nuclear Technology, 1984. 64: pp. 127-138.
20. Turnbull, J.A., et al. *An investigation into fuel pulverization with specific reference to high burnup LOCA*, 2014. In: Enlarged Halden Programme Group Meeting, September 7-12, 2014, Røros, Norway: OECD Halden Reactor Project, Halden, Norway.
21. Yagnik, S., et al. *An investigation into fuel pulverization with specific reference to high-burnup LOCA*, 2014. In: 2014 Water Reactor Fuel Performance Meeting (WRFPM 2014), September 14-17, 2014, Sendai, Japan.
22. Turnbull, J.A., et al., *An assessment of the fuel pulverization threshold during LOCA-type temperature transients*. Nuclear Science and Engineering, 2015. 179: pp. 477-485.
23. Lassmann, K., et al., *Modelling the high burnup UO₂ structure in LWR fuel*. Journal of Nuclear Materials, 1995. 226: pp. 1-8.
24. Baron, D., et al., *Discussion about HBS transformation in high burn-up fuels*. Nuclear Engineering and Technology, 2009. 41(2): pp. 199-214.
25. Geelhood, K.J. and W.G. Luscher, *FRAPCON-3.5: A computer code for the calculation of steady-state, thermal-mechanical behavior of oxide fuel rods for high burnup*, 2014, Report NUREG/CR-7022, Vol. 1, Rev. 1, Pacific Northwest National Laboratory, Richland, WA, USA.
26. Lassmann, K., et al., *The radial distribution of plutonium in high burnup UO₂ fuels*. Journal of Nuclear Materials, 1994. 208(3): pp. 223-231.
27. Jernkvist, L.O. and A.R. Massih, *Models for fuel rod behaviour at high burnup*, 2005, Report SKI 2005:41, Swedish Nuclear Power Inspectorate, Stockholm, Sweden.

28. Cumberland, D.J. and R.J. Crawford, *The packing of particles*. Handbook of Powder Technology. Vol. 6. 1987, Amsterdam, The Netherlands: Elsevier Science.
29. German, R.M., *Particle packing characteristics*. 1989, Princeton, NJ, USA: Metal Powder Industries Federation.
30. Torquato, S. and F.H. Stillinger, *Jammed hard-particle packings: From Kepler to Bernal and beyond*. Reviews of Modern Physics, 2010. 82(3): pp. 2633-2672.
31. Westman, A.E.R., *The packing of particles: Empirical equations for intermediate diameter ratios*. Journal of the American Ceramic Society, 1936. 19: pp. 127-129.
32. Yu, A.B., et al., *Porosity calculation of binary mixtures of nonspherical particles*. Journal of the American Ceramic Society, 1993. 76(11): pp. 2813-2816.
33. Finkers, H.J. and A.C. Hoffman, *Structural ratio for predicting the voidage of binary particle mixtures*. AIChE Journal, 1998. 44(2): pp. 495-498.
34. Oberländer, B.C. and W. Wiesenack, *Overview of Halden reactor LOCA experiments (with emphasis on fuel fragmentation) and plans*, 2014, Report IFE/KR/E-2014/001, Institute for Energy Technology, Kjeller, Norway.
35. Garlick, A. and P. Hindmarch, *Cladding deformation and fuel stack mechanical stability during internal pressurisation tests on irradiated PWR fuel*, 1983, Report ND-R-628(W), UKAEA Windscale Nuclear Power Development Labs, Windscale, UK.
36. Manley, A.J., et al. *Application of X-radioscopic techniques to LOCA simulation tests on irradiated PWR fuel*, 1990. In: Post-Irradiation Examination Techniques for Water Reactor Fuel, September 11-14, 1990, Workington, UK: IAEA International Working Group on Water Reactor Fuel Performance and Technology, Proceeding IWGFPT/37, Vienna, Austria.
37. Jernkvist, L.O., *Observed and corrected errors in source code and algorithms of FRAPTRAN-1.5*, 2015, Report TR15-002, Quantum Technologies AB, Uppsala, Sweden.
38. Wagner, R.J., *HEAT-1: A one-dimensional time dependent or steady state heat conduction code for the IBM-650*, 1963, Research report IDO-16867, Phillips Petroleum Company, Atomic Energy Division, Idaho Falls, ID, USA.
39. Brankov, V., et al. *Fuel relocation in IFA-650 LOCA tests based on gamma scan data*, 2014. In: Enlarged Halden Programme Group Meeting, September 7-12, 2014, Røros, Norway: OECD Halden Reactor Project, Halden, Norway.
40. Freshley, M.D. and G.M. Hesson, *Summary results of the LOCA simulation program conducted in NRU*, 1983, Conference paper presented at the Eleventh NRC Water Reactor Safety Meeting, Gaithersburg, MD, USA, October 14-28, 1983, Report PNL-SA-11536, Pacific Northwest Laboratory, Richland, WA, USA.
41. Tofino, Y., et al. *Evaluation of ECR and PCT in balloon region under LOCA conditions of the Halden IFA 650 tests (single rod tests)*, 2009. In: Water Reactor Fuel Performance Meeting 2009 (TopFuel 2009), September 6-10, 2009, Paris, France: European Nuclear Society, pp. 573-580.

42. Khvostov, G., et al., *Some insights into the role of axial gas flow in fuel rod behaviour during the LOCA, based on Halden tests and calculations with the FALCON-PSI code*. Nuclear Engineering and Design, 2011. 241: pp. 1500-1507.
43. Manngård, T., et al. *Evaluation of Halden IFA-650 loss-of-coolant accident experiments 2, 3, 4, 5, 6 and 7*, 2013. In: Enlarged Halden Programme Group Meeting, March 10-15, 2013, Storefjell, Norway: OECD Halden Reactor Project, Halden, Norway.
44. Manngård, T., et al., *Evaluation of the Halden IFA-650 loss-of-coolant accident experiments 2, 3 and 4*, 2014, Report SSM 2014:18, Swedish Radiation Safety Authority, Stockholm, Sweden.
45. Jernkvist, L.O., *Implementation of models for cladding high temperature metal-water reactions, phase transformation, creep and failure in the FRAPTRAN-1.4 computer program*, 2012, Report TR10-005V2, Quantum Technologies AB, Uppsala, Sweden.
46. Manngård, T. and A.R. Massih, *Modelling and simulation of reactor fuel cladding under loss-of-coolant accident conditions*. Journal of Nuclear Science and Technology, 2011. 48(1): pp. 39-49.
47. Knuutila, A., *Improvements on FRAPCON3/FRAPTRAN mechanical modelling*, 2006, Research report VTT-R-11337-06, VTT Technical Research Centre of Finland, Helsinki, Finland.
48. Modest, M.F., *Radiative Heat Transfer*. 3rd ed. 2013, Oxford, UK: Academic Press.
49. Oberländer, B.C., et al. *PIE results from the high burnup (92 MWd/kgU) PWR segment after LOCA testing in IFA 650-4*, 2008. In: Enlarged Halden Programme Group Meeting, May 18-23, 2008, Loen, Norway: OECD Halden Reactor Project, Halden, Norway
50. Tradotti, R., *LOCA testing at Halden, the BWR fuel experiment IFA-650.14*, 2014, Report HWR-1084, OECD Halden Reactor Project, Halden, Norway.
51. Oberländer, B.C. and H.K. Jenssen, *PIE on the rod from the LOCA test IFA-650.14 on high burn-up BWR fuel*, 2014, Report HWR-1096, OECD Halden Reactor Project, Halden, Norway.
52. Killeen, J.C., *Notes on the first research coordination meeting of the Coordinated Research Programme on Fuel Modelling in Accident Conditions (FUMAC), held in coordination with the 20th QUENCH workshop at the Karlsruhe Institute of Technology (KIT), Karlsruhe, Germany, November 11-14, 2014*, 2014, International Atomic Energy Agency, Vienna, Austria.
53. Struzik, C., et al. *LOCA tests IFA 650 analysis through the fuel state at the end of base irradiation and its thermo-mechanical behaviour during the experiment*, 2014. In: Enlarged Halden Programme Group Meeting, September , 2014, Røros, Norway: OECD Halden Reactor Project, Halden, Norway.
54. Routledge, K.T., et al. *Calculations of the effects of fuel pellet fragment axial relocation on the peak clad temperature during a loss-of-coolant accident in a pressurized water reactor*, 1988. In: Second UK National Conference on Heat Transfer, September 14-16, 1988, Glasgow, UK: Institution of Mechanical Engineers, Mechanical Engineering Publications, London, UK, 2, pp. 1531-1540.

55. Chung, H.M. and T.F. Kassner, *Deformation characteristics of Zircaloy cladding in vacuum and steam under transient-heating conditions: summary report 1978*, Report NUREG/CR-0344, U.S. Nuclear Regulatory Commission, Washington, DC, USA.
56. Markiewics, M.E. and F.J. Erbacher, *Experiments on ballooning in pressurized and transiently heated Zircaloy-4 tubes*, 1988, Report KfK-4343, Kernforschungszentrum Karlsruhe, Karlsruhe, Germany.
57. Mezzi, G.P., *Thermoelastic stresses in pellet fragments and conditions for fragments formation*. Nuclear Engineering and Design, 1983. 73: pp. 83-93.
58. Oguma, M., *Cracking and relocation behaviour of nuclear fuel pellets during rise to power*. Nuclear Engineering and Design, 1983. 76: pp. 35-45.
59. Coindreau, O., et al., *Nuclear fuel rod fragmentation under accidental conditions*. Nuclear Engineering and Design, 2013. 255: pp. 68-76.
60. Oguma, M., *Integrity degradation of UO₂ pellets subjected to thermal shock*. Journal of Nuclear Materials, 1985. 127: pp. 67-76.
61. Helin, M. and J. Flygare, *NRC LOCA tests at Studsvik: Design and construction of test train device and tests with unirradiated cladding material*, 2012, Report STUDSVIK/N-11/130, Studsvik Nuclear AB, Studsvik, Sweden.
62. Jernkvist, L.O., *A continuum model for cracked UO₂ fuel*. Nuclear Engineering and Design, 1997. 176: pp. 273-284.
63. Michel, B., et al., *3D fuel cracking modelling in pellet cladding mechanical interaction*. Engineering Fracture Mechanics, 2008. 75: pp. 3581-3598.
64. Williamson, R.L. and D.A. Knoll. *Simulating dynamic fracture in oxide fuel pellets using cohesive zone models*, 2009. In: 20th International Conference on Structural Mechanics in Reactor Technology (SMiRT-20), August 9-14, 2009, Espoo, Finland.
65. Une, K., et al., *Fission gas release behavior from high burnup UO₂ fuels under rapid heating conditions*. Journal of Nuclear Science and Technology, 2006. 43(9): pp. 1161-1171.
66. Hiernaut, J.-P., et al., *Fission product release and microstructure changes during laboratory annealing of a very high burnup fuel specimen*. Journal of Nuclear Materials, 2008. 377: pp. 313-324.
67. Puranen, A., et al. *Burnup effects on fine fuel fragmentation in simulated LOCA testing*, 2013. In: 2013 LWR Fuel Performance Meeting (TopFuel 2013), September 15-19, 2013, Charlotte, NC, USA: American Nuclear Society.
68. DiMelfi, R.J. and J.M. Kramer, *Modeling fragmentation and spallation of oxide reactor fuel during transient heating including the effects of burnup and fission product distribution*. Nuclear Technology, 1983. 62(1): pp. 51-61.
69. Tsotsas, E. and H. Martin, *Thermal conductivity of packed beds: a review*. Chemical Engineering and Processing: Process Intensification, 1987. 22(1): pp. 19-37.
70. Cheng, P. and H. Chin-Tsau, *Heat Conduction*, 1998. In: Transport Phenomena in Porous Media, D.B. Ingham and I. Pop, Editors. Pergamon Press: Oxford, UK. pp. 57-76.

71. Achenbach, E., *Heat and flow characteristics of packed beds*. Experimental Thermal and Fluid Science, 1995. 10(1): pp. 17-27.
72. Chiew, Y.C. and E.D. Glandt, *The effect of structure on the conductivity of a dispersion*. Journal of Colloid and Interface Science, 1983. 94(1): pp. 90-104.
73. Maxwell, J.C., *A Treatise on Electricity and Magnetism*. 1873, London, UK: Clarendon Press.
74. Gonzo, E.E., *Estimating correlations for the effective thermal conductivity of granular materials*. Chemical Engineering Journal, 2002. 90: pp. 299-302.
75. Eian, C.S. and R.G. Deissler, *Effective thermal conductivities of magnesium oxide, stainless steel, and uranium oxide powders*, 1953, NACA Research Memorandum NACA RM E53G03, National Advisory Committee for Aeronautics, Washington, DC, USA.
76. Boegli, J.S. and R.G. Deissler, *Measured effective conductivity of uranium oxide powder in various gases and gas mixtures*, 1955, NACA Research Memorandum NACA RM E54L10, National Advisory Committee for Aeronautics, Washington, DC, USA.
77. Bich, E., et al., *The viscosity and thermal conductivity of pure monatomic gases from their normal boiling point up to 5000 K in the limit of zero density and at 0.101325 MPa*. Journal of Physical and Chemical Reference Data, 1990. 19(6): pp. 1289-1305.
78. Kolstad, E., et al. *High burn-up fuel behaviour under LOCA conditions as observed in Halden experiments*, 2011. In: IAEA Technical Meeting on Fuel Behaviour and Modelling under Severe Transient and Loss-of-Coolant Accident (LOCA) Conditions, October 18-21, 2011, Mito, Japan: International Atomic Energy Agency, IAEA-TECDOC-CD-1709.
79. Kolstad, E. *LOCA experiments with high burnup fuel in the Halden programme*, 2010. In: Swedish Radiation Safety Authority Research Seminar on Reactor Safety, April 22-23, 2010, Stockholm, Sweden.
80. Kekkonen, L., *LOCA testing at Halden: The fourth experiment - IFA-650.4*, 2007, Report HWR-838, OECD Halden Reactor Project, Halden, Norway.

Appendix A: Fuel fragmentation and pulverization

A.1. Fuel fragmentation

A strong radial temperature gradient arises in UO_2 or mixed $(\text{U,Pu})\text{O}_2$ fuel pellets during normal reactor operation, due to the low thermal conductivity of the material. The temperature gradient induces thermo-elastic stresses in the material. Tensile stresses are found at the cold outer surface of the pellet, predominantly in the hoop direction. These stresses cause radial cracks to form at a linear heat generation rate of $5\text{--}6\text{ kWm}^{-1}$. The cracking proceeds as the power is increased, and the strength of the temperature gradient caused by the applied power dictates how many fragments need be created to keep the tensile stresses below the fracture threshold for the material [57, 58]. The number of radial cracks (or fragments) therefore increases almost linearly with increasing linear heat generation rate, as illustrated by Fig. 26. However, the tendency for further cracking declines at an LHGR above $40\text{--}45\text{ kWm}^{-1}$, as a result of increased material plasticity at high temperature. It should also be remarked that thermal stresses in annular fuel pellets are lower than in solid pellets, and that annular pellets therefore generally exhibit coarser crack patterns than depicted in Fig. 26.

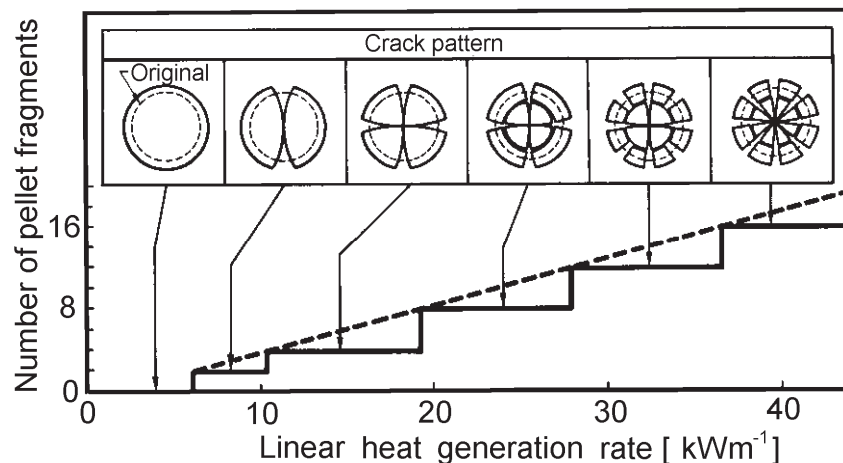


Fig. 26: Changes in ideal cross sectional crack pattern with increasing LHGR.
Reprinted from [58], copyright 1983, with permission from Elsevier.

Because of the characteristics of the thermally induced stress state, most pellet cracks are along the radial direction (“radial cracks”), as shown in Fig. 27. Some cracks are also formed in planes normal to the axial direction (“axial cracks”) and normal to the radial direction (“circumferential cracks”). In ceramographic investigations of irradiated fuel, the number of pellet cracks is observed to increase with fuel operating time or burnup. The reason is not clear, but it is likely that

thermal stresses are particularly strong during fast and/or large changes of fuel power. Consequently, the number of cracks is believed to increase for each reactor shutdown or fast power change. Build-up of internal stresses by differential swelling and weakening of the material by element transmutation and by accumulation of fission product gas along grain boundaries may also ease cracking at higher burnup.

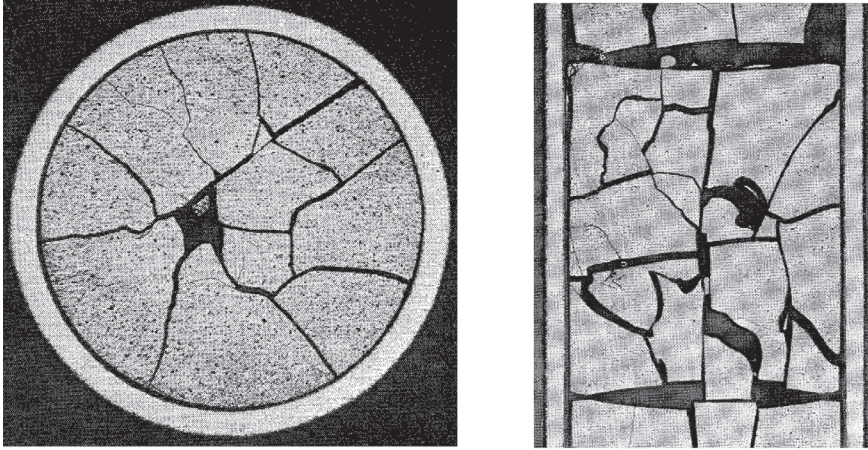


Fig. 27: Typical crack pattern in low burnup (2.5 MWd/kgU) UO₂ fuel, caused by normal reactor operation at high (40–45 kW/m) linear power; rod C6 in the FR2 test series [1].

A database on crack patterns observed in more than 60 investigated cross sections of irradiated UO₂ and (U,Pu)O₂ fuel rods with solid fuel pellets has been presented by Walton and Husser [18]. The database covers peak LHGRs up to nearly 70 kWm⁻¹ and pellet average burnups to approximately 35 MWd(kgHM)⁻¹. For each investigated cross section, the number of radial cracks intersecting the pellet outer surface was counted. Walton and Matheson [19] used these data to formulate an empirical correlation between the number of radial fuel cracks, n_f , and the fuel burnup and peak LHGR. The best-estimate correlation is

$$n_f = 0.8 \left(\sqrt{E_{av}} + \sqrt{3.3 \{q'_M - 6.0\}} \right), \quad (28)$$

where E_{av} is the fuel pellet average burnup in MWd(kgHM)⁻¹ and q'_M is the maximum LHGR experienced by the fuel in kWm⁻¹. In eq. (28), the number of radial cracks n_f is treated as a float rather than an integer, and $\{ \}$ denotes the Macaulay brackets

$$\{x\} = \begin{cases} 0, & x < 0 \\ x, & x \geq 0 \end{cases}. \quad (29)$$

The correlation in eq. (28) is compared with its supporting database for UO₂ fuel in Fig. 28 and Fig. 29. It should be remarked that, in eq. (28), the fuel burnup and maximum LHGR are treated as *independent* parameters for calculating the fuel pellet crack density. This must be considered as a crude approach; it is likely that

cases where the peak power is reached late in life is more detrimental to fuel cracking than cases where the peak power is reached at beginning of life.

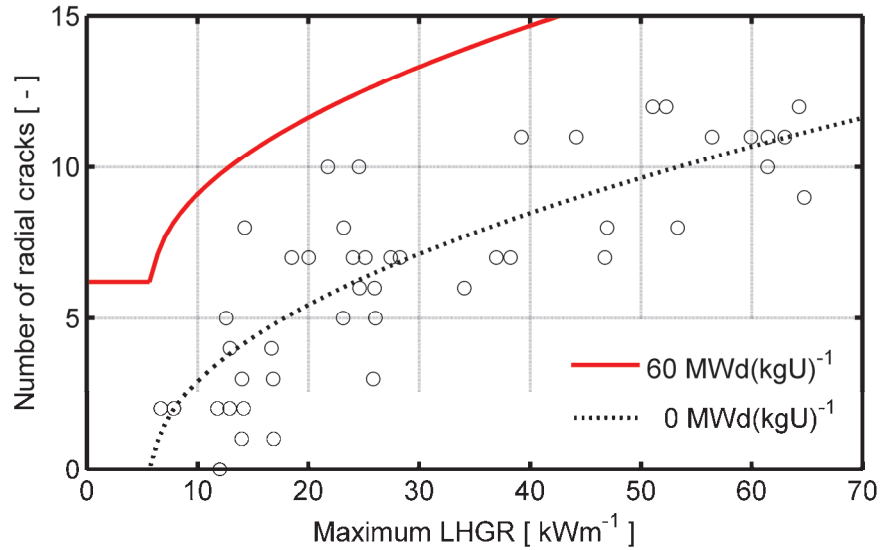


Fig. 28: Number of radial cracks in the fuel pellet, calculated through eq. (28), in comparison with data from [18]. The data are for UO₂ fuel pellets with an average burnup between 0 and 5 MWd(kgU)⁻¹.

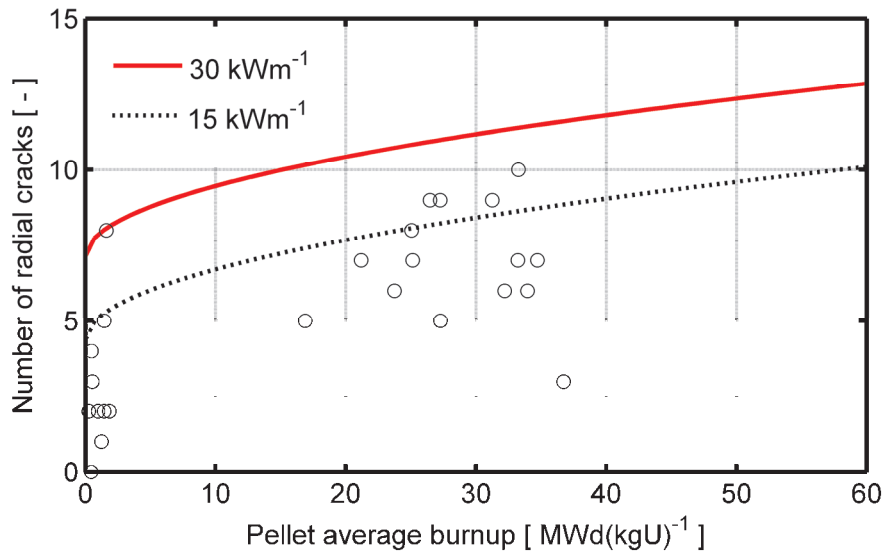


Fig. 29: Number of radial cracks in the fuel pellet, calculated through eq. (28), in comparison with data from [18]. The data are for UO₂ fuel pellets that were operated at a maximum LHGR below 15 kWm⁻¹.

In recent work [59], Coindreau et al. presented correlations for estimating the number of radial fragments in irradiated UO₂ fuel pellets; by “radial fragments”, they meant pieces as those illustrated in Fig. 26. Without showing the underlying database, they proposed the following correlations

$$n_f^o = \text{Max} \left(1, \text{Min} \left(7q'_M / 17 - 8/17, 16 \right) \right), \quad (30)$$

$$n_f = \text{Min} \left(n_f^o + (16 - n_f^o) E_{av} / 50, 16 \right). \quad (31)$$

Here, n_f^o is the number of radial fragments in fresh fuel, subjected to power at beginning of life. From the above equations, it follows that there will never be more than sixteen radial fragments in the fuel pellet. The correlations are used for calculating fragment characteristics and debris bed properties in the severe accident analysis software ASTEC [59].

The works presented above suggest that fuel fragments formed by stresses induced by temperature gradients are fairly large; a maximum number of about 15 radial cracks or radial fragments are consistently reported by Oguma [58], Walton and Husser [18], and Coindreau et al. [59]. Consequently, the fragment side stemming from the pellet periphery should on average be larger than $\pi D_{FP} / 15$ in size, where D_{FP} is the fuel pellet diameter. This minimum fragment size estimate is in fair agreement with typical fragment sizes reported from ceramographic examinations of irradiated commercial fuel with moderate burnup. A summary of average fragment sizes reported from LOCA-tested fuel in Halden, Studsvik, PBF and FR2 was presented in [12], from which Fig. 30 is reproduced. Most of the data reported for fuel with a pellet average burnup less than 60 MWd(kgU)⁻¹ fall between 2 and 3.5 mm. For fuel with higher burnup, the fragment average size drops considerably as a result of fuel pulverization.

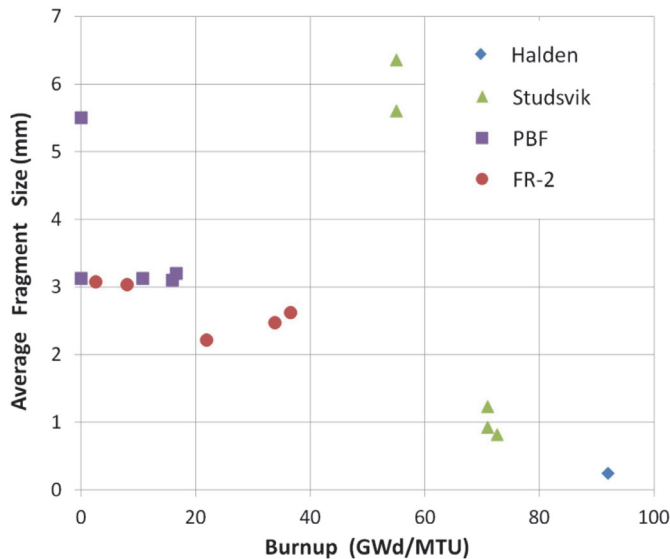


Fig. 30: Average fuel fragment size, determined from ceramography of fuel rod cross sections and reported in [12]. Burnup is the radial average fuel pellet burnup and average fragment size is the average cross section dimension [12].

Ceramographic investigations of irradiated fuel just before and after LOCA testing generally reveal that negligible additional cracking occurs during the LOCA transient in fuel with burnup below about $60 \text{ MWd}(\text{kgU})^{-1}$ [1, 34]. This can be understood from the fact that fuel fragmentation at these burnup levels is driven mainly by stresses induced by temperature gradients. These stresses are usually lower during LOCA than during normal reactor operation, since the fuel temperature is generally more uniform. A notable exception is the case when the fuel is re-wetted (quenched) at termination of the LOCA. The thermal shock induced in the fuel when it comes into contact with cold water may lead to fragmentation of the solid fuel pellets, if the temperature drop is sufficiently large and sufficiently fast. This phenomenon seems not to be particularly well studied; most studies found in literature are concerned with interaction of *molten* UO_2 with water. A notable exception is the study by Oguma, who carried out thermal shock tests on solid unirradiated UO_2 fuel pellets by quenching them into room temperature water [60]. After quenching, the material fracture strength was measured at room temperature to detect damage in the form of microcracks in the material. Oguma reported a significant drop in fracture strength for pellets quenched from temperatures higher than about 430 K, i.e. about 140 K above the water temperature. For higher quenching temperatures, macroscopic cracks were clearly visible in the material. As shown in Fig. 31, quenching from fuel temperatures expected under LOCA resulted in fuel fragments that were much finer than those created by thermal stresses under normal reactor operation.

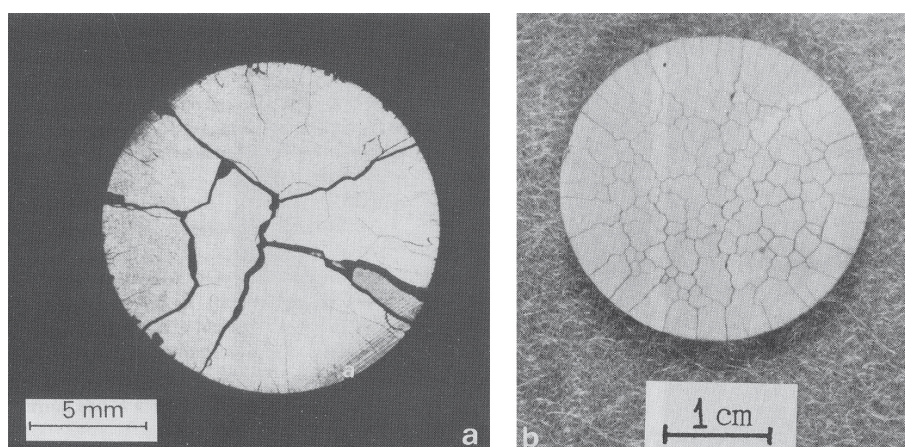


Fig. 31: Crack patterns resulting from quenching as-fabricated UO_2 fuel pellets in room temperature water. The pre-quench fuel temperature was: a) $\sim 770 \text{ K}$, b) $\sim 1070 \text{ K}$.

Reprinted from [60], copyright 1985, with permission from Elsevier.

It is likely that thermal shock may have contributed to creation of the fine fuel fragments that were observed in LOCA tests done in Studsvik, Sweden. Four of the six Studsvik tests were terminated by quenching the test rig with room temperature water, which means that at least the fuel expelled from the fuel rod and residing at the bottom of the test rig at time of quenching must have been subjected to thermal shock [11, 61]. The pre-quench temperature in the Studsvik tests, as

measured with thermocouples attached to the cladding, was typically 1050 K. The cooling rate during quenching, as measured with the same thermocouples, was around 60 K s^{-1} . These testing conditions are thus different from those used in the IFA-650 series of LOCA tests done in Halden, where all tests are terminated by slow cooling of the test rig rather than by quenching [10].

Finally, it should be remarked that advanced computational methods and models have been presented in the literature, by which pellet crack formation is mechanically modelled from the true stress state in the fuel pellet under various operating conditions [62-64]. These methods and models are not reviewed here, but they could possibly be used to formulate more accurate correlations for crack formation and for correlations that relate fuel fragment size to fuel operating conditions.

A.2. Fuel pulverization

The first reports of extensive disintegration of high burnup UO_2 fuel into fine fragments originated from out-of-reactor tests that involved heating of the fuel material above its steady-state irradiation temperature. Some of these tests were laser flash thermal diffusivity measurements, whereas others were studies on fission gas release from high burnup fuel [65, 66]. The latter tests clearly showed that the disintegration of the material was accompanied by release of gaseous fission products, and it was early hypothesized that the disintegration occurred by cracking initiated at overpressurized bubbles and pores in the high burnup material [65]. Today, this hypothesis seems to be widely accepted, not least since later tests have shown that fuel cracking and the burst-type fission gas release that it brings about can be suppressed by imposing a hydrostatic pressure on the fuel.

The mechanism produces much finer fragments than the cracking induced by thermal stresses under normal fuel operation. It is therefore often referred to as fuel *pulverization*, in order to discriminate it from the larger-scale fragmentation normally seen in the fuel. Fig. 32 shows the appearance of very high burnup UO_2 fuel after out-of-reactor heating to 1500 K at a heating rate of 0.17 K s^{-1} . The insert in Fig. 32 shows the measured fragment frequency-size distribution [66]. It is clear that virtually all fragments are smaller than $100 \mu\text{m}$.

In-reactor as well as out-of-reactor LOCA simulation tests on high burnup fuel rods have later shown that the pulverization mechanism may come into play under LOCA as the high burnup material at the pellet periphery is overheated [34, 67]. The LOCA tests suggest that there is a strong threshold effect of fuel burnup on the propensity for fuel pulverization: No or negligible pulverization is seen in LOCA tests on fuel rods with pellet average burnup less than $60 \text{ MWd}(\text{kgU})^{-1}$, whilst nearly complete pulverization is seen in tests with fuel having a pellet average burnup above $80 \text{ MWd}(\text{kgU})^{-1}$. This is illustrated in Fig. 33, which shows the

cumulative fuel fragment size distributions measured in five 17×17 type PWR fuel rods after out-of-reactor LOCA simulation tests in Studsvik, Sweden.

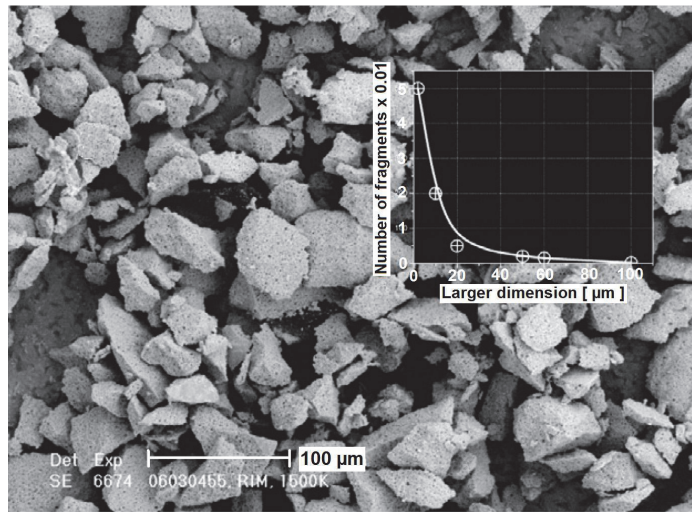


Fig. 32: Micrograph showing pulverized UO_2 fuel with a local burnup of $200 \text{ MWd}(\text{kgU})^{-1}$ after heating to 1500 K. The measured frequency-size distribution for the fuel fragments is shown in the insert. Reprinted from [66], copyright 2008, with permission from Elsevier.

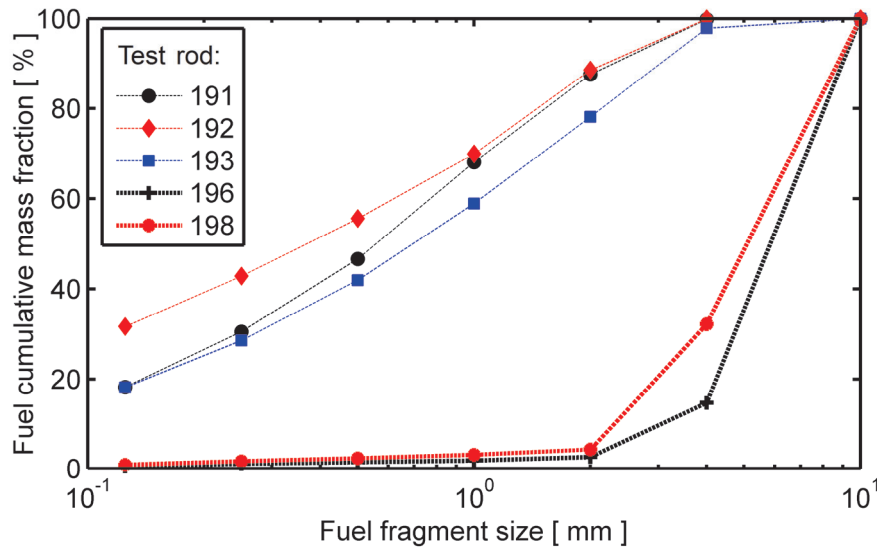


Fig. 33: Cumulative fragment size distributions measured for five fuel rods after LOCA simulation tests in Studsvik [12]. The pellet radial average burnup was about $78 \text{ MWd}(\text{kgU})^{-1}$ in tests 191/192/193 and $60 \text{ MWd}(\text{kgU})^{-1}$ in tests 196/198.

Following the LOCA simulation tests in Studsvik, bend tests were conducted on the rods to measure the mechanical strength of the ballooned and ruptured region. The two halves of each broken rod were then inverted and gently shaken, in order to dislodge any loose fuel fragments within the cladding tube. All loose fuel frag-

ments were collected and processed through a series of sieves to determine the fragment size distribution. The results are shown in Fig. 33. There is a significant difference in the amount of fine fragments between rods 191/192/193 with a pellet radial average burnup around $78 \text{ MWd}(\text{kgU})^{-1}$ and rods 196/198, which had a burnup around $60 \text{ MWd}(\text{kgU})^{-1}$. The latter had virtually no fragments smaller than 2 mm. We note that all tests presented in Fig. 33 were terminated by quench, except for the test on rod 196. This rod had the lowest fraction of small-size fragments [11], which suggests that additional fuel fragmentation by thermal shock under quenching could possibly have occurred in the other tests; see section A.1.

A review and assessment of proprietary as well as open literature data from out-of-reactor experiments on fuel pulverization has recently been published [20-22]. The reviewers draw the following conclusions from these data:

- At high burnup and low irradiation temperature, UO_2 fuel is liable to form fine fragments when subjected to temperature excursions above the steady-state irradiation temperature. The susceptibility to pulverization is highly correlated to the formation of a high burnup structure at the pellet rim, but pulverization occurs also outside the re-structured rim; the pulverization is related to a high local population of overpressurized gas bubbles in the fuel material, and not to the HBS formation per se.
- Pulverization and fission gas release can be substantially reduced by the imposition of a hydrostatic pressure on the fuel material. A pressure of about 50 MPa seems sufficient to suppress pulverization, which means that pellet-cladding mechanical interaction may limit pulverization in LWR fuel rods.
- The degree of pulverization, and hence, the resulting fragment size, depends on the heating rate and the temperature reached during the transient. The higher the heating rate and peak temperature, the smaller the fragments. Typically, the fragment size is in the range 20–200 μm .
- The data at hand can be used to devise an empirical temperature threshold for pulverization of high burnup fuel. The threshold depends on the local burnup of the fuel, as shown in Fig. 34.

The empirical temperature threshold presented in [20-22] states that a local burnup of at least $71 \text{ MWd}(\text{kgU})^{-1}$ is required for pulverization. As shown in Fig. 34, the threshold temperature at this burnup is $920 \text{ }^\circ\text{C}$. It drops linearly with increasing burnup and reaches a constant value of about $640 \text{ }^\circ\text{C}$ for fuel burnups beyond $94 \text{ MWd}(\text{kgU})^{-1}$.⁵

By combining their pulverization threshold (Fig. 34) with calculations of the local burnup distributions and measured peak temperatures for fifteen fuel rods that have been LOCA tested in Halden and Studsvik, the aforementioned reviewers estimated the amount of pulverized fuel in each test rod [20-22]. The estimates were found to agree fairly well with the observed amounts of pulverized fuel. In

⁵ It is indicated in [20] that unpublished results from more recent experiments suggest that the temperature threshold would in fact be somewhat higher than $640 \text{ }^\circ\text{C}$.

particular, the strong threshold effect of fuel burnup observed in the range 60–80 $\text{MWd}(\text{kgU})^{-1}$ (pellet radial average value) was well reproduced. This threshold effect is further discussed in section 2.2.2 of the report.

The empirical threshold shown in Fig. 34 is based on currently available data, open as well as proprietary, and reflects the current state of knowledge regarding the pulverization phenomenon. The only parameter considered in this simple threshold is the fuel local burnup, although other parameters are known to be important. Additional experiments are needed and underway to quantify for example the effects of heating rate and hydrostatic pressure, and also to determine the size of fragments produced under different conditions [20-22]. Mechanistic models for the pulverization phenomenon observed in high burnup LWR fuel are not yet available, but reported to be underway [53]. However, it should be remarked that models for fission gas driven fragmentation and spallation of UO_2 fuel for fast breeder reactors were developed and verified against experiments in the early 1980s [68].

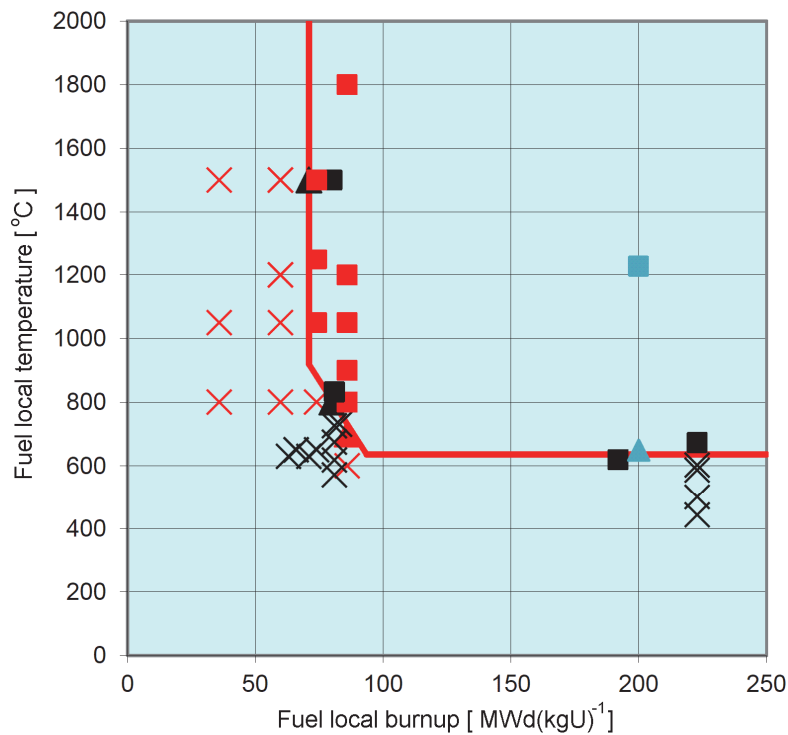


Fig. 34: Empirical temperature threshold for fuel pulverization in comparison with its supporting database [20-22]. Solid squares represent samples that were fully pulverized, crosses denote samples for which no pulverization was observed, and solid triangles indicate samples showing partial pulverization. Colours represent various data sets.

Appendix B: Effective thermal conductivity of crumbled fuel

Over the years, various models and formulas have been proposed for calculating the effective thermal conductivity of particle beds, in which the voids between the particles contain a stagnant fluid. Reviews of the subject are given in [69-71]. In general, all models express the effective thermal conductivity as a function of the volume fraction of solid particles or fluid and the thermal conductivities of the two phases. Some models also take into consideration other parameters, such as the shape of the solid particles, their orientation and size distribution. These more elaborate models usually provide better accuracy for the effective thermal conductivity, but they are useful only if the properties of the particles and the particle bed are well defined. Since this is not the case for crumbled fuel pellets in distending cladding tubes, we have to rely on simple models.

In our model, we calculate the effective thermal conductivity of crumbled fuel pellets through a correlation proposed by Chiew and Glandt [72]. Input to this correlation consists of the thermal conductivities of the solid particles (fuel fragments in our case) and the surrounding gas (helium mixed with gaseous fission products released from the fuel), together with the packing fraction of the particles. This input is available from other models and correlations in our version of FRAPTRAN-1.5. The correlation is

$$\frac{\lambda_{eff}}{\lambda_f} = \frac{(1-\beta)}{(1+2\beta)(1-\beta\phi)} \left(1 + 2\beta\phi + (K_2 - 3\beta^2)\phi^2 \right). \quad (32)$$

Here, λ_{eff}/λ_f is the ratio of the effective thermal conductivity to the conductivity of the solid fuel fragments, ϕ is the packing fraction of fuel fragments, K_2 is a function defined below, and β is the reduced thermal polarizability

$$\beta = \frac{\lambda_f - \lambda_g}{\lambda_f + 2\lambda_g}, \quad (33)$$

where λ_g is the thermal conductivity of the gas surrounding the fuel fragments. We note that $-1/2 \leq \beta \leq 1$ as the ratio λ_f/λ_g varies from zero to infinity.

Chiew and Glandt approximated the function K_2 in eq. (32) by

$$K_2(\beta, \phi) \approx K_2^{(0)}(\beta) + K_2^{(1)}(\beta)\phi, \quad (34)$$

and provided the coefficients $K_2^{(0)}(\beta)$ and $K_2^{(1)}(\beta)$ as functions of β in tabular form [72]. In our model, we use a best fit to these tabulated values, given by

$$K_2^{(0)}(\beta) = 1.7383\beta^3 + 2.8796\beta^2 - 0.11604\beta, \quad (35)$$

$$K_2^{(1)}(\beta) = 2.8341\beta^3 - 0.13455\beta^2 - 0.27858\beta . \quad (36)$$

The correlation given by eqs. (32)–(36) is an extended form of Maxwell’s classical mixture equation [73]. It is plotted in Fig. 35 for the parameter range of interest for our application.

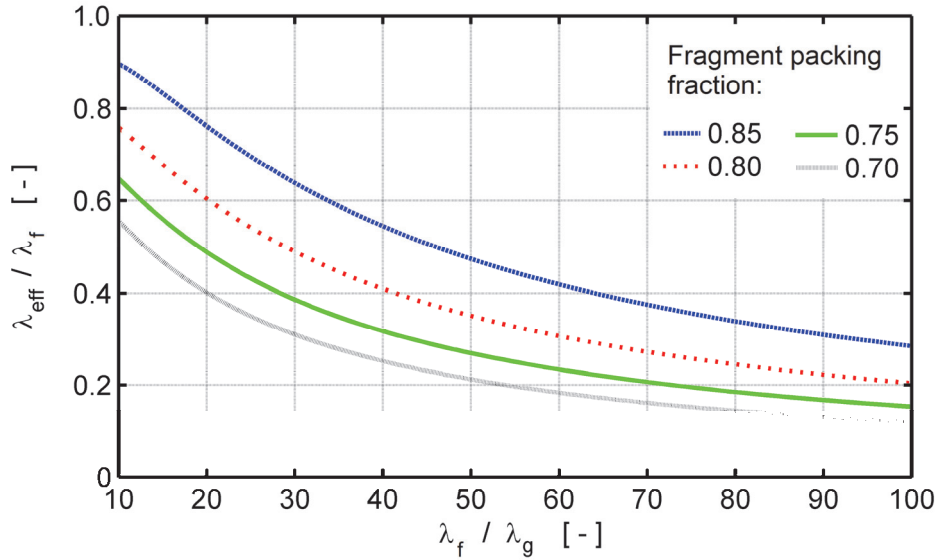


Fig. 35: Calculated effective thermal conductivity (normalized) for various packing fractions of fuel fragments, plotted versus the thermal conductivity ratio between the fuel fragment material and the surrounding gas.

Notwithstanding its simplicity, the effective thermal conductivity correlation by Chiew and Glandt [72] is known to successfully reproduce experimental data on the effective thermal conductivity of granular materials over a wide range of phase conductivity ratios and particle packing fractions [74]. Some experimental data are available for the effective thermal conductivity of UO_2 powders in helium, argon and mixtures of helium and argon [75, 76]. The powders examined in these experiments were of unirradiated UO_2 , and had a mean particle size of about 85 μm and a packing fraction around 0.63. The gas pressures ranged from 0.27 to 1.1 MPa, which is high enough for the thermal conductivity of the gas to be practically independent of pressure [75, 76]. Fig. 36 is a comparison of measured data for the effective thermal conductivity at 850 K with results calculated through eqs. (32)–(36). The calculations were done for an assumed packing fraction of 0.63. In the calculations, the thermal conductivity of UO_2 at 850 K was assumed to be 3.98 W(mK)^{-1} . The conductivity of the gas was taken from reference data [77] (pure He or Ar) or from [76] (He/Ar mixtures).

It is clear from Fig. 36 that the correlation by Chiew and Glandt reproduces the experimental data quite well. The largest discrepancy is found for the tests with pure argon gas. This is probably due to the fact that the correlation considers heat transfer merely by conduction through solid particles and stagnant gas. Other modes of heat transfer, e.g. by natural or forced convection of the gas or by radia-

tion between surfaces of the solid particles, are not accounted for. The underestimated effective thermal conductivity in the low-conductivity argon gas is most likely a consequence of neglecting the radiative heat transfer in the calculations.

In conclusion, Fig. 35 and Fig. 36 suggest that collapse of the fuel pellet column, leading to fuel crumbling in ballooned segments of the fuel rod, is likely to have a large effect on the effective thermal conductivity of the crumbled fuel material. This is particularly true for high burnup fuel rods, in which the void volume free gas inventory comprises a large amount of fission products Xe and Kr with low thermal conductivity. Yet, it should be remembered that the thermal conductivity degradation of the crumbled fuel is balanced by closure of the wide pellet-cladding gap, as the fuel pellet stack collapses into the balloon.

Finally, it should be remarked that the correlation defined by eqs. (32)–(36) gives unphysical results for high packing fractions ($\phi > 0.85$) in combination with small differences between the thermal conductivities of the solid fragments and the surrounding gas ($\lambda_f / \lambda_g < 5$). However, this parameter range is not of concern for our application of the correlation.

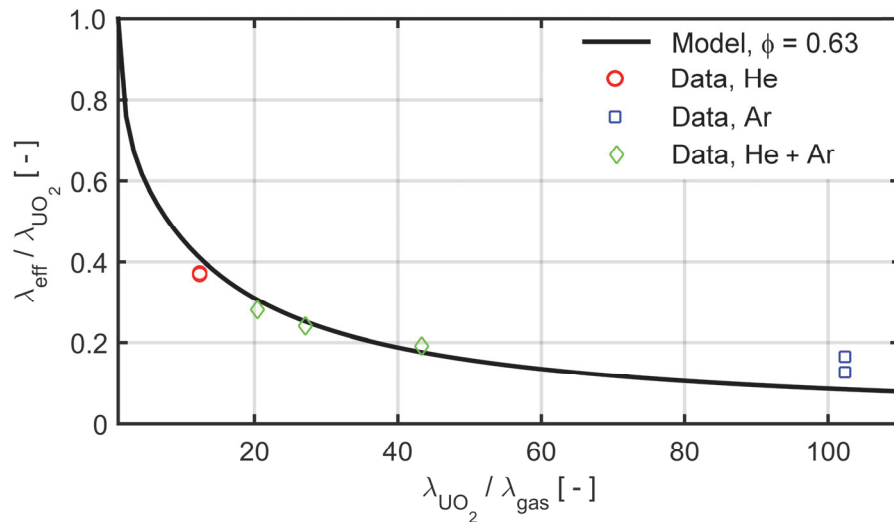


Fig. 36: Calculated effective thermal conductivity of UO_2 powder in various gases, in comparison with experimental data [75, 76]. The mixed gas data are for different compositions of He and Ar. Data as well as calculations pertain to a temperature of 850 K and fragment packing fractions around 0.63.

Appendix C:

The Halden LOCA test IFA-650.4

The IFA-650 series of tests are conducted since 2003 in the Halden heavy water test reactor, Norway. To date, fourteen tests on short-length fuel rodlets have been carried out under simulated loss-of-cooling accident conditions. Eleven of the tests have been made on pre-irradiated fuel rods [10, 78]. One of the primary objectives of the tests is to quantify the extent of fuel fragment axial relocation into the ballooned regions of the rods, and to study possible effects of fuel relocation on cladding temperature and oxidation. Several tests have exhibited axial relocation of fuel fragments; the most notable relocation resulted from tests 4 and 9.

C.1. Design and operation of the IFA-650 test rig

The design of the IFA-650 test rig is shown in Fig. 37, and a schematic drawing of the heated section of the rig is given in Fig. 38. In each test, a single test rodlet with an active (fuelled) length of about 500 mm is instrumented and placed in the centre of the rig, which in turn is placed in one of the experimental channels of the test reactor. The rodlet is surrounded by an electrically heated shroud and a pressure flask. The heated shroud is part of a flow separator, which separates the coolant into a central channel adjacent to the fuel rod and an outer annulus. The heated shroud provides boundary conditions that resemble the heating effects of nearby fuel rods with similar power. The temperature of the test rodlet is affected both by nuclear heating of the rodlet itself and the electrical heating of the shroud. The inner/outer diameters of the shroud and pressure flask are 20/26.2 mm and 34/40 mm, respectively.

The pressure flask is connected to a water loop. During the precondition phase before the test, the loop is filled with heavy water at a pressure and temperature of about 7 MPa and 515 K, which is circulated by pumps through the loop. Shortly before the test, the pressure flask is isolated from the loop and the test rodlet is cooled only by natural circulation within the flask. The LOCA simulation test is then initiated by opening valves to a blowdown tank, which causes a sudden pressure drop in the flask. The coolant flashes to steam, which flows to the blowdown tank and condensates. The flashing lowers the temperature of the remaining coolant. At the end of this blowdown phase, which typically lasts for a minute, the coolant pressure in the flask stabilizes at 0.2–0.3 MPa [10].

After the blowdown phase, the test rodlet heats up with a rate that depends on the predetermined power levels of the rod and the electrically heated shroud. Small amounts of water are periodically injected during this high temperature phase to maintain a sufficient amount of steam for cladding oxidation, but otherwise, no actions are taken until the test is terminated by switching off the electrical heater

and scrambling the reactor. The test rod is then left to cool down slowly, without quenching, in order to minimize any disturbances that could influence the fuel fragmentation and relocation that may have occurred during the high temperature phase.

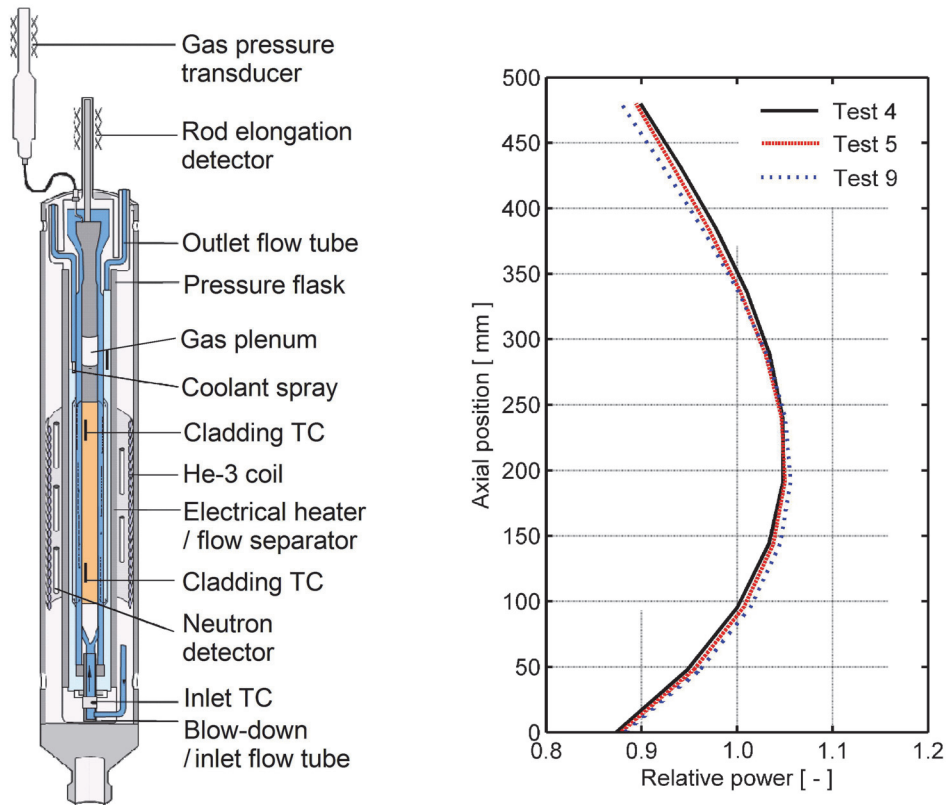


Fig. 37: Design of the IFA-650 test rig (left) and rodlet axial power profiles from three tests on pre-irradiated PWR fuel rods in the IFA-650 series (right) [10, 79].

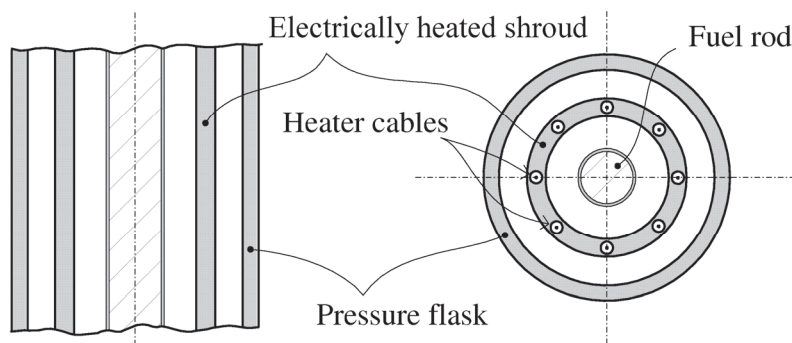


Fig. 38: Schematic drawing of the heated section of the IFA-650 test rig [44].

The general test procedure includes a preconditioning period of 7–8 hours, during which the test rodlet is operated at an LHGR around 8.5 kWm^{-1} . The reactor and rod power is decreased prior to the test. During the test, the rod power is held nearly constant, typically at $1\text{--}3 \text{ kWm}^{-1}$, depending on the target peak cladding temperature. The axial power profile in the rodlet during the test is nearly symmetric, with an axial peak to average power factor of 1.04–1.08. Fig. 37 shows the axial power profiles for three different IFA-650 LOCA tests on PWR fuel rods. The variation from one test to another is fairly small.

As indicated in Fig. 37, the IFA-650 test rig instrumentation consists of a fuel rod elongation detector, a fuel rod gas pressure transducer, and coolant thermocouples at the inlet and outlet of the rig. For most tests, there are also 2–4 cladding surface thermocouples, three vanadium neutron detectors and 2–3 heater surface thermocouples. All of these are axially distributed along the rod. Tests 3 and 4 were also equipped with thermocouples at the axial level of the rod gas plenum; the gas plenum is located about 250 mm above the top of the fuel pellet column, away from the heated region.

C.2. The IFA-650.4 test rodlet

The test rodlet for IFA-650.4 was re-fabricated from a full-length PWR fuel rod, manufactured by Framatome ANP and operated in the Gösigen nuclear power plant, Switzerland, to very high burnup [80]. The test rodlet was sampled from the span between the fifth and sixth spacer grid. The active length of the re-fabricated rodlet was 480 mm, and the sampled section had reached a burnup of $92.3 \text{ MWd}(\text{kgU})^{-1}$ during seven reactor cycles of operation in the Gösigen reactor. The estimated average linear heat generation rate for the sampled section during each cycle was 33.5, 27.5, 30.0, 19.0, 18.0, 17.0 and 16.0 kWm^{-1} [80].

As part of the re-fabrication process, the test rodlet was filled with a gas mixture consisting of 95 vol% argon and 5 vol% helium to a pressure of 4 MPa at room temperature. Argon was used to mimic the low conductivity fission product gases Xe and Kr, while a small amount of helium was needed to leak test the rodlet. The gas plenum volume of the rodlet was made sufficiently large to maintain stable pressure conditions until cladding rupture. The design and pre-test material conditions of the IFA-650.4 test rodlet are summarized in Table 4. It should be remarked that the Duplex-type cladding had a good corrosion resistance, which explains the low hydrogen concentration and thin oxide layer, in spite of the long operating life of the mother fuel rod. The variation in pre-test oxide layer thickness along the rodlet was insignificant.

Table 4: Design specification and pre-test conditions for the IFA-650.4 test rodlet [80].

Rodlet active length	[mm]	480
Cold free volume	[cm ³]	21.5
Fill gas composition	[vol%]	95 Ar + 5 He
Fill gas pressure at 295 K	[MPa]	4.0
<hr/>		
Fuel material		UO ₂
As-fabricated enrichment of ²³⁵ U	[wt%]	3.5
As-fabricated fuel pellet density	[kgm ⁻³]	10 421
As-fabricated fuel pellet diameter	[mm]	9.13
As-fabricated fuel pellet height	[mm]	11.00
As-fabricated dishing volume per pellet	[mm ³]	16
Pre-test average fuel burnup	[MWd(kgU) ⁻¹]	92.3
<hr/>		
Cladding tube material		Duplex
Cladding tube base material		Zircaloy-4
Outer surface liner material		Zr-2.6wt%Nb
Heat treatment		SRA
Outer surface liner thickness (nominal)	[μm]	100
As-fabricated cladding outer diameter	[mm]	10.75
As-fabricated cladding wall thickness	[mm]	0.725
Pre-test oxide thickness (mean)	[μm]	10
Pre-test oxide thickness (max)	[μm]	11
Pre-test hydrogen concentration	[wppm]	50
Pre-test fast neutron fluence (> 1 MeV)	[m ⁻²]	1.52×10 ²⁶

C.3. Summary of test results

In the IFA-650.4 LOCA test, the average linear heat generation rate of the rodlet was about 1.0 kWm⁻¹ and that of the electrically heated shroud 1.5 kWm⁻¹ [80]. These power levels were kept constant during the heat-up phase and most of the high temperature phase. The power for the heated shroud was uniformly distributed along the test section, while the axial power profile for the rodlet was peaked to the rodlet mid-plane; see Fig. 37.

Fig. 39 presents temperature measurements from eight different thermocouples, the positions of which are defined in Table 5. Time $t = 0$ refers to the time at which the test was initiated by opening the valves to the blowdown tank. It should be remarked that cladding thermocouples were attached only at the upper end of the IFA-650.4 test rodlet. This was done to ensure that the cladding was not weakened in the centre and lower end of the rodlet, where cladding ballooning and burst were expected.

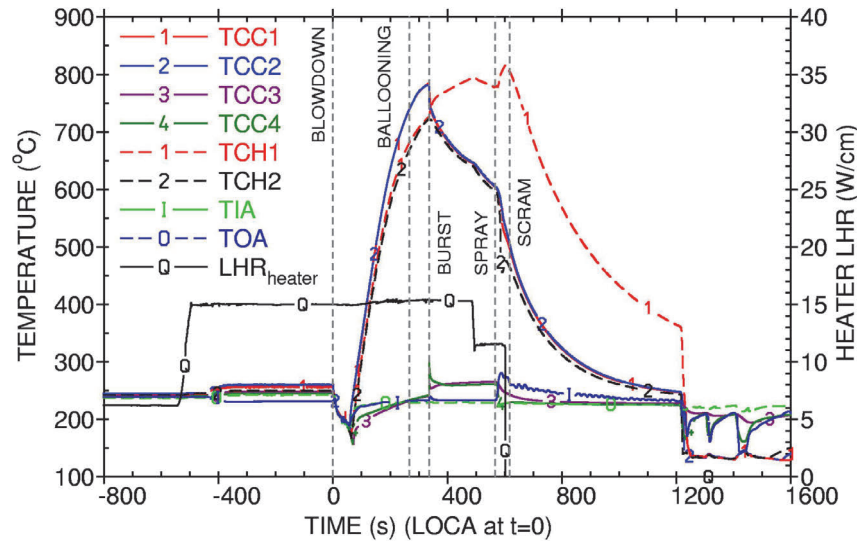


Fig. 39: Measured temperatures during the IFA-650.4 LOCA simulation test [79].
See Table 5 for definition of the thermocouples listed in the legend.

Table 5: Thermocouple (TC) positions in the IFA-650.4 LOCA simulation test.
The axial position z refers to the height above the bottom of the fuel pellet column.

TC	Position and measured property	z [mm]
TCC1	Cladding surface (upper part of active length)	400
TCC2	Cladding surface (upper part of active length)	400
TCC3	Cladding surface (gas plenum position)	678
TCC4	Inner flow channel (upper part)	670
TCH1	Heater surface (mid position)	205
TCH2	Heater surface (top part)	380
TIA	Coolant inlet (average signal from 2 TCs)	-
TOA	Coolant outlet (average signal from 2 TCs)	-

Fig. 40 presents the recorded rod internal gas pressure, rod elongation and the gamma activity in the pipeline to the blowdown tank. From these recordings, it is clear that the cladding ruptured at $t = 336$ s. The rod internal gas pressure dropped instantaneously to about 0.8 MPa, according to Fig. 40. In reality, the gas pressure fell to that of the coolant (0.3–0.4 MPa), but mechanical constraints in the pressure transducer limited the measuring range.

From Fig. 39, it is clear that the cladding temperature at the upper part of the fuel pellet column started to decrease significantly, approximately at time of cladding rupture. This is a consequence of axial fuel relocation, which emptied the cladding tube at the thermocouple locations (TCC1 and TCC2). At the same time, the heater temperature at the rodlet mid position (TCH1) started to increase dramatically. This is a result of fuel accumulation in the ballooned cladding at this position,

together with a much reduced gap between the ballooned cladding and the heater. Water spraying was started at $t = 566$ s and the reactor was scrammed at $t = 617$ s, i.e. more than 10 minutes after start of blowdown.

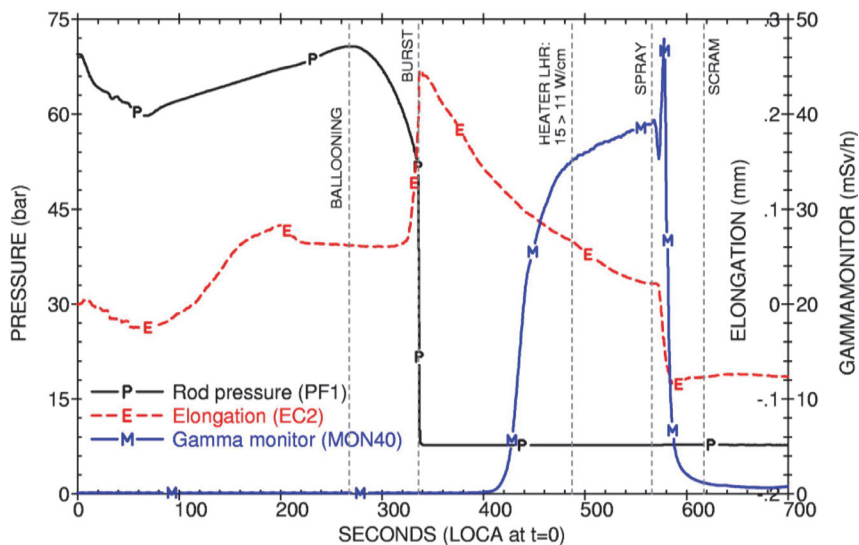


Fig. 40: Measured rod elongation, rod internal gas pressure and coolant gamma activity during the IFA-650.4 LOCA simulation test [79].

The entire pressure flask was gamma scanned 105–115 days after the test. The flask was thereafter filled with epoxy and sent to the hot cell laboratory for ceramographic and metallographic examinations of the test rodlet. The epoxy was intended to stabilize the fuel relocation that had occurred during the test. However, the impregnation failed below the balloon, which was located slightly below the mid-plane of the rodlet. The balloon filled the entire cross section, and the cladding was in contact with the inner surface of the heated shroud.

A detailed presentation of the results from gamma scanning, ceramography and metallography of the IFA-650.4 rodlet can be found in [49], and selected data from the investigations are compared with our calculated results in section 4.2.2. With regard to fuel fragmentation and axial relocation, the post-test characterization of the rodlet showed that about 190 mm of the fuel pellet column was missing from the upper part of the rod. This fuel had relocated axially to the balloon, and some of it had been expelled through the cladding breach and had accumulated above the balloon and at the bottom of the pressure flask. Ceramography revealed extensive fragmentation and pulverization of the fuel in the balloon and its vicinity, where mechanical restraint from the cladding had disappeared [49]. The pulverization had occurred across the entire cross section of the pellet, and was not confined to the high burnup structure at the pellet rim. The fuel fragment size distribution was determined by image analysis of two cross sections, both located within the ballooned and ruptured region of the rodlet. Most of the fuel fragments were less than 200 μm in size [78].



2015:37

The Swedish Radiation Safety Authority has a comprehensive responsibility to ensure that society is safe from the effects of radiation. The Authority works to achieve radiation safety in a number of areas: nuclear power, medical care as well as commercial products and services. The Authority also works to achieve protection from natural radiation and to increase the level of radiation safety internationally.

The Swedish Radiation Safety Authority works proactively and preventively to protect people and the environment from the harmful effects of radiation, now and in the future. The Authority issues regulations and supervises compliance, while also supporting research, providing training and information, and issuing advice. Often, activities involving radiation require licences issued by the Authority. The Swedish Radiation Safety Authority maintains emergency preparedness around the clock with the aim of limiting the aftermath of radiation accidents and the unintentional spreading of radioactive substances. The Authority participates in international co-operation in order to promote radiation safety and finances projects aiming to raise the level of radiation safety in certain Eastern European countries.

The Authority reports to the Ministry of the Environment and has around 300 employees with competencies in the fields of engineering, natural and behavioural sciences, law, economics and communications. We have received quality, environmental and working environment certification.

Strålsäkerhetsmyndigheten
Swedish Radiation Safety Authority

SE-171 16 Stockholm
Solna strandväg 96

Tel: +46 8 799 40 00
Fax: +46 8 799 40 10

E-mail: registrator@ssm.se
Web: stralsakerhetsmyndigheten.se